Evaluation of an *In Situ* Measurement Technique for Streambank Critical Shear Stress and Soil Erodibility

Cami Marie Charonko

Thesis submitted to the faculty of the Virginia Polytechnic Institute and State University in partial fulfillment of the requirements for the degree of

Master of Science
In
Biological Systems Engineering

Theresa M. Wynn (Co-Chair)
Saied Mostaghimi (Co-Chair)
Panayiotis Diplas

May 18, 2010
Blacksburg, Virginia

Keywords: submerged jet test device; critical shear stress; soil erodibility; cohesive soil erosion; flume erosion test

Evaluation of an *In Situ* Measurement Technique for Streambank Critical Shear Stress and Soil Erodibility

Cami Marie Charonko

ABSTRACT

The multiangle submerged jet test device (JTD) provides a simple *in situ* method of measuring streambank critical shear stress (τ_c) and soil erodibility (k_d). Previous research showed streambank k_d and τ_c can vary by up to four orders of magnitude at a single site; therefore, it is essential to determine if the large range is due to natural variability in soil properties or errors due to the test method. The study objectives were to evaluate the repeatability of the JTD and determine how it compares to traditional flume studies.

To evaluate the repeatability, a total of 21 jet tests were conducted on two remolded soils, a clay loam and clay, compacted at uniform moisture content to a bulk density of 1.53 g/cm^3 and 1.46 g/cm^3, respectively. To determine the similarity between JTD and a traditional measurement method, JTD τ_c and k_d measurements were compared with measurements determined from flume tests.

The JTD k_d and τ_c ranged from 1.68-2.81 cm^3/N-s and 0.28-0.79 Pa, respectively, for the clay loam and 1.36-2.69 cm^3/N-s and 0.30-2.72 Pa, respectively, for the clay. The modest variation of k_d and τ_c for the remolded soils suggests the JTD is repeatable, indicating the wide range of parameters measured in the field was a result of natural soil variability. The JTD median k_d and τ_c, except clay loam k_d (clay loam k_d = 2.31 cm^3/N-s, τ_c = 0.45 Pa; clay k_d = 2.18 cm^3/N-s, τ_c = 1.10 Pa) were significantly different than the flume values (clay loam k_d = 2.43 cm^3/N-s, τ_c = 0.23 Pa; clay k_d = 4.59 cm^3/N-s, τ_c = 0.16 Pa); however, considering the range of potential errors in both test methods, the findings indicate the multiangle submerged jet test provides reasonable measurement of erosion parameters in a field setting.

This work is dedicated to my wonderful husband, John Charonko, and my grandfather, Bob Beye, who will always be in my heart.

Acknowledgements

I would like to thank my major professor, Dr. Tess Wynn, for all her time, effort, guidance, and continuous support during my graduate studies. Her encouragement and motivation throughout the project helped me complete this project. I would also like to thank Drs. Saied Mostaghimi and Panos Diplas for serving on my committee, and for all of their support and expertise.

Thank you to Dr. David Vaughan for offering me my first opportunity to come to Virginia Tech. His invitation to participate in a summer NSF Research Experience for Undergraduates changed my life. This one opportunity not only introduced me to research, but it gave me the chance to meet the most important person in my life, my husband, John. And thank you to Dr. Mostaghimi for encouraging me to return for graduate school at Virginia Tech.

I would like to thank Laura Teany, the person who spent more days with me in the lab and at Prices Fork facility fixing equipment and overcoming obstacle after obstacle than anyone else during my research. Thank you for all of your ideas, advice, help, support, and friendship. And thanks to Henry Lehmann for his help with construction of my research equipment. Many thanks go to those who helped me during experiments: Justin Summers, Matt Gloe, and Dan Laird. I would like to thank Dr. Joseph Dove and Jonathan Resop for their help and support experimenting with the use of the LiDAR. I would also like to thank the Biological Systems Engineering faculty, staff, and my fellow graduate students for their support over the years.

I would especially like to thank my husband, John. Without his endless love, support, motivation, and help, I would not have had the strength to complete my degree. You are the one person who got me through graduate school. Thank you to my parents, Patty and Blaine Johnson, for their undying love and encouragement throughout my life, and for all the long

distance support. Many thanks also go to Caroline and John Charonko for their encouragement over the years, and being my family on this side of the country. Thank you to all of my family and friends back in Idaho, as well as thanks to Sara Morris for her friendship and support through the good and bad days.

This material is based upon work supported under a National Science Foundation Graduate Research Fellowship. Photos made by author, 2010.

Table of Contents

List of Figures

List of Tables

Chapter 1: Introduction

1.1. Introduction

Soil erosion affects everyone: it negatively impacts water quality, drinking water treatment, aesthetics, and agricultural productivity, as well as aquatic ecosystems (Harder et al., 1976; Clark, 1985; Owoputi and Stolte, 1995; USEPA, 2002). According to the United States Environmental Protection Agency (EPA) (2002), sediment is the top pollutant for assessed streams and rivers in the country. The physical, chemical, and biological damage of sediment pollution in streams cost approximately $16 billion annually in North America (Pons, 2003). Sediment damages aquatic habitats, smothers benthic organisms and fish eggs, and serves as a carrier for pollutants, such as heavy metals, pesticides, nutrients, and bacteria, which increase the health risk to public waters (Clark, 1985; USEPA, 2002). Excessive sedimentation can also hinder public recreational use of streams, interfere with drinking water treatment procedures, and decrease reservoir water-storage capacity (Harder et al., 1976; Clark, 1985).

The major source of sediment is non-point source (NPS) pollution, including erosion from urban, agricultural, and construction areas (USEPA, 2002). However, excessive streambank erosion usually has been disregarded as an important sediment source in a watershed. Channel degradation can contribute as much as 85% of the total stream sediment load (Simon et al., 2000). Knowledge of stream sediment transport is important for hydraulic engineering and ecological applications, erosion and sedimentation estimates, and pollutant transport (Graf, 1984; Aberle et al., 2002). Quantification of stream sediment load is required for the development of Total Maximum Daily Loads (TMDLs) and sound watershed management strategies, as required by the U.S. Clean Water Act. Streambank retreat also impacts riparian ecosystems, floodplain structures, and floodplain residents (Lawler et al., 1997; ASCE, 1998).

Streambank retreat is the overall lateral recession of the bank over time from a cyclic process of three natural processes: subaerial weakening, fluid entrainment (fluvial erosion), and mass failure (Thorne, 1982; Lawler, 1995; Lawler et al., 1997). Researchers often use the term erosion loosely to mean fluid entrainment or mass failure or sometimes both processes. Fluid entrainment, or the direct detachment and removal of sediment by the eroding fluid, is hereafter called "erosion".

To prevent fluvial entrainment, the applied fluvial shear stress on the bank must stay below erosive levels. When applied shear stresses are below the soil critical shear stress, erosion rates are considered zero (Osman and Thorne, 1988; Hanson, 1989; Nearing et al., 1989; Hanson, 1990a, 1990b; Hanson and Cook, 1997; Ravens and Gschwend, 1999; Hanson and Simon, 2001). Soil critical shear stress (τ_c) is the hydraulic force required to initiate the removal of sediment, and represents the critical condition for erosion.

Since stream channels can include cohesive soils (sediment particles held in place by interparticle forces, not gravitational forces), standard sediment transport theory for non-cohesive soils is not applicable. The most common method to estimate cohesive erosion rates is the excess shear stress equation, which relates erosion to soil erodibility (k_d) and critical shear stress (Partheniades, 1965; Osman and Thorne, 1988; Hanson, 1989, 1990a, 1990b; Stein et al., 1993; Hanson and Cook, 1997; Stein and Nett, 1997; Allen et al., 1999; Hanson and Cook, 2004; Wan and Fell, 2004; Julian and Torres, 2006; Knapen et al., 2007). Numerous erosion models, such as HSPF, CONCEPTS, SWAT, and HEC-6, utilize this equation to predict streambank erosion (USACE, 1993; Allen et al., 1997; Bicknell et al., 1997; Langendoen, 2000). Reliable erosion prediction is needed for planning effective erosion control programs, TMDL development and implementation, and watershed management (Harder et al., 1976). Empirical methods, such as

Smerdon and Beasley (1961), Julian and Torres (2006) and Osman and Thorne (1988), are available to estimate the parameters, but recent research has shown they significantly underestimate both k_d and τ_c (Clark and Wynn, 2007). In addition, the soil parameters are difficult to determine by traditional flume studies, because many biological, physical, and chemical factors impact cohesive soil erosion and some are difficult to replicate in the laboratory (Kamphuis and Hall, 1983; Osman and Thorne, 1988; Aberle et al., 2002; Debnath et al., 2007). *In situ* tests are needed to incorporate natural field conditions and the influence of soil structure and variability on streambank erosion.

Erosion models and stream restoration need accurate measurements of k_d and τ_c for accurate erosion predictions and successful restoration designs. Currently, stream restoration is based on natural channel design using empirical methods, which are design equations that represent average conditions based on observations of several stable streams. These equations are only applicable for similar streams, and usually the equations include empirical parameter values chosen by the designer based on experience. To apply these methods for natural channel design, the reference and design watersheds must have similar characteristics. These methods also do not apply to urban watersheds, where more disturbances impact the stream and "stable" reference streams are difficult to find.

An accurate field testing device will permit stream restoration design to advance from empirical methods toward process-based analytical designs. Considering over $1 billion was spent annually since 1990 in the U.S. alone for stream restoration (Bernhardt et al., 2005), improved design methodologies will ensure a more efficient use of scarce conservation resources. Using analytical methods would allow the application of fundamental fluvial geomorphology principles in a quantitative manner that would be applicable to any watershed,

instead of using empirical methods that only apply to similar streams. The difficulty with analytical methods lies with determining the model parameters.

The multiangle submerged jet test device (JTD) represents a relatively simple, inexpensive *in situ* method of measuring k_d and τ_c (Hanson, 1990b). Since the late 1950's, submerged water jets have been used for studying cohesive erosion in both laboratory and field studies (Dunn, 1959; Moore and Masch, 1962; Hollick, 1976; Hanson, 1990b, 1991; Hanson and Robinson, 1993; Allen et al., 1997, 1999; Hanson and Simon, 2001; Mazurek et al., 2001; Potter et al., 2002; Wynn and Mostaghimi, 2006; Mallison, 2008; Thoman and Niezgoda, 2008; Wynn et al., 2008). The portable jet test device produces a jet of water perpendicular to the bank, causing soil scour as the jet dissipates horizontally along the streambank face. Soil k_d and τ_c are calculated from the scour rate and jet velocity. Previous research has shown k_d and τ_c can vary by up to four orders of magnitude at a single site (Wynn and Mostaghimi, 2006; Wynn et al., 2008). Therefore, it is essential to determine if the large range of *in situ* jet test measurements is due to natural variability in soil properties or errors due to the test method and jet test device.

Determining the repeatability of the JTD and the similarity between the JTD and a traditional method are critical in developing this tool to measure soil erodibility and critical shear stress for estimating streambank erosion. Currently, there are few available data regarding the accuracy and precision of the JTD. The ASTM International Standard D5852 (ASTM, 2007b) for Hanson's (1990b) submerged jet device contains no accuracy, bias, or precision information. Recognizing the measurement uncertainty of any device is essential for understanding the data and formulating strong, solid conclusions. In research, documenting the measurement error is needed for accurate evaluation of data (Moldwin and Rose, 2009). The repeatability of the JTD and measurement similarity to traditional method results need to be determined for the JTD

before further research relies on the data, which could result in questionable results and conclusions. The JTD evaluation is also important for research advances in the areas of water quality management and modeling, fluvial geomorphology, and stream restoration.

1.2. Goals and Objectives

The overall goal of this research was to evaluate the *in situ* measurement tool, the multiangle submerged jet test device, for measuring streambank critical shear stress and soil erodibility. The specific objectives include the following:

1. Determine the repeatability of the multiangle submerged jet test device for measuring critical shear stress and soil erodibility; and,
2. Compare the critical shear stress and soil erodibility measured using the multiangle submerged jet test device to results from traditional flume studies.

The research hypothesis was that the jet test device is repeatable and provides statistically similar results ($\alpha = 0.05$) to traditional laboratory flume-based measurements. The jet test device was judged to be repeatable based on the standard deviations and 95% confidence intervals of k_d and τ_c.

Chapter 2: Literature Review

2.1. Cohesive Soil Erosion

The mechanisms and factors influencing soil erosion differ for non-cohesive and cohesive soils. Non-cohesive soils consist of gravel (diameter > 2.0 mm) and sand particles (0.062 mm > diameter < 2.0 mm), which detach and act as individual grains with no interaction between particles. A combination of the particle submerged gravitational weight and hydrodynamic drag and lift forces influence non-cohesive detachment and transportation (Figure 2.1) (Graf, 1984). Cohesive soils are predominately a mixture of silt (0.004 mm < diameter < 0.062 mm) and clay (diameter < 0.004 mm) particles, which interact with each other and act as a group instead of individually (Knighton, 1998). The electrochemical interactions between cohesive grains bond them together and increase the resistance to hydraulic erosion. Without the complex particle interactions, non-cohesive sediment detachment and transport is simpler and better understood than cohesive erosion.

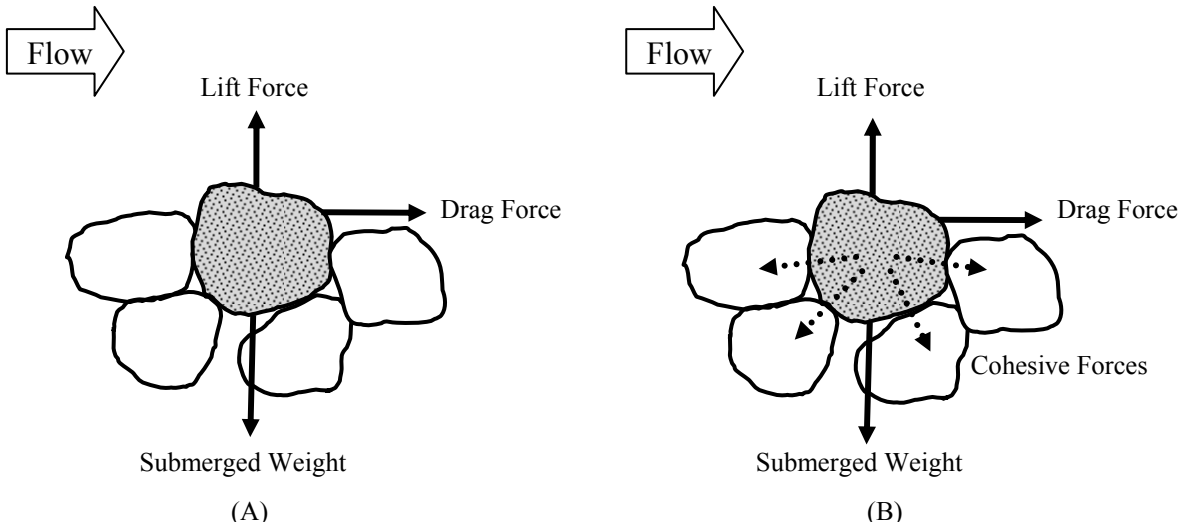

Figure 2.1. Force diagrams on submerged sediment particles in (A) non-cohesive and (B) cohesive soils.

More factors influence cohesive soil erosion than non-cohesive erosion due to the electrochemical interactions between particles. Physical, chemical, environmental, and biological factors affect cohesive erosion, resulting in high temporal and spatial variability (Osman and Thorne, 1988; Aberle et al., 2002; Debnath et al., 2007).

2.1.1. Physical Factors

Both sediment and flow physical properties affect cohesive erosion. Sediment properties include moisture content, bulk density, soil type, clay and organic content, clay plasticity and activity, grain-size distribution, aggregate size distribution and stability, soil structure, dispersion ratio, and stress history of the soil (Smerdon and Beasley, 1961; Lyle and Smerdon, 1965; Harder et al., 1976; Hollick, 1976; Ariathurai and Arulanandan, 1978; Arulanandan et al., 1980; Grissinger, 1982; Kamphuis and Hall, 1983; Thorne and Osman, 1988; Hanson and Robinson, 1993; Owoputi and Stolte, 1995; Lawler et al., 1997; Knighton, 1998; Allen et al., 1999; Potter et al., 2002; Wan and Fell, 2004; Wynn and Mostaghimi, 2006; Knapen et al., 2007; Thoman and Niezgoda, 2008; Wynn et al., 2008). Research has suggested erodibility decreases with increasing clay content (Smerdon and Beasley, 1961), increasing initial soil moisture content (Allen et al., 1999), or increasing bulk density (Hanson and Robinson, 1993; Allen et al., 1999; Wynn and Mostaghimi, 2006). In addition, increases in soil plasticity can decrease soil erodibility (Lyle and Smerdon, 1965; Allen et al., 1999; Potter et al., 2002). Flow properties that influence cohesive soil erosion include applied hydraulic shear stress, velocity, complex secondary flows, and turbulence (Grissinger, 1982; Knighton, 1998). Partheniades, (1965) concluded from a flume study that erosion rates of cohesive soils strongly depend on the bed shear stress.

2.1.2. Chemical Factors

Cohesive soil erosion is influenced by chemical factors, such as soil, eroding fluid, and pore fluid chemistry. Soil chemistry parameters include pH, temperature, ion type and concentrations, dielectric dispersion, and electrochemical forces (Hollick, 1976; Ariathurai and Arulanandan, 1978; Moody et al., 2005; Julian and Torres, 2006; Wynn and Mostaghimi, 2006; Thoman and Niezgoda, 2008). The Sodium Adsorption Ratio (SAR), ratio of exchangeable sodium ions to calcium and magnesium ions, has been shown to impact cohesive erosion. As SAR decreases, sediment particle interaction and bonding increases, and soil erodibility decreases (Ariathurai and Arulanandan, 1978). In addition, Ariathurai and Arulanandan (1978) concluded temperature increases increase soil erodibility due to the decrease in clay attractions between particles. Pore water pressure in the soil also affects cohesive erosion by increasing the distance and, hence the attraction, between clay plates (Grissinger, 1982).

The eroding fluid temperature, pH, electrical conductivity, and chemical composition affect cohesive erosion (Harder et al., 1976; Hollick, 1976; Ariathurai and Arulanandan, 1978; Arulanandan et al., 1980; Grissinger, 1982; Kamphuis and Hall, 1983; Lawler et al., 1997; Wynn and Mostaghimi, 2006; Wynn et al., 2008). In addition, the pore fluid chemistry and the interaction between the eroding fluid and the pore water in the soil influence cohesive soil erosion. Ion type and concentration in pore fluid can impact erosion rate by affecting the soil structure and osmotic potential. Increasing the pore water ion concentration can increase erosion by creating an ionic gradient, which results in water movement into the soil pores (Ariathurai and Arulanandan, 1978).

2.1.3. Environmental Factors

Climate and environmental factors have a large influence on cohesive soil erosion. Air temperature, freeze-thaw cycling, water table changes, and wet-dry cycling weaken and detach soil particles. Freeze-thaw cycling usually increases erodibility due to soil weakening by ice crystals (Wynn et al., 2008).

2.1.4. Biological Factors

Vegetation, animal burrows, and animal trampling affect cohesive soil erosion. Vegetation usually protects and supports cohesive soil from erosion. Vegetation type, above-ground density, and root density impact erosion in several ways (Lawler et al., 1997; Knighton, 1998; Julian and Torres, 2006; Wynn and Mostaghimi, 2006).

2.2. Streambank Retreat Processes

Streambank retreat is the overall lateral recession of the bank over time from a cyclic process of erosion and mass failure (Lawler et al., 1997). This complex phenomenon is dependent on bank erodibility and the sediment quantity entrained in the water (Thorne and Osman, 1988). Research has recognized three processes which contribute to retreat: subaerial weakening and erosion, fluid entrainment, and mass failure (Thorne, 1982; Lawler, 1995; Lawler et al., 1997).

Excessive bank erosion typically results in bank retreat, which impacts floodplain residents, riparian and aquatic ecosystems, and riparian and floodplain structures. In addition to the factors listed earlier that influence cohesive erosion, bank material composition, and channel geometry also contribute to the extent and frequency of bank erosion (Thorne, 1982; Thorne and Osman, 1988; Lawler et al., 1997; Knighton, 1998; Allen et al., 1999). Subaerial processes, fluid

entrainment, and mass failure processes are affected by these influencing factors to varying degrees.

Subaerial processes reduce the soil resistance to future erosion and directly remove soil particles from the bank surface. The weakening process depends on climate conditions and bank properties, particularly soil temperature and bank material composition (Thorne, 1982; Lawler et al., 1997; Wynn et al., 2008). Lawler et al. (1997) classified subaerial processes into three categories based on soil moisture: pre-wetting, desiccation, and freeze-thaw. Pre-wetting encompasses processes that increase bank moisture content, including precipitation infiltration, rise in water table, and high flows. Water seepage and piping can significantly increase bank erodibility. Desiccation, or the reduction of moisture in the soil, can lead to cracking and crumbling of the bank face. Freeze-thaw processes weaken the soil structure, especially in cohesive banks, making the bank more susceptible for future erosion (Lawler et al., 1997; Wynn et al., 2008) .

Fluid entrainment is the detachment, removal, and transport of sediment by the eroding fluid. Entrainment, or fluvial erosion, is a function of stream power (Lawler, 1995) and is influenced by flow peak intensities (Julian and Torres, 2006). Erosion occurs when the fluid shear stress is greater than the soil resisting force (Thorne, 1982; Owoputi and Stolte, 1995). Bank material composition and cohesiveness influence the degree of fluvial erosion. Channel morphology, soil moisture content, and flow properties are also factors in fluvial erosion (Lawler et al., 1997). Fluid entrainment of non-cohesive soils involves lift and drag forces of the water that detach individual grains from the bank (Thorne, 1982; Knighton, 1998). In cohesive soils, erosion occurs by the detachment of aggregates, and many elements influence the degree of erosion in cohesive material, as listed earlier. Cohesive soil erosion is more complex and less

understood than non-cohesive soil erosion, because of the interaction between particles and influencing elements mentioned above (Grissinger, 1982; Thorne, 1982; Lawler et al., 1997; Knighton, 1998; Knapen et al., 2007).

Mass wasting results from large sediment blocks, typically from the upper bank, collapsing due to gravitational forces. The collapse occurs after fluvial entrainment scours and undercuts the lower bank or the stream bed, causing the bank height or angle to increase (Osman and Thorne, 1988; Thorne and Osman, 1988). Bank failure depends on bank height, angle, material composition and properties, and moisture content (Osman and Thorne, 1988; Lawler et al., 1997). Mass stability is not dependent directly on fluvial shear stress, but fluvial erosion influences mass failure rates (Osman and Thorne, 1988).

Subaerial processes, entrainment, and mass failure dominate at different scales in the fluvial system. Lawler (1995) developed a conceptual model of downstream change in dominant retreat processes, which suggested watershed scale is a significant factor in streambank retreat. Headwater reaches are typically confined with low banks, coarse bed particles, and low stream power. Subaerial processes are dominant at this scale. Middle reaches in a watershed usually have the highest stream power with low banks. Since entrainment is a function of stream power, erosion dominates the retreat process at this scale with interaction of subaerial processes (Lawler, 1995). Mass failure is the dominant process in downstream reaches, where bank heights are greater. The fine sediment found in the downstream reaches tends to resist fluvial erosion more than the medium-sized particles in the middle reaches because of an increase in soil cohesion. Preparation processes, particularly desiccation, also occur at this scale.

In summary, streambank retreat is a cyclic, complex phenomenon with three main processes. Subaerial processes weaken the soil structure and detach particles. Fluvial

entrainment erodes weakened soil, scours and undercuts the lower bank, and increases bank height and angle. Without the support from the lower bank sediment, the upper bank fails under gravitational force and slides to the toe. Entrainment moves and transports this sediment mass downstream during subsequent high flows, reducing bank stability and generating more mass failure (Thorne, 1982; Osman and Thorne, 1988; Lawler et al., 1997; Knighton, 1998). To determine the rate of streambank recession, erosion rate estimation is required (Arulanandan et al., 1980) .

2.3. Critical Shear Stress and Soil Erodibility

To maintain streambank stability, the applied fluvial shear stress on the bank must stay below erosive levels. The critical condition for erosion is typically quantified by the soil critical shear stress. Critical shear stress (τ_c) is the hydraulic force required to initiate the detachment of sediment particles or aggregates. This critical force is a theoretical threshold for sediment movement: erosion rates are considered zero when the applied shear stresses are below the critical shear stress (Ariathurai and Arulanandan, 1978; Osman and Thorne, 1988; Hanson, 1989; Nearing et al., 1989; Hanson, 1990a, 1990b; Hanson and Cook, 1997; Ravens and Gschwend, 1999; Hanson and Simon, 2001). Some researchers have questioned the critical shear stress concept (Einstein, 1942; Paintal, 1971; Lavelle and Mofjeld, 1987; Zhu et al., 2001). Paintal (1971) concluded there was no specific critical point for soil movement; to have no erosion there needs to be no flow because turbulent velocity spikes can cause movement at any flow. Despite criticisms, determining τ_c and accurately predicting erosion rates are still important for understanding and modeling streambank retreat (Owoputi and Stolte, 1995).

Since channel boundaries can include cohesive soils, standard sediment transport theory for non-cohesive soils is not applicable. The excess shear stress equation is frequently used to

estimate the erosion rate of cohesive soils (Partheniades, 1965; Osman and Thorne, 1988; Hanson, 1989, 1990a, 1990b; Stein et al., 1993; Hanson and Cook, 1997; Stein and Nett, 1997; Hanson and Cook, 2004; Wan and Fell, 2004; Julian and Torres, 2006; Knapen et al., 2007):

$$\varepsilon = k_d \left(\tau_a - \tau_c \right)^a \tag{2.1}$$

where,

ε = erosion rate (m/s);

k_d = soil erodibility coefficient (m^3/N-s);

τ_a = applied hydraulic boundary shear stress on the soil (N/m^2);

τ_c = soil critical shear stress (N/m^2), and;

a = exponent typically assumed to be 1.

Two assumptions limit the excess shear stress equation: 1) soil erodibility remains constant throughout the soil depth; and, 2) erosion rate and shear stress are linearly related after reaching critical shear stress (Osman and Thorne, 1988; Moody et al., 2005). During an erosion study with undisturbed and remolded samples, Ariathurai and Arulanandan (1978) observed a non-linear relationship between erosion rate and shear stress for a few of the undisturbed samples. Paintal (1971) and multiple researchers also found a non-linear relationship between applied shear stress and bedload transport rate for non-cohesive bedload (2.5 mm and 7.95 mm particles) during a flume study (Garcia, 2008). Some erosion studies have found a power relationship fits better, with the exponent a in Equation 2.1 varying 1.05 to 6.8 (Knapen et al., 2007). Another limitation of the excess shear stress equation is the question of whether the average applied shear stress is adequate for predicting erosion. Grass (1970) recognized turbulence affects sediment detachment, so the shear stress of the drag force may not be the most representative parameter. Research addressing the non-linear relationship and other possibilities

to represent turbulence effects is limited, so the simple linear excess shear stress equation is still currently applied to cohesive erosion data.

Two of the parameters in the excess shear stress equation (τ_c and k_d) are considered soil properties, and are needed to estimate erosion rates. The soil erodibility coefficient (k_d) quantitatively describes the ease of particle detachment from soil. This coefficient incorporates both processes of particle motion initiation (soil-property dependent) and sediment transport (fluid-property dependent) (Moody et al., 2005). Knapen et al. (2007) suggested factors that influence erosion resistance, like moisture content and bulk density, affect k_d more than τ_c. Some erosion studies have indicated an inverse relationship between τ_c and k_d (Ariathurai and Arulanandan, 1978; Arulanandan et al., 1980; Hanson and Cook, 1997; Hanson and Simon, 2001; Wynn, 2004). Knapen et al. (2007) compiled τ_c and k_d values from field and laboratory erosion studies in literature, and concluded τ_c and k_d were not related to each other, although a weak inverse relationship ($R^2 = 0.36$) was observed when τ_c and k_d were grouped by soil type (sand, sandy loam, loam, silt loam, silty clay, clay loam and clay). Silt loams had a low critical shear stress and high erodibility, clay had high critical shear stress and low erodibility, and clay loam had a similar erodibility as clay with a lower critical shear stress.

Forms of the excess shear stress equation are used for estimating channel erosion, rill erosion, and detachment capacity from overland flow (Foster et al., 1977; Osman and Thorne, 1988; Nearing et al., 1989; Owoputi and Stolte, 1995). Numerous models, such as HSPF, CONCEPTS, SWAT, and HEC-6, utilize the linear relationship between erosion rate and applied hydraulic shear stress to predict streambank erosion (USACE, 1993; Allen et al., 1997; Bicknell et al., 1997; Langendoen, 2000). While empirical methods are available for τ_c and k_d estimation, recent research has shown they can significantly underestimate both parameters (Clark and

Wynn, 2007). In addition, the soil parameters are difficult to determine by traditional flume studies, because of the different factors (listed earlier) that can impact soil erodibility in the field. Some of the factors are difficult to replicate in the lab, including subaerial processes, stream water chemistry, climate, and soil structure.

2.4. Critical Shear Stress and Soil Erodibility Measurement Techniques

Estimating τ_c and k_d accurately is difficult; however several different methods exist. Critical shear stress and soil erodibility can be estimated empirically from soil properties, or experimentally in the laboratory or in the field. In some cases, critical shear stress is assumed zero (Foster et al., 1977; Hanson, 1990a, 1991; Allen et al., 1997, 1999; Potter et al., 2002). The Shield's curve provides a critical shear stress estimate based on grain size and density for non-cohesive soils (Shields, 1936).

2.4.1. Shields Diagram for Non-cohesive Soils

Shields (1936) developed a relationship between critical shear stress and representative grain size for non-cohesive sediment. Using two dimensionless parameters (dimensionless critical shear stress and boundary Reynolds number), Shields (1936) plotted an initiation of motion curve (Shields curve), where any point below this line indicated no sediment motion and any point above the curve indicated motion. To determine τ_c from the graph, the boundary Reynolds number is calculated from representative grain size (usually d_{50}), fluid kinematic viscosity, and the shear velocity. The dimensionless critical shear stress is determined by the point where the Shields curve and calculated boundary Reynolds number intersect. Critical shear stress is calculated from the dimensionless critical shear stress, representative grain size, and specific weight of the fluid and sediment (Shields, 1936; Graf, 1984). Even today, the Shields diagram is commonly accepted and utilized in non-cohesive sediment transport.

Although Shields (1936) influenced non-cohesive sediment transport, his work does not apply to cohesive soils. With particle interactions, critical shear stresses are typically greater for cohesive soils than non-cohesive soils. Since few methods estimate critical shear stress for fine sediment, the Shields diagram has been extended to include smaller diameter grains, and is occasionally used to estimate τ_c (Temple and Hanson, 1994; Hanson and Cook, 1997). However, this extension of the curve is not based on actual data. In cohesive soils, particle interactions influence soil resistance to erosion more than gravitational forces. Therefore, the Shields curve will most likely provide an underestimation of critical shear stress. Using Shields diagram, particles smaller than 0.1 mm would have a critical stress for incipient motion equal to 0.14 Pa, assuming critical shear stress as a function of incipient motion for discrete particles (Hanson and Cook, 1997). In addition, many factors influence cohesive erosion that do not affect non-cohesive erosion, as stated earlier.

2.4.2. Empirical Estimation

Many empirical methods estimating critical shear stress exist; these methods typically estimate critical shear stress and soil erodibility based on soil parameters, such as particle size and percent clay content. Smerdon and Beasley (1961) conducted a flume erosion study on eleven Missouri soil samples to develop a relationship between critical shear stress (0.73 – 4.24 Pa) and four physical properties of cohesive soil: plasticity index (22.4 – 30.5), dispersion ratio (4.9 – 73.1), mean particle size (0.0003 – 0.0215 mm), and percent clay (15.3 – 57.5%). The soil samples were leveled in the flume bed to a thickness of 6.35 cm, but not compacted (void ratios ranged from 1.23 to 1.84). After an initial pre-wetting period, the flow rate was increased incrementally until the visual observation of "general movement of soil" was made, which signified critical shear stress. Plotted data of critical shear stress (logarithmic scale) and soil

physical properties (arithmetic or logarithmic scale) showed correlation between the parameters. The developed empirical relationships between critical shear stress and the four soil physical properties are as follows:

$$\tau_c = 0.163(I_w)^{0.84} \tag{2.2}$$

$$\tau_c = 10.199(D_r)^{-0.63} \tag{2.3}$$

$$\tau_c = 3.543 \times 10^{-28.1 D_{50}} \tag{2.4}$$

$$\tau_c = 0.493 \times 10^{0.0183 P_c} \tag{2.5}$$

where,

τ_c = critical shear stress (Pa);

I_w = plasticity index;

D_r = dispersion ratio;

D_{50} = median particle size (mm); and,

P_c = percent clay by weight (%).

Of these four empirical correlations, the relationships of critical shear stress with plasticity index and dispersion ratio were considered most reliable, because these two properties directly relate to soil cohesiveness (Smerdon and Beasley, 1961).

Julian and Torres (2006) used results presented by Dunn (1959) and Vanoni (Vanoni, 1977) to estimate critical shear stress based on soil silt and clay percentage (< 0.063 mm). A rating curve was developed by fitting a third-order polynomial relationship to Dunn's (1959) average τ_c values, assuming 100% and 0% silt and clay percentage result in a maximum and a

minimum τ_c value, respectively. The resulting curve intersects the τ_c-axis (0% silt and clay) at Shields curve lower limit (0.1 Pa) (Shields, 1936):

$$\tau_c = 0.1 + 0.1779(SC) + 0.0028(SC)^2 - 2.34E - 5(SC)^3 \quad (2.6)$$

where *SC* is the silt and clay percentage (<0.063 mm). Julian and Torres (2006) considered vegetation effects on critical shear stress by multiplying the resulting τ_c with a vegetation coefficient (ranging from 1 to 19.20).

There are two empirical methods to estimate k_d if τ_c is known. Osman and Thorne (1988) presented a method to estimate lateral erosion rate for cohesive soils with a critical shear stress greater than 0.6 Pa. This method is based on laboratory work conducted by Arulanandan et al. (1980) at the US Army Corps of Engineers (USACE) Waterways Experiment Station in Vicksburg, Mississippi with 42 undisturbed cohesive soil samples collected from streambanks throughout the United States. Soil erodibility was estimated by dividing the initial soil erosion rate by the critical shear stress. The initial soil erosion rate was calculated as follows:

$$dB = \frac{233 \times 10^{-4} \tau_c e^{-0.13\tau_c}}{\gamma} \quad (2.7)$$

where,

dB = initial soil erosion rate (m/min per unit area);

τ_c = critical shear stress (dynes/cm^2); and,

γ = soil unit weight (kN/m^3).

Assuming a linear relationship between erosion rate and shear stress once critical shear stress was reached, the actual soil erosion rate was calculated by the following form of the excess shear stress equation:

$$dW = dB * \left(\frac{\tau - \tau_c}{\tau_c} \right) \tag{2.8}$$

where dW was the actual erosion rate (m/min), and τ was the flow shear stress (dynes/cm^2). Osman and Thorne (1988) recommended using a calibration factor if the predicted value was unrealistic and not consistent with field observations.

Hanson and Simon (2001) observed an inverse relationship between τ_c and k_d data from 83 submerged jet tests on highly erodible loess streambeds in the Midwestern United States. The typically silt-bedded streams (50 to 80% silt-sized material) had τ_c values ranging from 0.00 to 400 Pa and k_d values between 0.001 to 3.75 cm^3/N-s. Although there was a wide variation among τ_c and k_d parameters, an inverse relationship was observed in the data. Hanson and Simon (2001) found the following relationship for k_d as a function of τ_c ($R^2 = 0.64$):

$$k_d = 0.2\tau_c^{-0.5} \tag{2.9}$$

where k_d is the soil erodibility coefficient (cm^3/N-s).

Clark and Wynn (2007) evaluated and compared different empirical methods for estimating τ_c and k_d, and found the methods underestimate the parameters for streambanks in southwest Virginia, resulting in inaccurate erosion estimation and prediction.

2.4.3. Laboratory Techniques

Typically, laboratory techniques use apparatuses, such as hydraulic flumes or rotating cylinders, to estimate τ_c and k_d. Experimentally, critical shear stress can be defined in a descriptive or quantitative manner.

Visual observation of critical shear stress during experiments requires descriptive criteria for the point of erosion initiation. This defined initiation point of sediment movement is

subjective and difficult to determine (Partheniades, 1965; Hollick, 1976; Kamphuis and Hall, 1983; Graf, 1984; Owoputi and Stolte; Hanson et al., 1999). Multiple definitions of τ_c exist. Dunn (1959) defined τ_c as the point at which "water became cloudy," whereas Kamphuis and Hall (1983) defined the value at the point where "normal pitting of surface…appearance of small pit marks over entire surface of soil" occurred. Smerdon and Beasley (1961) described the critical condition as "general movement of soil." Houwing and van Rijn, (1998) used a camera to document the initiation of erosion and defined it based on "particle movement". Due to the difficulty of the establishing a point of motion, Moody et al. (2005) defined three criteria for erosion initiation depending on the parent material type and the temperature at which the soil was exposed to in the furnace: 1) "movement of the coarser sediment fraction (1 – 2 mm) over the finer fraction (typically 0.125 – 0.500 mm) as opposed to just winnowing of the fine fraction"; 2) "steady erosion or scour of the surface"; or 3) "erosion of several large (1 – 2 mm) soil aggregates in succession from the surface." Visually observed critical shear stress values depend on the definition of soil erosion initiation.

Quantitative methods for determining critical shear stress are recommended to remove the subjectivity of visual initiation definitions. A common graphing technique to estimate τ_c and k_d is based on the excess shear stress equation (Hanson, 1989; Hanson and Cook, 1997; Knapen et al., 2007). By assuming a linear relationship between erosion rate and hydraulic boundary shear stress, a regression line is drawn through the plotted erosion rate and applied shear stress data. The critical shear stress is equal to shear stress at the point where the regression line crosses the x-axis, and k_d is determined from the slope of the line (Figure 2.2). This graphical technique is the most common method in cohesive erosion research (Knapen et al., 2007). Several researchers (Smerdon, 1964; Lyle and Smerdon, 1965; Zhu et al., 2001) estimated τ_c

using a graphing method based on slope change in erosion rate versus applied shear stress curve, by applying two separate linear relationships to low (<1 – 2.5 Pa) and high shear stress (>1 – 2.5 Pa) observations. The critical shear stress equaled the point where an abrupt slope change occurred, which was the intersection of the two linear regressions.

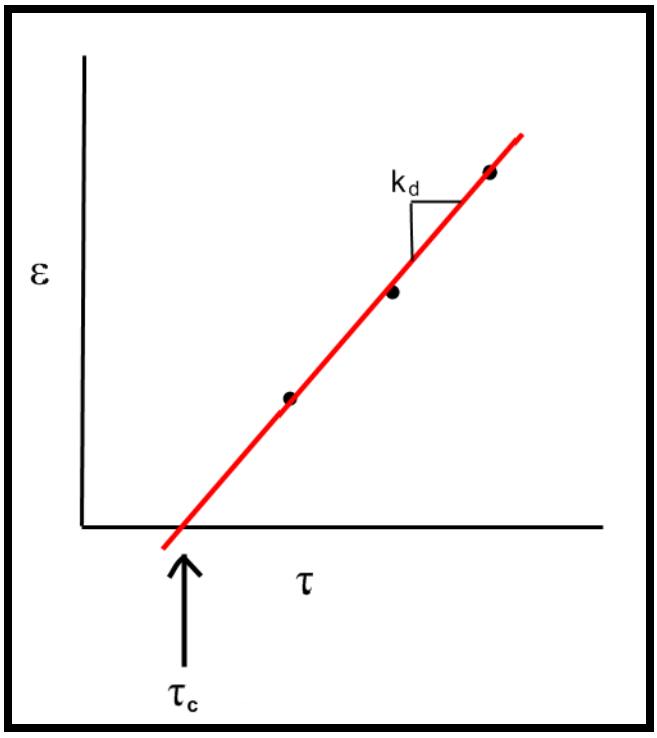

Figure 2.2. Diagram of the excess shears stress equation graphing technique to determine critical shear stress (τ_c) from plotting erosion rate (ε) and hydraulic boundary shear stress (τ), assuming linear relationship.

Another technique to determine τ_c and k_d quantitatively is to fit the data to a hyperbolic asymptote (Blaisdell et al., 1981). The hyperbolic logarithmic method analytically estimates the ultimate or equilibrium scour depth and the corresponding time to reach the depth based on experimental scour data (Blaisdell et al., 1981). The critical shear stress can be estimated from the equilibrium scour depth, and the soil erodibility coefficient can be determined independently of the shear stress based on diffusion principles (Hanson and Cook, 1997). This procedure is further discussed further in section 2.7.3.

2.4.4. Laboratory Erosion Testing Apparatuses

Researchers have used flumes (large, small, straight, and circular), submerged jets, rotating cylinders, annular channels, circular tanks and impellers, pipes, pin-hole testing apparatus, water tunnels, disks, and propellers for erosion tests (Hollick, 1976; Grissinger, 1982; Hanson and Simon, 2001). All of the devices have advantages and disadvantages depending on cost, complexity, simulation accuracy, sample size, and quantitative or qualitative measurements.

Hydraulic flumes have been commonly used for erosion tests for decades, so results from flume tests are generally accepted. Erosion tests with flumes have been conducted on soil samples with many different testing conditions: undisturbed natural and remolded samples; moisture content conditions including saturated, saturated and drained, air-dried, and natural field moisture content; different flume slopes and velocities; and, sample surface area ranging from 0.002 m^2 and 5.5 m^2 (Partheniades, 1965; Moody et al., 2005; Knapen et al., 2007). Partheniades and Paaswell (1968) recommended a large width-to-depth ratio in flume studies to minimize sidewall effects and secondary currents, and Knapen et al. (2007) found k_d measurements were higher in laboratory erosion studies compared to results from field studies, indicating the difference was probably because the field plot tests were usually done with natural soils, while the laboratory tests usually tested remolded soils.

2.5. Hydraulic Flume Erosion Studies

Smerdon (1964) researched the influences of rainfall on critical shear stress in low flow channels by conducting erosion tests on 5.5-m long soil samples in a 21.9-m flume. Tests started with a water depth of 2.29 cm, which was increased in 0.76 cm increments until the soil was rapidly eroding. Erosion rates were estimated by sediment concentrations from water collected by a total-load sediment sampler downstream of test section. From the erosion tests with no

rainfall, critical shear stress ranged from 0.72 Pa to 1.29 Pa for the five different soils from Texas (clay percentage ranging from 13.5% to 55.5%) (Smerdon, 1964).

Heinzen (1976) used a small recirculating flume (2.5 m long x 0.15 m wide x 0.3 m deep) to compare erodibilities of eleven natural undisturbed soils with soil properties. Applied shear stress was measured with a Presten tube located upstream of the sample, and erosion rate was determined by mass of soil lost. A screw underneath the flume allowed the soil to be raised during the 2-minute testing to keep the sample flush with the bed. Heinzen (1976) concluded useful correlations between soil erodibility and clay type and amount, and pore fluid composition

Arulanandan et al. (1980) conducted flume studies with 42 undisturbed soil and stream water samples from around the U.S. to develop relationships to estimate erosion based on soil composition and structure and eroding water composition. Erosion tests in a recirculating flume started at low shear stresses, which were increased during the duration of the test. Soil erosion rates were calculated based on weight loss. The researchers observed erosion rates increased exponentially with decreases in τ_c; soil erodibility and critical shear stress were inversely related. Results indicated increasing sodium adsorption rate of the soil pore water decreases τ_c. Erosion resistance was observed to increase when salt concentrations of eroding water increased (Arulanandan et al., 1980).

Kamphuis and Hall (1983) determined erosion initiation of compacted silty clay soils from a riverbed in Northwest Territories of Canada using a flume tunnel. Soils were compacted at different pressures (48 kPa to 350 kPa), and eroded in unidimesional flow to estimate critical velocity and shear stress. Critical shear stress (0.2 Pa to 18.4 Pa) was calculated based on critical velocity, and was compared to the soil properties. During testing, erosion rates increased as the soil surface and roughness were altered by the flow. Results indicated τ_c was positively related

to consolidation pressure, plasticity index, and clay content (Kamphuis and Hall, 1983). Hanson (1989, 1990a) conducted large-scale open channel flume tests (30.5 m long and 0.91 m wide) on four soils (two sandy loam, loam, and clay loam) under high shear stresses to determine erodibilities. The soil beds were compacted at different slopes (0.5%, 1.5%, and 3.0%) and tested under a range of shear stresses (1 Pa to 36 Pa), starting with low stresses and increasing incrementally during the test. Total stress was calculated from slope of the energy grade line and water depth, and erosion rates were estimated by change in bed elevation. Results indicated a general relationship between erodibility and soil properties (Atterberg limits and grain-size distribution) where the soils with the highest clay content, lowest sand content, and highest plasticity index had the lowest values for k_d.

Moody et al. (2005) used a recirculating flume to determine the effect of wildfire temperatures on critical shear stress of forest soils. Forest soil samples from eight sites in Colorado and New Mexico were placed in porcelain crucibles (0.020 m wide, 0.105 m long, and 0.012 m deep) and subjected to different temperatures before being set in the flume, flush with the bed. Critical shear stress was visually assessed during the tests, where the slope was incrementally increased every five to ten seconds until one of the pre-determined erosion criteria was met. Critical shear stress ranged from 0.45 Pa to greater than 3.2 Pa (maximum shear stress produced by flume in study).

Although the application of hydraulic flumes for erosion research is appealing due to the ability to control the environment and flow, there are many limitations that need to be considered when designing tests and evaluating erosion results, especially for cohesive erosion. Flumes are expensive and fairly complex equipment. Determining the erosion initiation point quantitatively during an erosion test is difficult, and visual observation is usually required in the flume. Soil

roughness and elevation level between a soil sample and a flume bed changes with time during erosion. Although an average shear stress is known, the roughness changes during erosion introduce uncertainties and variations of the actual shear stress (Hollick, 1976). Small sample sizes in erosion flume tests limit the options of erosion rate measurement. Sediment concentrations and weight loss are typically too low to measure accurately, and increase of soil moisture content can affect soil weight. Soil swelling during tests can result in inaccurate volume loss measurements (Hollick, 1976).

2.6. *In Situ* Erosion Tests

The limitations of traditional flume tests restrict the ability to determine soil erosion for undisturbed field sites accurately. *In situ* tests are needed to incorporate natural field conditions and the influence of soil structure and variability on streambank erosion. Kamphuis and Hall (1983) concluded tests need to simulate naturally occurring conditions accurately. The only way to accurately simulate natural soils is to test *in situ* soils; however, to test *in situ* soils in a flume, samples must be removed from the site. Disturbance*s* are introduced when moving large streambed or bank samples into a flume for testing (Hanson and Cook, 2004). Erosion studies have shown numerous elements influence cohesive soil erodibility, and some of the elements, like subaerial processes, are very difficult to replicate in the laboratory. These elements are either modified or lost when removing samples from the site. *In situ* erosion measurements may not be as easy to control as for erosion tests are in the laboratory, but field observations are essential for accurate measurements for natural soils.

Several apparatuses and methods have been used by researchers to determine erosion in the field: submerged jets, *in situ* flumes, cohesive strength meter, benthic annular flumes, and ISIS (*I*nstrument *S*hear *In Situ*) (Houwing and van Rijn, 1998). Each device has its own

limitations for field applications and operation. The multiangle submerged jet test device has recently been used in many studies and has demonstrated strong potential to be useful tool in erosion research.

2.7. Multiangle Submerged Jet Test Device

The multiangle submerged jet test device (JTD) represents a relatively simple, inexpensive *in situ* method of measuring k_d and τ_c (Hanson, 1990a). Since the late 1950's, submerged water jets have been used for studying cohesive erosion in both laboratory and field studies (Dunn, 1959; Moore and Masch, 1962; Hollick, 1976; Hanson, 1990a; Hanson et al., 1990; Hanson, 1991; Hanson and Robinson, 1993; Allen et al., 1997, 1999; Hanson and Simon, 2001; Mazurek et al., 2001; Potter et al., 2002; Wynn and Mostaghimi, 2006; Mallison, 2008; Thoman and Niezgoda, 2008; Wynn et al., 2008).

Dunn (1959) determined τ_c of cohesive soils with a laboratory vertical submerged water jet, and related τ_c to soil properties (Atterberg limits, grain size, and shear strength). During the tests, the water head was increased until erosion initiation, and critical shear stress was visually estimated when the "water became cloudy." Dunn (1959) observed the location of the initial erosion and peak shear stress occurred a short distance from the jet centerline. The location of the initial erosion was not affected by changes in water head or nozzle height above the soil surface.

Moore and Masch (1962) used a laboratory vertical impinging jet to measure scour rates of remolded and undisturbed cohesive soils by weight loss. Different nozzle diameters and nozzle heights above the soil were also investigated. Two scour hole shapes were observed during the tests: 1) deep and narrow, and 2) shallow and wide. Moore and Masch (1962) found the hole shape depended on the jet impingement height (jet height above soil surface divided by

the nozzle diameter). Deep and narrow scour holes formed when the impingement height was less than seven and the potential core reached the soil surface, creating a reversed jet. When the potential core did not reach the surface (impingement height greater than seven), a shallow and wide scour hole formed (Moore and Masch, 1962). When the impingement height remained constant, Hollick (1976) observed other factors affected the scour hole shape. Mazurek et al. (2001) found deep and narrow scour holes had a strongly deflected jet regime, while the shallow and wide holes exhibited a weak deflected jet regime.

Hollick (1976) tried to correlate soil mass eroded by a laboratory submerged jet with visually observed τ_c values from flume tests. The researcher compared several different apparatuses for the study, and decided to use a submerged jet because it was inexpensive, simple, and could test a variety of soil types. The difference between flow from a submerged jet and typical channel flow could cause limitations because: 1) the jet has normal and tangential stress components; 2) jet turbulence is different than turbulence in a channel; 3) eroded particles must be transported horizontally and vertically out of the developed scour hole; 4) the eroded surface is not horizontal, which could be important for oriented or layer soil structures; and, 5) the soil samples must be uniform with depth (Hollick, 1976). Jet tests ran for either 100 min. (33.0 cm and 12.5 cm water heads) or 10 min. (maximum 10 m head) on a minimum of 10 samples (10-cm diameter x 6.3 cm deep) for two artificial (kaolin/sand mixtures) soils to develop calibration curves. Nine samples (35.0 cm x 7.5 cm) for two artificial soils, positioned flush with a sand-roughened bed, were tested in a 3-m long 10.0-cm wide flume. Soil mass eroded during the flume and jet test was determined by dry mass lost during testing. The calibration curves were tested using natural soils. Testing both natural and artificial soils, Hollick (1976) found the jet critical shear stress results varied more for natural soils than for artificial soils, and in the flume,

defining a consistent erosion initiation point visually was difficult, especially for natural soils. Although the correlation between erosion rate results from a jet and critical shear stress results from a flume were not completely successful, Hollick (1976) concluded that a submerged jet had potential for successful soil erosion measurements, and the scour hole shape should be considered in analysis.

2.7.1. Development of the Multiangle Submerged Jet Test Device

At the USDA-Agricultural Research Service Hydraulic Engineering Laboratory in Stillwater, Oklahoma, Hanson (1990b) developed a vertical submerged jet device for testing soil erodibility *in situ*. This field device consisted of a base ring and tank (46 cm soil surface testing diameter), interchangeable pin profiler (31 pins spaced 15 mm apart) and jet (13 mm nozzle diameter), and a constant head tank. To calibrate and verify the jet device, Hanson (1990b) used erodibility data for four soils (two sandy loam, loam, and clay loam) obtained from large-scale open channel tests conducted in previous studies (Hanson, 1989, 1990a). The soil erodibility was calculated based on the Reynolds number of the jet.

To describe soil erosion resistance, Hanson (1991) developed the jet index, a dimensionless soil parameter, based on the change of the maximum scour depth over time caused by an impinging jet. The jet index is a semi-empirical relationship, and was related to k_d (Hanson, 1991). ASTM Standard D5852 (ASTM, 2007b) describes the procedure to determine the soil jet index using Hanson's (1990b) submerged jet device. To remove the empiricism of the jet index, Hanson and Cook (1997) developed an analytical procedure for a circular submerged jet to estimate τ_c and k_d based on diffusion principles.

Allen et al. (1997) simplified Hanson's (1990b) original submerged jet device to be more portable and better adapted for *in situ* testing. The jet nozzle diameter was reduced from 12.7

mm to 6.35 mm to decrease the water volume required for testing and the testing procedure was simplified. Allen et al. (1997) conducted three jet tests at each of three sites with different specific jet velocities for each test (305, 457, and 610 cm/s). Depth measurements were taken in 10-minute intervals, and the jet index was used to compare soil erodibilities. Allen et al. (1997) concluded the jet test device could be effectively used for *in situ* erosion measurements. Further modifications by Allen et al. (1999) improved the jet test device for field testing. A single pin was used to measure the maximum scour depth instead of the pin profiler. The constant head during testing was achieved by overflow ports rather than a pressure-control device. Hanson and Simon (2001) used a similar modified submerged jet test device (6.4-mm nozzle diameter and 30-cm diameter base ring) in the field to determine streambed erodibilities.

2.7.2. Submerged Impinging Circular Jet Theory

The submerged jet test device produces a circular water jet perpendicular to the soil surface, causing the soil to erode as the jet dissipates horizontally along the surface. The initial jet velocity along the centerline, U_o, remains constant for a short distance after exiting the submerged nozzle, diameter, d_o, defining the potential core length, H_p. The potential core length is usually about nine nozzle diameters (Hanson et al., 1990). Beyond the potential core, the jet average velocity decreases by diffusion with the maximum velocity occurring along the centerline. With the nozzle set at an initial height above the soil surface, H_i, the jet impinges and scours the soil surface. The scour continues until a maximum depth is reached, H_e.

Several studies on the flow characteristics of a submerged impinging circular jet on a smooth planar surface have shown four distinct flow zones exist (Poreh and Cermak, 1959; Beltaos and Rajaratnam, 1974; Viegas and Borges, 1986; Hanson et al., 1990). The potential core length of the jet defines Zone 1, known as the "zone of flow establishment." Zone 2, or the

"zone of established flow", occurs after the potential core when the centerline velocity decreases due to jet diffusion before impacting the boundary. Zone 3 is the "deflection zone," where the jet changes from a vertical flow to a horizontal flow as it impacts the planar surface. A stagnation point forms where the jet centerline meets the planar boundary. Zone 4, or the "wall jet zone," occurs after the jet changes to a horizontal flow, moving parallel to the planar surface (Beltaos and Rajaratnam, 1974; Hanson et al., 1990; Hanson and Cook, 1997).

Hanson et al. (1990) examined the pressure and applied shear stress distribution along a smooth boundary in the impingement region (Zone 3 and 4) using a vertical laboratory submerged jet. Differential pressures and shear stresses were measured at different radial distances along the boundary from the jet centerline. The maximum differential pressure occurred at the centerline, and as the water dissipated a short distance away from the center, the pressure quickly decreased to zero (Hanson et al., 1990). The shear stress distribution was not uniform; the shear stress peaked a short distance from the center, similar to what Dunn (1959) observed as the location of erosion initiation. As the water flowed outward from the center, the shear stress increased to its maximum and then decreased. The maximum shear stress was a function of average fluid velocity at the nozzle and fluid density, with constant nozzle diameter and nozzle height above surface (Beltaos and Rajaratnam, 1974; Hanson et al., 1990). The applied shear stress at the stagnation point, theoretically, is zero. However, the experimental results indicated shear stress at the stagnation point was $0.6\tau_{om}$, where τ_{om} is the maximum shear stress (Hanson et al., 1990).

The initial centerline velocity of the jet, before reaching the potential core length, H_p ($H > H_p$), is as follows (Albertson et al., 1950):

$$\frac{U}{U_o} = C_d \frac{d_o}{H} \tag{2.10}$$

where,

U = jet velocity (m/s);

U_o = initial centerline jet velocity at origin (m/s);

C_d = diffusion constant;

d_o = nozzle diameter (m); and

H = distance along the centerline from the origin (m).

The initial jet velocity U_o is calculated from the differential change in pressure (Beltaos and Rajaratnam, 1974):

$$U_o = \sqrt{2gh} \tag{2.11}$$

where,

g = gravity acceleration constant (m/s^2), and

h = differential head (m).

When $U = U_o$ and $H = H_p$, Equation 2.10 can be used to determine the potential core length (Albertson et al., 1950; Hanson and Cook, 1997; Hanson et al., 2002):

$$H_p = C_d d_o \tag{2.12}$$

The diffusion constant, C_d, is commonly accepted as a value of 6.3, though values have ranged from 5.8 to 7.4 (Beltaos and Rajaratnam, 1974).

Several scour characteristics have been observed for an impinging submerged jet. As the scour hole increases with time, the applied shear stress decreases, because the increasing

diffusion throughout the surrounding water decreases the jet energy (Stein et al., 1993; Stein and Nett, 1997). The erosion rate of the scour hole is high at the start of erosion, and asymptotically approaches zero as the applied shear stress decreases and approaches the critical shear stress. Scour depth and logarithm of time are linearly related, except near the beginning of erosion and as erosion approaches equilibrium (Moore and Masch, 1962; Mazurek et al., 2001).

2.7.3. Submerged Impinging Circular Jet τ_c and k_d Analysis

Hanson and Cook (1997) developed an analytical method, similar to Stein et al. (1993), to estimate τ_c and k_d with the submerged jet test device based on diffusion and local scour principles. Stein et al. (1993) developed an analytical procedure for a planar jet at an overfall, which was validated by Stein and Nett (1997) in a laboratory experiment with six different soils. The analytical analysis for submerged jet erosion is based on three assumptions: 1) equilibrium depth is the depth when the applied shear stress no longer causes downward scour; 2) the rate of change in scour depth (*dH/dt*) is the erosion rate, and a function of the boundary maximum shear stress and k_d; and, 3) the maximum shear stress causes the maximum erosion beneath the jet (Hanson and Cook, 1997; Hanson et al., 2002; Hanson and Cook, 2004).

The critical shear stress, τ_c, is estimated from the equilibrium scour depth, H_e. However, the time required to reach the equilibrium depth can be very large (Blaisdell et al., 1981; Mazurek et al., 2001). During a study on erosion from a pipe outlet, Blaisdell et al. (1981) observed erosion of non-cohesive sand never reached equilibrium depth, even after 14 months. Using a vertical laboratory jet, Mazurek et al. (2001) observed the time to reach equilibrium scour depth in manufactured pottery clay usually took 80 to 100 hours, with the maximum measured time of 188.7 hours. Blaisdell et al. (1981) developed a hyperbolic logarithmic function that analytically estimated the equilibrium scour depth and the corresponding time to

reach the depth. This procedure was based on the concept that scour approaches a limit asymptotically. The general form of a rectangular hyperbola equation is (Blaisdell et al., 1981; Hanson and Cook, 1997):

$$x = \left[(f - f_o)^2 - A^2 \right]^{\frac{1}{2}} \tag{2.13}$$

where,

$$f = \log\left(\frac{H}{d_o}\right) - \log\left(\frac{U_o t}{d_o}\right) \tag{2.14}$$

$$f_o = \log\left(\frac{H_e}{d_o}\right) \tag{2.15}$$

$$x = \log\left(\frac{U_o t}{d_o}\right) \tag{2.16}$$

H = distance from jet nozzle along centerline (m);

H_e = distance from jet nozzle to maximum point of scour (equilibrium scour depth) (m);

d_o = jet nozzle diameter (m);

U_o = jet velocity (m/s);

t = time (s); and,

A = semitransverse axis.

A least squares curve-fitting method estimates the equilibrium scour depth by iteratively evaluating the best values for A and f_o, based on a minimum standard error of estimate (Hanson and Cook, 1997).

Erosion beneath a submerged jet is local scour, and scour rate decreases with time as the scour hole diameter increases due to erosion (Hanson, 1991). Based on the shear stress equation (Equation 2.1), the rate of scour *dH/dt* under a submerged circular jet for $H \geq H_p$ (potential core length from jet origin) is (Hanson and Cook, 1997):

$$\frac{dH}{dt} = k_d \left[\frac{\tau_o H_p^2}{H^2} - \tau_c \right], H \geq H_p \tag{2.17}$$

where, τ_o is the maximum applied shear stress in potential core. When equilibrium depth is reached, the previous equation (Equation 2.17) can be re-written to determine τ_c for submerged circular jet, when τ_o is greater than τ_c (Hanson and Cook, 1997):

$$\tau_c = \tau_o \left(\frac{H_p}{H_e} \right)^2 \tag{2.18}$$

Within the potential core ($H \leq H_p$), the maximum applied shear stress is (Hanson and Cook, 1997):

$$\tau_o = C_f \rho U_o^2 \tag{2.19}$$

where C_f is the friction coefficient, and ρ = water density. The recommended value for C_f is 0.00416, based on a study of shear stress distribution on a planar boundary conducted by Hanson et al.(1990).

The erodibility coefficient, k_d, is a function of scour depth, the calculated critical shear stress, τ_c, time, and a dimensionless time function. Integrating a dimensionless form of Equation 2.17 results in an equation for measured time t_m (Hanson and Cook, 1997):

$$t_m = T_r\left[0.5\ln\left(\frac{1+H^*}{1-H^*}\right) - H^* - 0.5\ln\left(\frac{1+H_i^*}{1-H_i^*}\right) + H_i^*\right] \quad (2.20)$$

$$T_r = \frac{H_e}{k_d \tau_c} \quad (2.21)$$

$$H^* = \frac{H}{H_e} \quad (2.22)$$

$$H_i^* = \frac{H_i}{H_e} \quad (2.23)$$

where,

T_r = reference time (s);

H = distance from the nozzle to the centerline scour depth (m);

H_e = equilibrium scour depth (m);

H^* = dimensionless scour term;

H_i^* = dimensionless scour term; and,

H_i = initial distance from the nozzle to soil surface (m).

The erodibility coefficient, k_d, is estimated by curve-fitting measured values of H versus t, and minimizing the error of measured time t_m versus predicted time (Hanson and Cook, 1997).

2.7.4. Laboratory and Field Studies with the Jet Test Device

Hanson and Robinson (1993) investigated how changes in bulk density and moisture content influence the erodibility of compacted soils, by comparing erodibility results from a submerged jet test to results from two large-scale channel tests. Typically, compaction increases soil strength and shrink-swell, and decreases permeability, though soil swell decreases as the moisture content at compaction increases. Twenty-nine soil samples were compacted either by

dynamic or static load procedures at different moisture contents and bulk densities, and wetted prior to jet testing. Erodibility decreased when either bulk density increased (compacted at same moisture content) or moisture content at compaction increased (compacted to same bulk density); except when the moisture content was at saturation, erodibility increased (Hanson and Robinson, 1993). The results from the jet tests suggest bulk density and compaction soil moisture content are major influences on soil erodibility, while the compaction method is not a major factor. These findings were similar to the two large-scale channel tests (compacted at different densities with same compaction moisture content) conducted by Robinson (Hanson, 1990a; Hanson et al., 1990)(1990a, 1990b), where the channel with the higher bulk density had lower erosion (Hanson and Robinson, 1993).

Allen et al. (1999) evaluated the potential of using the jet test device results to extend erosion prediction upstream and downstream of a test site based on local soil properties. Jet tests were conducted on 30 Texas alluvial stream channels with three tests per site, each at a different specific velocity. Soil samples were collected to determine local soil properties for the streams. A regression analysis between the jet index and soil properties (bulk density, soil moisture content, Atterberg limits, and grain size) resulted in the best correlation when the data set was grouped into three categories based on clay percentage and soil activity (plasticity index divided by clay percentage): 1) soils with less than 10% clay (n = 9); 2) soils with greater than 10% clay and soil activities less than 1.25 (n = 10); and, 3) soils with greater than 10% clay and soil activities greater than 1.25 (n = 11) (Allen et al., 1999). Results indicated moisture content and sand percentage were important for determining erodibilities of soils with less than 10% clay, while erodibilities of soils with greater clay percentage and low soil activities were best correlated to bulk density, plastic limit, and percent clay. Soil texture (percent sand, silt, and

clay) and liquid limit described the erodibilities of soils with clay percentage greater than 10% and high soil activities. These relationships between soil properties and erodibilities were used to estimate channel erosion upstream and downstream of the test sites (Allen et al., 1999).

Another field study utilized the jet test device to determine the erodibility of cohesive loess streambeds in the Midwestern United States (southeastern Nebraska, southwestern Iowa, and north central Mississippi) (Hanson and Simon, 2001). The maximum scour depth was recorded in ten-minute intervals during the 120-minute jet test. A wide range of erodibilities was observed for the 83 jet tests: τ_c and k_d values ranged six orders of magnitude (< 0.001 Pa to 400 Pa) and four orders of magnitude (0.001 cm^3/N-s to 3.75 cm^3/N-s), respectively. Erodibility varied within a streambed, between different streambeds, and from region to region. Hanson and Simon (2001) concluded the streambeds may consist of several different soil types exposed, each with a different erosion resistance. An inverse trend between τ_c and k_d was observed, which is similar to results found by Arunlanandan et al. (1980), Wynn and Mostaghimi (2006) and Thoman and Niezgoda (2008).

Unlike the previous studies, Potter et al. (2002) used the jet test device to estimate erodibility of agricultural soils, instead of channel erodibility. Agricultural soils at six locations (sandy loam, loam, silt loam, and 3 clays) in Central Mexico were jet tested, and the difference in erodibilities between soil types and between tilled and no-tilled practices were analyzed. The bulk densities varied from 0.51 Mg/m^3 to 1.41 Mg/m^3 with testing moisture contents ranging from 0.05 to 0.76. Potter et al. (2002) found significant differences between the jet index for four of the six locations, and those four soils had a higher erodibility for tilled soils than no-tilled soils, probably due to breaking of soil aggregates during tilling. Potter et al. (2002) concluded the submerged jet test device is a useful tool to determine agricultural soil erodibility.

Hanson and Cook (2004) compared jet test estimated erosion results to large-scale open channel flume erosion results. The predicted erosion results from the jet test were based on the average of three tests, as well as the maximum and minimum values. Soil (38% sand, 34% silt, 28% clay) with an average water content of 13.9%, was compacted to an average dry weight of 1.85 Mg/m^3 in a large-scale open channel (1.8 m wide by 29 m long by 2.4 m deep) at a 3% slope. Water discharge for the flume erosion test was 0.71 m^3/s and 2.89 m^3/s for 1089 minutes and 415 minutes, respectively, and erosion measurements in the center of the flume were used to estimate average erosion for the bed. The τ_c and k_d values from the jet test were 1.1 Pa and 0.089 $cm^3/N\text{-}s$, respectively, while the resulting k_d value from the flume was 0.096 $cm^3/N\text{-}s$, assuming the same critical shear stress of 1.1 Pa. Although the estimated overall average erosion of 15.7 cm (based on jet test results) was close to the average measured erosion of 14.5 cm from the flume, the predicted and measured values for the two discharges were different. The predicted average erosion was 7.6 cm and 8.1 cm for the respective discharges 0.71 m^3/s and 2.89 m^3/s, while the average measured erosion was 11.1 cm and 3.4 cm. If the soil had eroded uniformly with time throughout both discharges, Hanson and Cook (2004) believed the erosion would have been similar for both discharges, as the jet test results predicted.

In the first *in situ* testing of vegetated streambanks, root density, subaerial processes, and soil type were found to influence the critical shear stress and soil erodibility (Wynn and Mostaghimi, 2006). Wynn and Mostaghimi (2006) conducted 142 individual jet tests at 25 field sites (average six tests per site) in southwestern Virginia, and observed at an individual site, k_d and τ_c ranged as much as one and four orders of magnitude, respectively. For all the jet tests, streambank erodibility varied from 0.2 $cm^3/N\text{-}s$ to 13.1 $cm^3/N\text{-}s$ and critical shear stress ranged from 0 Pa to 21.9 Pa. A regression analysis was done to determine the influence soil properties

and field conditions have on streambank k_d and τ_c, which resulted in several correlations that explain the range of parameter values (Wynn and Mostaghimi, 2006). Results showed soil bulk density was a significant factor for determining both k_d and τ_c, where increases in bulk density result in decreases in k_d and increase in τ_c, similar to Hanson and Robinson (1993). Root densities (diameters of 2 to 20 mm) in streambanks were inversely related to k_d, and freezing and thawing processes had significant influences on k_d and τ_c, depending on soil type. Soil chemistry also affected soil erodibility. Increases in the ratio between soil pH and water pH tended to decrease τ_c and increase k_d, and as soil salt concentrations increased, k_d decreased (Wynn and Mostaghimi, 2006).

Another *in situ* study evaluated the temporal changes in k_d and τ_c from subaerial processes (desiccation and freeze-thaw cycling) in southwestern Virginia (Wynn et al., 2008). The submerged jet test device was used to measure k_d and τ_c monthly at six sites along a streambank for a year. Weather conditions, soil moisture and temperature, and bulk density were recorded during the study. Streambank erodibility varied from 0.01 cm^3/N-s to 8.6 cm^3/N-s and critical shear stress ranged from 0 Pa to 43.3 Pa; during any given month, measurements varied as much as four orders of magnitude for k_d and one order of magnitude for τ_c (Wynn et al., 2008). Results indicated k_d and τ_c varied significantly by month and by season. Soil erodibility in the winter was more than twice the erodibility in either spring or summer, while higher τ_c values were measured in the spring and fall compared to summer and winter. Freeze-thaw cycles that occurred during the 10 days prior to jet testing were strongly related to k_d and not related to τ_c, indicating freeze-thaw processes influence streambank erodibility. Streambank bulk density was inversely related to moisture content and freeze-thaw cycling (Wynn et al., 2008).

Thoman and Niezgoda (2008) correlated cohesive soil properties to critical shear stress of stream channels. Critical shear stress and soil erodibility of 25 streams in northeast Wyoming were measured with a submerged jet test device, with values ranging from 0.11 Pa to 15.35 Pa for τ_c and from 0.27 cm^3/N-s to 2.38 cm^3/N-s for k_d. Soil activity, dispersion ratio, soil pH, organic percentage, and cation exchange capacity were all significantly correlated to τ_c, and further multiple linear regression indicated five significant independent properties (activity, dispersion ratio, specific gravity, soil pH, and moisture content) (Thoman and Niezgoda, 2008). Soil activity, dispersion ratio, and moisture content were positively related to τ_c, while specific gravity and soil pH had an inverse relationship. Thoman and Niezgoda (2008) used this model to predict allowable discharge for cohesive channels, and to extend the results to other similar areas.

Mallison (2008) attempted to compare estimated τ_c and k_d results for 12 cohesive streambanks in Tennessee from submerged jet tests and erosion tests conducted in a circular closed-loop laboratory flume. Critical shear stress values measured with the jet test device ranged from 0.09 Pa to 5.84 Pa, while k_d values ranged from 0.37 cm^3/N-s to 10.07 cm^3/N-s. The flume could only produce a maximum bed shear stress of 1.83 Pa, so limited erosion was observed for many samples, and direct comparison between values from the flume and jet test device could not be determined. However, Mallison (2008) observed the moisture content and soil surface influenced how the sample eroded in the flume. Samples with high moisture content or a rough surface typically exhibited shearing from the soil surface, while samples from the same site with low moisture or a smooth surface did not eroded. Results from the study suggest erosion of cohesive soils is not primarily determined by τ_c and k_d alone, as indicated by the excess shear stress equation (Mallison, 2008).

Chapter 3: Methods

To evaluate the repeatability, a total of 21 jet tests were conducted on two remolded soil types, clay loam and clay. Soil samples were compacted at uniform moisture content to a bulk density of 1.53 g/cm^3/N-s for clay loam and 1.46 g/cm^3/N-s for clay. The compacted soil was set at 45°, and the jet tests were run for 45 minutes with scour depth and pressure readings recorded at 5-minute intervals. Critical shear stress and soil erodibility were calculated with a spreadsheet routine developed by Hanson and Cook (2004).

To determine the similarity of the jet test measurements to traditional flume values, soil critical shear stress and erodibility measurements from a submerged jet test device were statically compared with measurements estimated from a total of 12 traditional flume tests. Remolded soil samples were prepared using the same conditions as for the jet tests, and inserted into the bottom of a recirculating flume, flush with the bed. During the 45-minute flume tests, velocity profiles and water depth were measured. The erosion rate was estimated for different applied shear stresses by calculating soil mass loss during the test. By plotting the flume erosion rate versus the applied shear stress, soil erodibility and critical shear stress were calculated with the excess shear stress equation.

3.1. Soil Preparation

The two local cohesive soils used during the erosion tests were classified using the USDA texture system as clay loam and clay. These soils were selected because they were available locally in large quantities. The clay loam was from the upper 15 cm of a Groseclose silt loam (fine, mixed, semiactive, mesic Typic Hapludults), while the "clay" testing soil was a mixture the A and C horizons of the Groseclose silt loam. Particle size analysis and Atterberg limit tests were conducted to determine the size distribution and plasticity of the two soil types

tested in this study. The particle size analysis was conducted following the ASTM International standards D421-85 (ASTM, 2007a) and D422-63 (ASTM, 2007c), and Atterberg limits were determined using ASTM standard D4318-05 (ASTM, 2005).

The clay loam (29% sand, 40% silt, 31% clay; Plasticity Index = 9) preparation consisted of sieving the soil through a 0.64-cm opening mesh screen to remove any vegetation and gravel, and to break apart large soil masses (Figure 3.1). Small amounts of gravel passed through the screen and remained part of the clay loam. The soil was air-dried to an average gravimetric moisture content of 0.12 (at which the soil was easy to manage) and thoroughly mixed to ensure a homogeneous sample.

The clay testing soil (18% sand, 32% silt, 50% clay; Plasticity Index = 24) was a mixture of 50% clay loam (by weight; sieved as described above) and 50% clay subsoil excavated at a local construction site. After using a hand-operated sausage grinder to break apart the dry excavated clay masses, the clay was sieved through a series 12 sieve with 1.651-mm openings. The small amount of gravel in the soil was removed before grinding or by the sieve. The clay retained in the sieve was crushed with a wooden roller and re-sieved. Before mixing, the sieved clay and clay loam were air-dried to a gravimetric moisture content of 0.09 and 0.08, respectively, because the two soils mixed the best when dry, and these moisture contents were the lowest the soils would air-dry.

Figure 3.1. Clay preparation consisted of mixing (top left), wetting (top right), and sieving (bottom).

Using a cement mixer (BigCat Mixer Type B, Monarch Industries, Winnipeg, Manitoba, Canada), the soil was prepared in 27.22-kg batches (13.61 kg of each soil) for which 4.54 kg each of clay loam and sieved clay were mixed to attain a homogenous mixture (Figure 3.1). This procedure was repeated twice more, adding the additional amounts to the existing mixture and blending until the entire batch was thoroughly mixed. The clay testing mixture (hereafter called "clay") was moistened by sprinkling tap water onto the soil (Blacksburg, VA public water supply) with a watering can, and raking the soil and water. The clay was sieved through 0.64-cm opening screen to break apart large soil aggregates and air-dried to an average gravimetric moisture content of 0.16, a moisture content at which the soil was easy to manage during

compaction. A higher compacting moisture content would have been more difficult to manage, and would have increased the bulk density at compaction.

3.2. Submerged Jet Testing

3.2.1. Device Description

The multiangle submerged jet test device consisted of a steel base ring (30.5-cm diameter), a Plexiglas base ring lid with the jet nozzle, and an adjustable head tank (Figure 3.2) (Hanson and Cook, 2004). The base ring inserted into the soil approximately 7 cm to prevent water piping under the ring, which would cause the tank to drain. The lid latched to the base ring and secured the jet nozzle, which consisted of two concentric Plexiglas tubes centered perpendicularly to the lid. The jet nozzle was a tapered circular orifice (6.35-mm diameter) attached to the bottom of the outer tube. The inner tube stabilized the point gage, which was used to measure scour depth during the jet test. The point gage was inserted through the inner tube from the top and lowered through the nozzle.

A hose connected the adjustable head tank to the jet nozzle, while overflow hoses attached to the base ring and head tank. The adjustable head tank provided the water pressure needed to maintain the jet throughout the duration of the test. The eroding fluid filled the head tank either via a hose connection or pump, and flowed into the outer Plexiglas tube, through the nozzle, and into the JTD base ring. A deflecting plate below the nozzle protected the soil surface from the water jet as the tank filled, submerging the nozzle. The deflecting plate was moved away to begin testing, and the jet perpendicularly impinged the soil and dissipated horizontally along the soil surface, producing an applied shear stress.

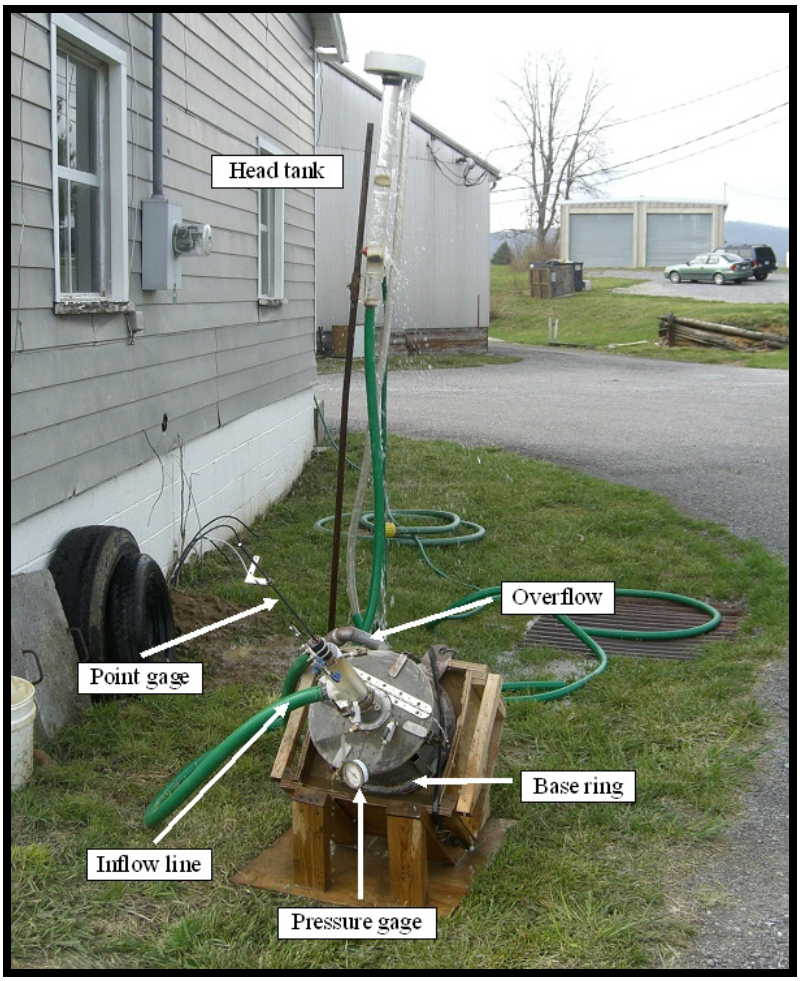

Figure 3.2. The multiangle submerged jet test device during testing of a remolded soil.

3.2.2. Testing Methods

The clay loam and clay were compacted into wooden boxes (39 cm long x 39 cm wide x 25 cm deep) at a bulk density of 1.5 g/cm^3. Each remolded soil consisted of 54.43 kg, compacted evenly in 4.54-kg lifts using a hydraulic press pressurized to at least 6.9 MPa (Dayton model 4Z194A; 0 to 17.2 MPa; 7.62 cm bore; 40.64 cm stroke; Dayton Electric Manufacturing Company, Chicago, Illinois) (Figure 3.3) with a circular head (22.2-cm diameter). Soil for jet tests were weighed using an Ohaus CW-11 balance (±4.5 g; Ohaus Corporation, Pine Brook, New Jersey). To compact the soil box, pressure was applied to a metal compacting board (36.0 cm x 37.5 cm x 0.5 cm thickness), placed on the soil, five times per compaction lift (once in each

box corner and the middle). After compacting 27.2 kg, a soil sample was collected from the remaining soil to be compacted to determine gravimetric moisture content. The collected soil sample was weighed with Mettler Toledo PG5002-S Delta Range balance (readability 0.01 g/ 0.1g, ± 0.02 g/0.05g, maximum 1000 g/5100 g; Mettler Toledo Inc., Columbus, Ohio, USA). To determine the moisture content and dry soil mass in the study, the soil was dried at 105°C for at least of 24 hours. After drying, the sample cooled in a desiccator before weighing again (USDA, 1996). Each compacted soil box was wetted (top to bottom) and drained with the eroding fluid (Blacksburg, VA public water supply) overnight for at least 16 hrs before jet testing. The water was gently applied to the soil surface by pouring it onto plastic lining with small holes. For the clay loam, a series of lined buckets, with small holes punctured in them, was positioned above the soil; these buckets supplied additional water for another 1 to 2 hours (Figure 3.3). Each box was compacted, saturated, and tested within the same time period (over a period of two days) to reduce variability among the tests due to soil consolidation.

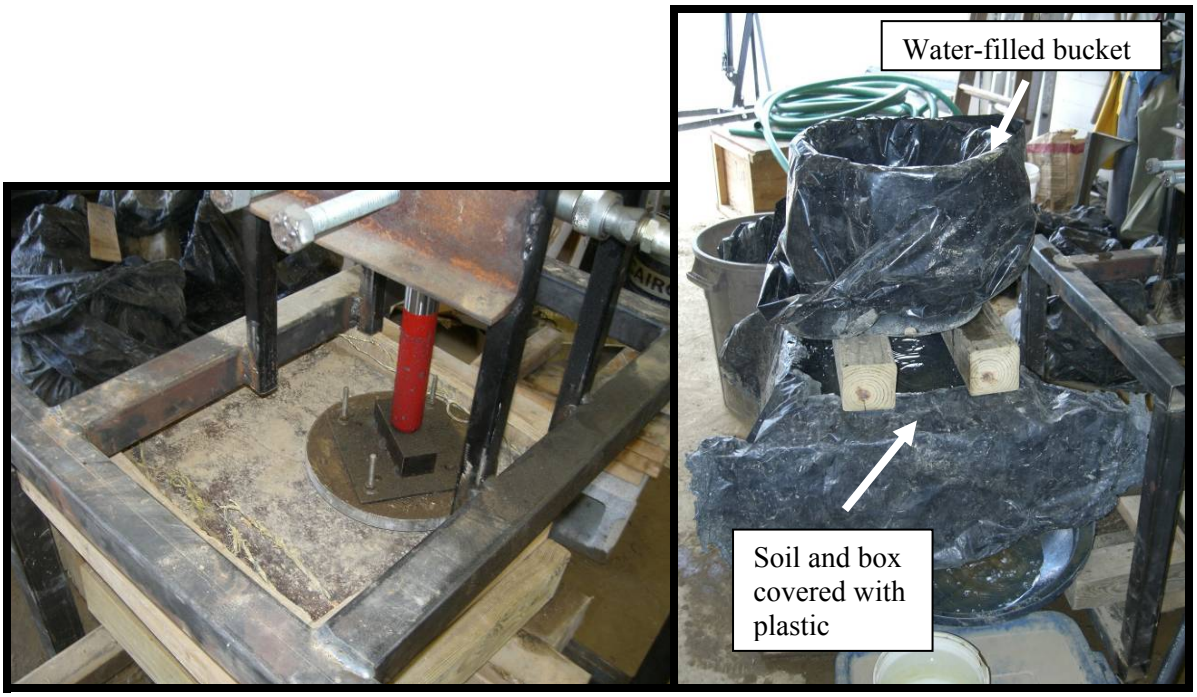

Figure 3.3. Compacting JTD soil (left) and clay loam wetting and draining overnight (right).

The soil-filled boxes were set at a 45° testing angle with a wooden platform. After inserting and securing the JTD base ring with bungee cords, bentonite was molded along the inside ring edge to seal the test area. The distance between the soil surface and jet nozzle and the point gage reading at the nozzle were recorded. With a preliminary head setting of 202 cm for clay loam and 203 cm for clay tests, municipal water filled the head tank via a hose connection and flowed through the nozzle to fill the JTD base ring. When the nozzle was submerged, the deflecting plate was moved and the testing started.

The 21 jet tests ran for 45 minutes with scour depth measurements taken every five minutes (nine scour measurements per test). During each measurement, the point gage was inserted through the nozzle, stopping the jet (and time), and lowered to eroded soil surface. Pressure differentials were measured during the five-minute testing intervals while the jet was running. For clay loam runs, temperature, and conductivity of the water inside the JTD base ring were recorded during the first scour measurement at five minutes and a second conductivity measurement was taken during the last scour measurement at 45 minutes. For clay runs, pre-test and post-test water temperature and conductivity were measured directly out of the hose connecting the head tank to the jet test lid and nozzle, in addition to the two measurements made during the test inside the base ring (at 5 minutes and 45 minutes). The additional measurements directly out of the hose for the clay runs were recorded, because the conductivity and water temperature inside the base ring could change due to the suspended sediment and the increase in temperature when the jet was stopped. Water temperature was measured with a Fisher Scientific Traceable handheld digital thermometer (-50°C to +300°C; +/- 1°C between -20°C and +100°C; SS stem; lollipop type; Fisher Scientific, Pittsburgh, PA, USA) and conductivity was measured with a Horiba compact Twin Cond conductivity meter B-173 (0 µS/cm to 19.9 mS/cm; +/- 2%

full scale +/- 1 digit; Horiba, Ltd., Kyoto, Japan). The conductivity meter was calibrated each day with a 4.41 mS/cm standard, and then rinsed with deionized water before collecting measurements.

At test completion, soil samples were taken with 5.0-cm diameter (90.5 cm^3 inside volume) metal sampling rings to measure bulk density and moisture content. Where possible, two sampling rings were used to obtain measurements at two depths (the soil surface and below the surface) (Figure 3.4). For clay loam runs, one sample was taken inside the JTD ring next to the scour hole, and one from an upper corner outside the JTD ring. For the clay runs, two samples were collected for both inside and outside the base ring, although no accurate bulk density samples were collected at the surface because the surface soil crumbled and fell out of the rings. The moisture content and dry soil mass of the collected samples were determined as described above.

Figure 3.4. Bulk density sample inside base ring after clay jet test.

3.2.3. Data Analysis

Test data were entered into a spreadsheet routine, developed by Hanson and Cook (2004), to estimate τ_c and k_d. Critical shear stress was calculated from the equilibrium scour depth, which was determined by fitting the scour depth versus time data to a logarithmic hyperbolic

function, following procedures of Blaisdell et al. (1981) (Hanson and Cook, 1997, 2004). The soil erodibility coefficient was determined using a least-squares regression based on measured scour depth, time, calculated τ_c, and a dimensionless time function (T*) (Hanson and Cook, 2004) (see Chapter 2.7.3. for more information).

Recently a new method to calculate τ_c and k_d from jet test data was developed by Dr. Robert Thomas (personal communication, 3 November 2009) The Blaisdell solver may not correctly solve the equation when the dimensionless time to reach the equilibrium scour depth is less than 0.2 (the jet test duration is less than 20% of the time estimated to reach equilibrium depth) or very close to 1.0 (Blaisdell et al., 1981; Stein and Nett, 1997; R. Thomas, personal communication, 3 November 2009). Recognizing this shortcoming in the Blaisdell method, Thomas' iterative $\tau_c + k_d$ method constrains the τ_c solution to a minimum value of 0.062 Pa and a maximum value based on nozzle diameter and maximum scour depth (R. Thomas, personal communication, 3 November 2009). The method with the minimum solver error (usually with maximum T^*) should be used estimate τ_c and k_d.

The jet test data consisted of eleven parameters for each soil type, including two τ_c and k_d values based on the two different analysis methods. Compacting gravimetric moisture content (θ_d), the ratio of the water mass to dry soil mass, was measured during compaction. The initial testing θ_d was estimated from the bulk density sample(s) collected outside of the JTD base ring in the upper corner(s) of the soil, under the assumption that the soil in the upper corners did not get wet during testing. The bulk density samples taken at the surface (except for Run 2 and Run 6, which were from the lower bulk density ring) were used to calculate the clay loam testing θ_d. The clay testing θ_d was the average of one, two, or three samples, which were a combination of incomplete bulk density samples from the surface (soil surface crumbled and fell out of rings, but

remaining soil was used to only determine testing θ_d) and complete bulk density samples below the surface. The testing bulk density (ρ_b) was estimated from the bulk density sample(s) collected inside the JTD base ring near the scour hole, assuming the density did not change during the test. The clay loam testing ρ_b was determined from the bulk density surface sample, and the clay testing ρ_b was the average of bulk densities from samples below the soil surface, again since the clay surface would crumble and fall out of the sampling rings. The testing water temperature for the clay loam runs was equal to the measured temperature during the first five or ten minutes of a test, and the water temperature for the clay runs was the average of the pre-test and post-test measurements. The water conductivity for the clay loam runs was the average of the test beginning and end measurements, and four conductivity measurements (pre-test, test beginning, test end, and post-test) were averaged together for the clay runs. The last two parameters were the total scour depth and the first scour depth after five minutes of testing.

Due to the small sample size, the data were analyzed using nonparametric tests ($\alpha = 0.05$) in Minitab® 15 (Minitab, Inc.; version 15.1.30.0). The ten pairs of τ_c and k_d data calculated by the Hanson and Cook (2004) procedure were analyzed to determine the test standard deviation and 95% confidence interval for each of the two soil types. Wilcoxon matched-pairs signed rank tests for related samples were conducted to statistically analyze the jet test data, with a null hypothesis for each test that the median of differences was equal to zero (alternative hypothesis that the median of differences $\neq 0$). The differences between the τ_c and k_d values calculated by the Blaisdell and Thomas methods were tested. The bulk density data were analyzed to confirm that the soil was uniformly compacted and to determine if it changed during the jet test. Four tests were conducted on the clay loam ρ_b data: 1) surface inside the JTD base ring compared to surface outside of the base ring; 2) inside the base ring compared to the outside; 3) the base ring

samples collected in the inside at the surface versus collected in the inside below the surface; and, 4) the surface compared to below the surface for inside and outside the base ring samples. Since there were no ρ_b data for the clay surface due to the difficulty of collecting an accurate sample, only one test was conducted: bulk density inside compared to outside the base ring. When a run had more than one ρ_b, sample for any specific location, the values were averaged.

To determine if the assumption that the testing θ_d did not vary with depth in the remolded soil box, a Wilcoxon matched-pairs signed rank test for related samples was attempted to compare the testing θ_d at the two sampling depths. However, the sample size ($n < 6$) was too small to determine a critical value for the Wilcoxon statistic (two-tailed test with $\alpha = 0.05$) to reject the null hypothesis (Ott and Longnecker, 2001).

The cumulative scour depth curves for the two remolded soil types were evaluated and compared to scour curves observed in field-testing. Additionally, changes in average τ_c and k_d values as a function of the number of jet tests were examined to provide guidance on the minimum number of tests required to confidently determine the erosion parameters. The variance for each erosion parameter was calculated after each additional run.

3.3. Flume Erosion Tests

A recirculating hydraulic flume was used to determine τ_c and k_d by fitting the test data to the excess shear stress equation. Erosion tests (seven for clay loam, five for clay) at different applied shear stresses were run for each soil. The erosion rate was determined gravimetrically by weighing the soil before the test and by collecting and weighing any soil that was not eroded. The applied bed shear stress was calculated from measured velocity profiles. The jet test results were compared to the flume results to evaluate the similarity of the jet test device to a traditional measurement technique.

3.3.1. Device Description

Traditional flume erosion tests were conducted within a hydraulic, recirculating sediment research flume (Engineering Laboratory Design, Inc.; Lake City, Minnesota, USA) (Figure 3.5). The straight, rectangular flume (6-m long; 1-m wide; 0.4-m deep) has a mid-channel test section (1.5-m long) with a removable acrylic bed section 2.5 m downstream of the water entrance.

For this study, the mid-channel bed section was removed, and a 6-m artificial bed was built in the flume out of marine-grade plywood, with a hole (15 cm x 15 cm) for soil placement in the mid-channel test section. The center of the hole was located in the middle of the mid-channel test section, 3.25 m downstream of the water entrance. The bed roughness was created using sand mixed with contact cement.

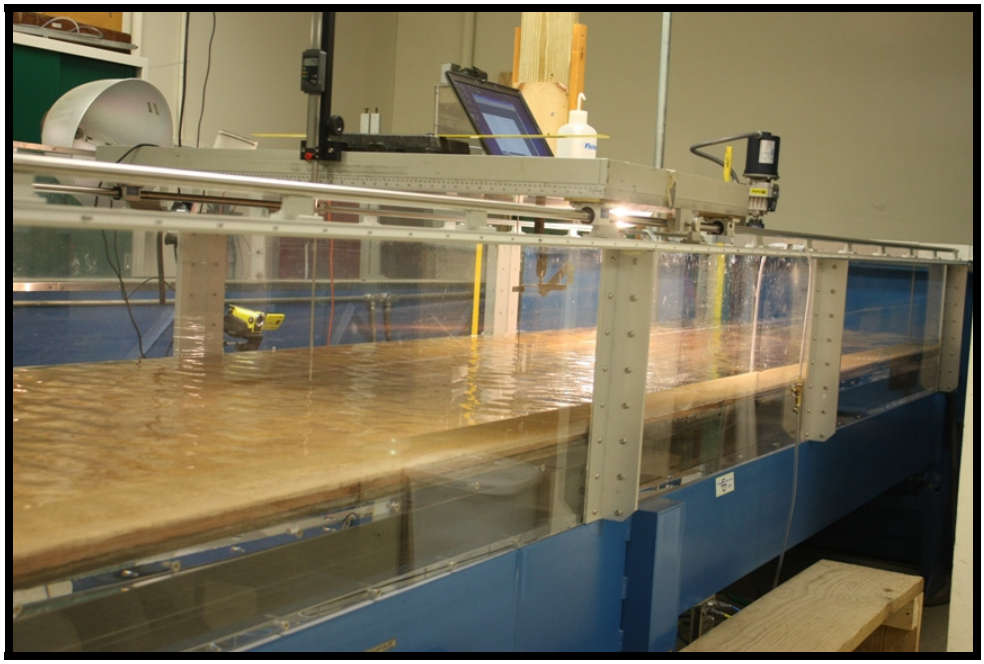

Figure 3.5. Hydraulic flume during testing.

3.3.2. Testing Methods

The clay loam and clay soils were compacted into a metal box (15 cm x 15 cm x 4.8 cm inside dimension) to the same bulk density as the jet test samples. The smaller sample size was needed to minimize sidewall effects, to reduce the sample size to a weight manageable with the

available equipment, and to permit vertical movement of the soil sample within the available space in the flume. The box was constructed from structural steel angle iron (6.35 cm x 3.81 cm x 6.35 mm) welded at the corners, which created a ledge to support a separate steel bottom plate (6.35 mm thickness) to raise the soil during testing (Figure 3.6). The box and bottom plate were painted with X-O Rust anti-rust glossy enamel spray paint (GPM; Cary, Illinois, USA) to prevent rusting of the iron. To reduce the friction from the compacted soil on the box sides, the box was lined with heavy 80-gage plastic film. A thin layer of petroleum jelly between the lining and the box kept the lining in place during compacting and allowed for easy soil removal after the test. The empty box with the lining was weighed before compacting. To reduce the soil pressure on the box sides, 1-mm thick acrylic spacers were placed in the lined box along each of the four sides before compacting to allow the soil to be raised during testing; these strips were removed before testing.

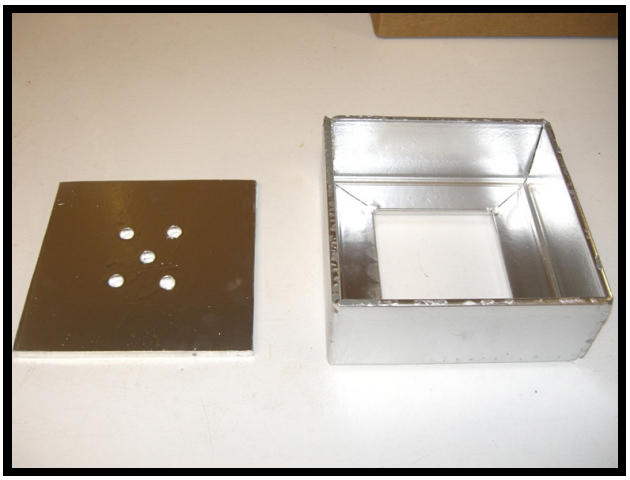

Figure 3.6. Flume soil box with removable bottom plate.

Two equal amounts of soil were weighed into separate plastic containers (847.00 g of clay loam per container; 816.00 g of clay per container). After weighing the soil, a sample was collected from the soil storage bag to determine gravimetric moisture content by the same procedure as for JTD tests (USDA, 1996). Using a square head (6 cm x 6 cm) on the same

hydraulic press used to prepare the JTD boxes, the soil was compacted evenly in two lifts by applying pressure to a wooden compacting board (14.6 cm x 14.6 cm x 6.2) two times per compaction lift (with one or two additional times after compaction of second lift if soil level was too high). During compaction, the hydraulic press was pressurized to a range of 2.1 MPa to 3.8 MPa. Because erosion rate in the flume study was determined based on the mass of soil lost, a soil budget was maintained throughout sample preparation and testing. The containers used to weigh and transport the soil were weighed after compacting to determine the soil amount remaining in them, assuming the soil moisture content had not changed. After slicing holes into the bottom lining through the draining holes in the bottom plate, the box was set over a pre-weighed aluminum pan and the compacted soil was wetted and drained (top to bottom) with the eroding fluid (Blacksburg, VA public water supply) overnight for at least 16 hrs before testing (Figure 3.8). Each box was compacted, saturated, and tested within the same time period (over a period of two days) to reduce variability among the tests due to soil consolidation.

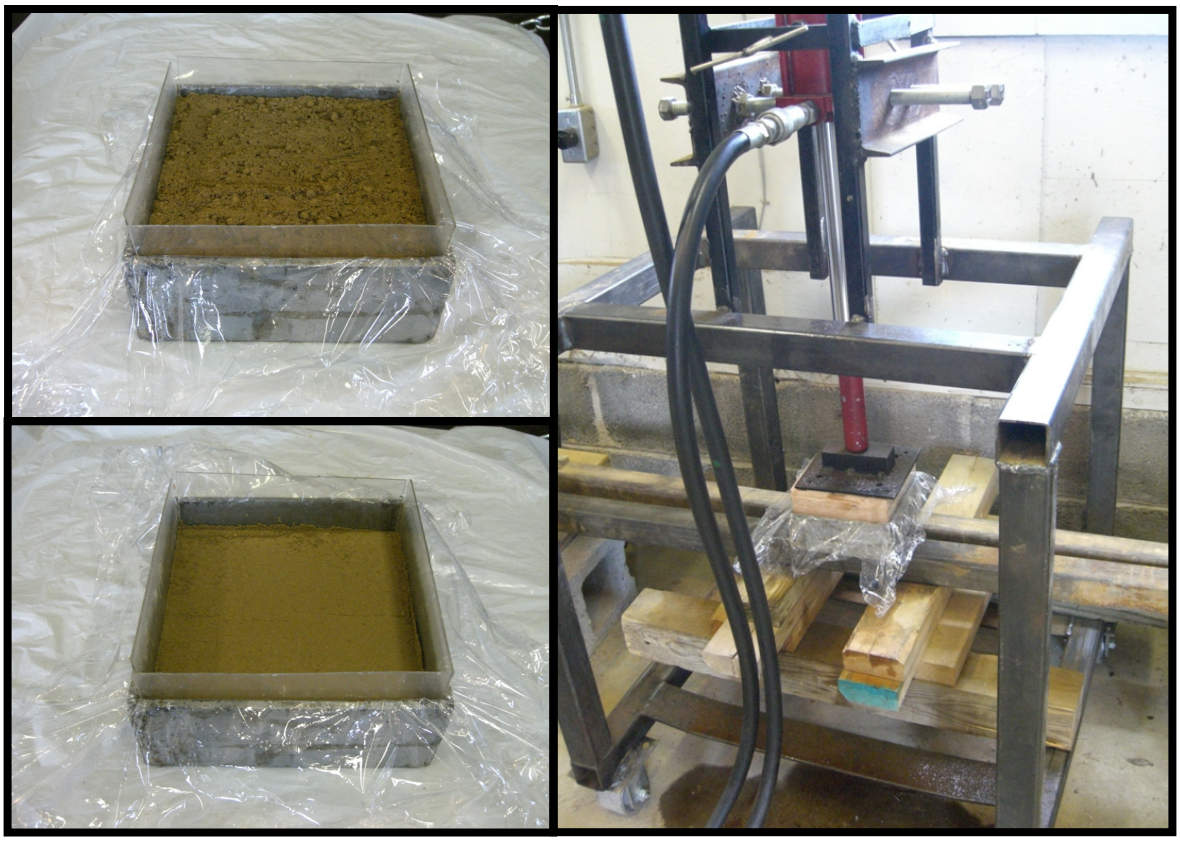

Figure 3.7. Remolded clay loam sample preparation; before (upper left) and after (lower left) compacting first lift with hydraulic press (right).

Figure 3.8. Remolded clay loam before (left) and during (right) wetting.

The acrylic spacers were removed on the test day. To collect any soil removed from the box before testing, the acrylic spacers were rinsed with deionized water into the same pre-weighed aluminum pan that the box drained into (Figure 3.9). For the clay soil samples, the box

sides usually were tapped with a hammer to help in the removal of the acrylic spacers. The dry mass of the soil from the acrylic spacers was determined. The remolded soil-filled box weight (±0.05 g, maximum 6100 g; Mettler Instrument Corp, Highstown, New Jersey, USA) and compacted soil volume were measured to calculate the testing gravimetric moisture content and bulk density. To calculate the compacted soil volume, the distance between the top edge of the box and the soil surface was measured with calipers at nine locations (3-by-3 grid along the upstream and downstream box sides and across the middle).

After taping the lining edges to the outside of the box, the soil box was inserted into the flume testing section and was sealed with GE Silicone II Kitchen and Bath mold and mildew resistant sealant (General Electric Company, Huntersville, North Carolina, USA) to prevent water leakage around the box (Figure 3.10). The soil was covered with plastic film to reduce moisture loss while the silicone cured for at least two hours before testing. A vertical Mitutoyo Digimatic Scale Unit series 572 (0 mm to 200 mm, +/- 0.03 mm, Mitutoyo Corporation, Kawasaki, Japan) was used to measure the distance to the flume bed in four locations along the length of the flume (50.0 cm and 6.5 cm upstream and downstream of the respective upstream and downstream soil edges).

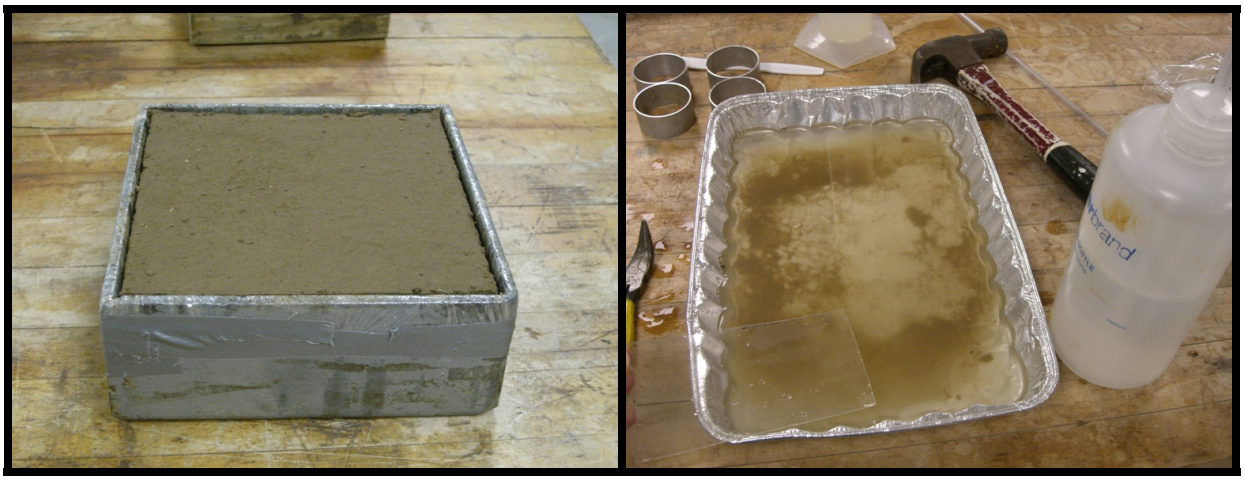

Figure 3.9. Clay loam box after removal of acrylic spacers (left) and after rinsing acrylic spacers (right).

Figure 3.10. Clay loam box sealed in flume bed.

The 45-minute flume tests (seven for clay loam; five for clay) were conducted at different applied bed shear stresses by adjusting the flume settings at 0% flume slope (Table 3.1). The artificial bed had a small bed slope of 0.009% over the length of the flume. A metal pot lid covered the soil when starting the water to protect the soil from the initial water surge. The test started when the flow was fully developed and approximately uniform after starting the flume, and the lid was lifted off the soil. Due to the bed roughness and the shallow depths, the water surface fluctuated, making comparison of the water surface and bed slopes difficult; however, the velocity profiles were logarithmic, providing a good estimate of the boundary shear stress on the soil samples. Water samples, temperature, and conductivity measurements were taken in the flume near the water entrance before, during, and after the test. Water temperature and conductivity were also measured in the water tank before starting the flume. Water samples were collected in 250-ml bottles for suspended sediment concentration (SSC), and temperature and conductivity were measured with the same instruments used during the jet tests. The flume Venturi meter readings were recorded three times: before, during, and after the test.

Table 3.1. Flume settings for each run.

Run Number	Flume Rate (Hz)	Tailgate Height (mm)	Average Discharge (m^3/s)
Clay Loam 1	15	35	0.0135
Clay Loam 2	15	25	0.0143
Clay Loam 3	15	---	0.0141
Clay Loam 4	45	---	0.0482
Clay Loam 5	15	10	0.0162
Clay Loam 6	35	---	0.0369
Clay Loam 7	45	---	0.0463
Clay 1	15	10	0.0178
Clay 2	15	---	0.0180
Clay 3	25	---	0.0301
Clay 4	35	---	0.0415
Clay 5	30	---	0.0360

Three velocity profiles were measured during each test with an Armfield H33 Propeller Velocity Meter with the H33-1 low-speed probe (5 cm/s to 150 cm/s; +/- 2% of true velocity; Armfield Limited, Hampshire, England) attached to the instrument carriage using a manual point gage (Figure 3.11). The propeller was used to measure velocity because it had greater range of depths than either side-looking or down-looking acoustic doppler velocimeters (ADVs). The propeller was aligned in the flow direction by aligning the upstream and downstream tips equal distance from the flume sides, and visually confirming the crossbar on the propeller was perpendicular to the flow. Miniature propeller measurements were compared to a SonTek 16-MHz MicroADV (1% of measured velocity, 0.25 cm/s; resolution 0.01 cm/s; YSI Inc., San Diego, California, USA) three times (before clay loam tests, between soil types, and after all tests) to verify the equipment was working properly. The miniature propeller (1.5 cm width x 2.5 cm length x 1.5 cm depth) center was positioned 6.5 cm upstream of the soil (propeller end 5.2 cm upstream) to prevent eroded material from interfering with the propeller. Each velocity profile consisted of four to eight measurements, with near-bed observations measured at intervals

of either 0.24 cm or 0.49 cm, depending on the water depth, and intervals of 1.0 cm or larger for observations higher in the flow depth. Velocities were recorded at a sampling interval of 50 msec for a 60-sec sampling time. The water surface was measured with the point gage three times during the test at the same four locations along the flume as the bed height measurements. Each erosion test was recorded with a video camcorder, either through the water or above the water surface, depending on the water clarity.

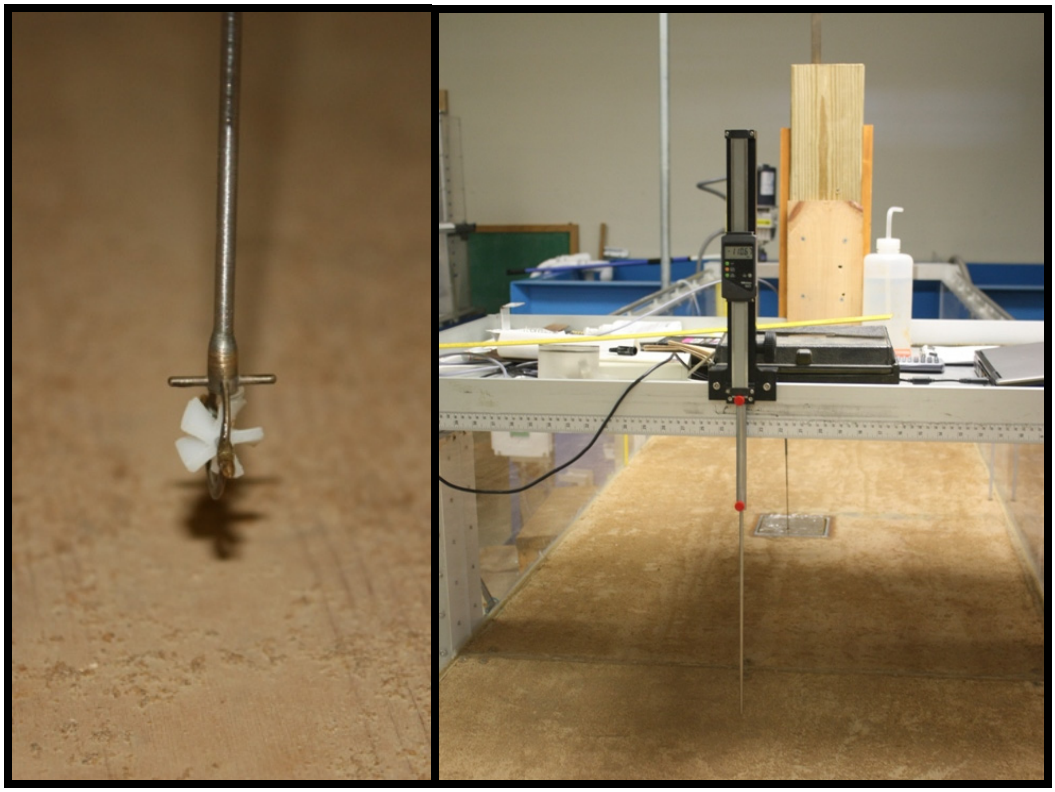

Figure 3.11. Miniature propeller (left) and digital point gage (right) setup.

As soil eroded during the test, a Numatics sleeve type ASNC6-1-1 air bellow (7.62 cm diameter, Numatics Incorporated, Novi, Michigan, USA) positioned underneath the box was used to raise the soil within the box to keep it flush with the bed (Figure 3.12). A Schwinn manual foot air pump (689.5 kPa maximum pressure, Schwinn, Madison, Wisconsin, USA) supplied air to the bellow. An inline check-valve and release-valve allowed for air release at test

end. During testing, the remolded soil was visually raised and kept level with the bed at the upstream edge to maintain consistent shear stress across the sample.

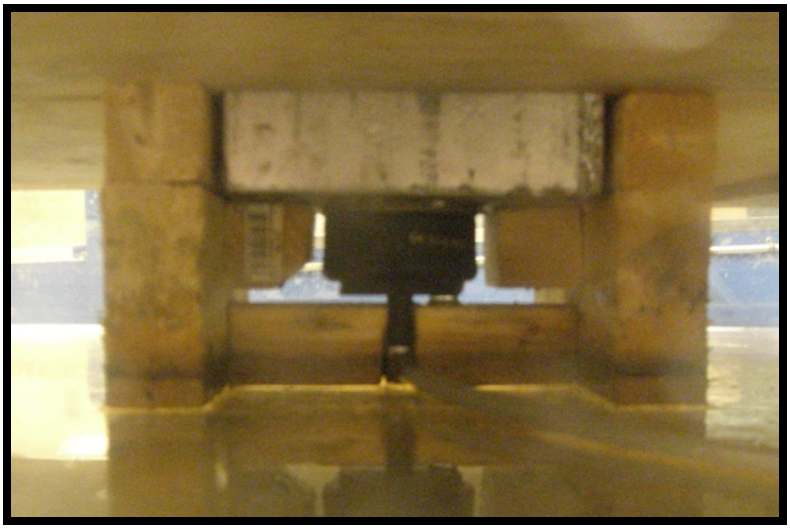

Figure 3.12. Air bellow setup underneath soil box.

After the test, the soil box was removed from the flume. A bulk density sample was collected from the clay loam soils with a 2.5-cm x 5.0-cm (45.2 cm^3 inside volume) metal sampling ring. The soil was not deep enough to sample bulk density in the clay, as the surface soil crumbled and fell out of the rings (similar to the jet test). In addition, the plasticity of the clay made removing the sampling rings from the sampler, without disturbing the sample, difficult. Soil on tools and sampling equipment was rinsed off with deionized water into a pre-weighed aluminum pan. The testing soil was pushed out of the box into the pan, and the lining, box, and bottom plate were rinsed off. The dry soil mass of the sample was determined, as described above.

The suspended sediment concentration (SSC) was determined from the water samples collected before, during, and after testing, to evaluate how the concentration changed over the duration of the test. The SSC was determined, by following ASTM International Standard D3977-97 (ASTM, 2007d) and Clesceri et al. (1998).

A control box for each soil type was prepared to determine approximately the amount of soil lost during the preparation and removal process, and to check the testing moisture content and bulk density calculations. The box underwent the same procedure as if it would be tested, including the time needed to cure the silicone seal without sealing the box in the flume. The calculated testing moisture content and bulk density were compared to the results from the collected bulk density sample. The soil for the control boxes was easier to work with and sample, because the soil was in testing condition (no additional water applied) and not in the wet condition after testing.

3.3.3. Data Analysis

The erosion rate was estimated by the dry mass of soil lost during the flume test. The soil parameters τ_c and k_d were estimated for each soil type with the excess shear stress equation by plotting the erosion rate versus the applied bed shear stress for all of the tests. To determine the statistically similarities to a traditional laboratory flume-based measurements, the jet test results were compared to the results from the flume erosion tests.

Erosion Rate: To estimate erosion rate for each flume test, the total dry mass of soil eroded was calculated from the difference between the dry mass before and after flume testing. All soil loss during sample preparation (e.g. on acrylic spacers) and post-testing measurements was collected, dried, and weighed. However, there was minimal soil loss during box preparation (during compaction, on compacting board, and on hands), pre-test preparation (on lining edge, and sealing box in flume) and soil removal (water leakage, and on lining, tools, bulk density sampler, and hands).

The testing bulk density (ρ_b) and testing gravimetric moisture content (θ_d) were estimated from dry mass, because the compacted soil could not be sampled before testing. The testing ρ_b

for the flume runs was the total dry soil mass after compacting (including the soil loss from the wetting and removal of acrylic spacers) divided by the compacted soil volume. The compacted volume was estimated by the soil width, length, and depth, with the soil depth equal to the difference between the inside box height and the average distance from top of the box to the soil surface calculated from the nine-point grid. The difference between the mass of the compacted box before sealing in the flume and the combined mass of the empty box and total dry soil before testing (not including the soil loss from the wetting and removal of acrylic spacers) was divided by the total dry soil mass before testing to estimate the testing θ_d.

Using the testing bulk density (ρ_b), the erosion rate for each flume test was calculated by:

$$\varepsilon = \frac{\dot{m}}{\text{testing } \rho_b * A} \tag{3.1}$$

where,

ε = erosion rate (m/s);

$\dot{m}$ = mass rate of soil loss (kg/s); and,

A = soil surface area (m^2).

The average rate of soil loss ($\dot{m}$) during a test equaled the total soil loss divided by the test duration in seconds.

Applied Bed Shear Stress: The applied hydraulic shear stress along the bed during flume testing was calculated three ways: 1) the basic law of the wall; 2) the velocity defect law; and 3) average total shear stress. The first two calculation methods were determined from the three velocity profiles measured during each test. Based on the calibration curve from Armfield for the miniature propeller low-speed probe, a positive offset of 3.6 cm/s was added to all

velocity measurements. The velocity profiles were created from averaging the time-series measurements at each depth location within the profile.

The measured average velocities during testing were compared to the average depth-averaged velocity (average of the three depth-averaged velocities from the three discharge measurements). Using this average depth-averaged velocity, the Reynolds and Froude numbers were determined.

The first applied shear stress calculation method was based on the law of the wall (Wilcock, 1996; Sturm, 2010):

$$\frac{\overline{u}}{u_*} = \frac{1}{\kappa} \ln\left(\frac{z}{z_o}\right) \tag{3.2}$$

where,

$$u_* = \sqrt{\frac{\tau}{\rho_w}} \tag{3.3}$$

$\overline{u}$ = time-averaged point velocity (m/s);

u_* = shear velocity (m/s);

κ = von Karman's constant (0.40);

z = height above bed corresponding to velocity measurement location (m);

z_o = bed roughness length corresponding to u = 0 (m);

τ = shear stress (Pa); and,

ρ_w = water density (kg/m^3).

The water density was adjusted for the water temperature during the flume tests. The law of the wall assumes a logarithmic velocity profile, and is applicable within the near-bed region of

uniform flow, usually the lower 20% of water depth (Robert, 2003; Sturm, 2010). The log profile closely resembles the velocity distribution with depth in wide, straight channels with steady, uniform subcritical flows where the bed grains strongly influence roughness (Wilcock, 1996). However, using the law of the wall for the entire flow depth in uniform flow, instead of the lower 20%, tends to underestimate the shear stress (Charlton, 2008).

Using the law of the wall, the approximate applied shear stress was estimated from the measured velocity profile with multiple observations. Rearranging Equation 3.2 resulted in the linear equation form:

$$\ln z = \frac{\kappa}{u_*}\bar{u} + \ln z_o \tag{3.4}$$

In this form, the shear velocity can be determined with z_o unknown. For each profile, the natural logarithmic of z was plotted versus the corresponding average velocity observation measured at that height. A fitted linear regression line and equation were determined for the plot, and the line slope was equal to $\frac{\kappa}{u_*}$. After solving for u_*, assuming κ was 0.40, the applied bed shear stress was calculated by rearranging Equation 3.3 (Wilcock, 1996; Robert, 2003):

$$\tau = {u_*}^2 * \rho_w \tag{3.5}$$

The shear stresses were averaged together for the three velocity profiles during a flume test.

The second applied shear stress calculation method was based on a modified law of the wall, which is the velocity defect law in logarithmic form (Sturm, 2010):

$$\frac{u_{\max} - \bar{u}}{u_*} = -\frac{1}{\kappa}\ln\frac{z}{y_o} + A_1 \tag{3.6}$$

where,

u_{max} = maximum velocity at the water surface (m/s);

y_o = flow depth (m); and,

A_1 = constant.

This form of the law of the wall can be extended into the logarithmic transitional layer of uniform flow, and is valid for rough and smooth walls. By rearranging Equation 3.6 to a linear form, a best-fit line was determined for the velocity measurements plotted as ln (z) versus (u_{max} - $\bar{u}$), where u_{max} was the highest average velocity of the profile (near the surface):

$$\ln z = -\frac{\kappa}{u_*}\left(u_{\max} - \bar{u}\right) + \left(A_1\kappa + \ln y_o\right) \tag{3.7}$$

Only velocity observations in the lower 60% of water depth should be plotted and used to determine the line slope (Sturm, 2010). The shear velocity was estimated from the slope of the linear line $\left(-\frac{\kappa}{u_*}\right)$, and the applied shear stress was calculated by Equation 3.5 for each velocity profile. The three shear stresses were averaged together.

The average bed shear stress (τ_o) for uniform flow was the third calculated applied shear stress (Robert, 2003):

$$\tau_o = \gamma DS \tag{3.8}$$

where,

γ = specific weight of water (kN/m^3);

D = water depth (m); and,

S = water slope (m/m).

The specific weight was adjusted for the water temperature during the flume tests. The average of the two average water depths for the upstream of the box and downstream of the box locations represented the water depth over the soil sample. The slope of the regression line for the four average water depths versus the distance between the measurement locations corresponded to the water slope.

Critical Shear Stress and Soil Erodibility: The critical shear stress and soil erodibility for each soil were determined by the excess shear stress equation (Equation 2.1). Assuming a linear relationship, a Theil-Sen non-parametric regression line was fitted to the erosion rate and applied shear stress observations. The critical shear stress was equal to shear stress at the point where the regression line intersected the x-axis, and k_d was determined from the slope of the line.

Statistical and Error Analysis: Non-parametric statistical tests were selected to analyze the flume data, as they were used to analyze the jet test data. The data for each flume parameter were evaluated with descriptive statistics, box plot, histogram, and 95% confidence intervals using Minitab® 15 (Minitab, Inc.; version 15.1.30.0). To determine if the testing soil conditions were similar for the jet tests and flume tests, a Mann-Whitney test ($\alpha = 0.5$) for independent samples was conducted to compare the testing bulk density, the compacting moisture content, and the testing moisture content.

Assuming the τ_c and k_d estimated from the flume test were accurate for each soil type, the τ_c and k_d from the jet tests were statistically compared to the flume test values, by Mann-Whitney test ($\alpha = 0.5$), to evaluate the similarity of the jet test device measurements. The null hypothesis stated that the median of the jet test τ_c and k_d were equal to the median of the flume τ_c and k_d.

To evaluate the error and sensitivity in the flume test measurements, possible sources of error were identified that could affect the outcome of the calculated critical shear stress and soil erodibility values:

- Soil loss in sample preparation and handling;
- Applied shear stress estimation method;
- Soil bulk density;
- Soil surface area; and
- The assumed linear relationship between erosion rate and applied shear stress.

To determine the impact of soil loss overestimation on critical shear stress and soil erodibility values, due to unaccounted for soil loss error during the preparation and soil removal processes, 5.5 g was subtracted from the amount of soil loss measured during testing. This subtracted amount was measured using the control boxes. This adjusted soil loss was used to determine an adjusted estimated erosion rate for each test, and τ_c and k_d were estimated based on this adjusted rate. The resulting τ_c and k_d were compared to the previous values.

To evaluate the sensitivity and possible range of critical shear stress and soil erodibility values, the erosion parameters were estimated by applied shear stress and erosion rate values calculated by different methods. The three different methods for approximating the applied shear stress (basic law of the wall, velocity defect law, and average bed shear stress) were used in the τ_c and k_d estimation with eight different erosion rates for clay loam and four erosion rates for clay. The erosion rate used to estimate τ_c and k_d was a function of the soil bulk density and surface area. For the clay loam, the erosion rate (from test data and adjusted erosion rate) were calculated based on four combinations of two bulk density values and two soil surface areas. The two bulk density values were the calculated testing bulk density before testing and the post-

test bulk density from the soil sample. The two soil surface areas were the area after removing the acrylic spacers before testing and before soil swelling (14.8 cm x 14.8 cm) and the testing surface area after the soil swelled, filling the spacer gaps (15.0 cm x 15.0 cm). Since a soil sample could not be collected for the clay soil, only the calculated bulk density was used to estimate erosion rate with the two different soil surface areas for each of the two different erosion rate methods (from test data and adjusted erosion rate).

Chapter 4: Results and Discussion

4.1. Multiangle Submerged Jet Test Device Repeatability

The clay loam and clay soils both eroded as aggregates during the jet tests. There was more deposition of eroded aggregates in the bottom of the base ring for the clay than for the clay loam. The clay loam usually eroded uniformly with a circular scour hole, while the clay eroded irregularly over the entire testing area. There was some possible erosion by compaction lifts for both soils. An inverse relationship between compacted bulk density and the erodibility of the soil was observed, when bulk density of a test slightly varied compared to the other tests.

4.1.1. Soil Condition Verification

The compacting gravimetric moisture content (θ_d), testing θ_d, and testing bulk density (ρ_b) were compared to ensure the testing soil conditions were similar among tests for each soil type. A ρ_b outlier was identified: the clay loam Run 11 bulk density (1.46 g/cm^3) was significantly less than the densities of the other previous ten runs (1.51 – 1.56 g/cm^3). The ρ_b for Run 11 was the only soil condition that statistically varied compared to the other runs, which suggests the lower τ_c (0.05 Pa) and higher k_d (3.47 cm^3/N-s) values were due to the lower bulk density and/or other unknown factors. This relationship between bulk density and k_d was similar to the results of Hanson and Robinson (1993), who found k_d increased with lower soil bulk density (for constant compaction moisture). In addition, clay loam Run 11 soil did not drain properly, forcing the remolded soil to be tested four days after compacting, instead of the next day as in all other tests. Instead of draining overnight, the soil appeared to absorb and retain the water, resulting in wet and pliable conditions the next day. For previous tests, the soil was firm to the touch prior to testing. After sitting an additional three days, the soil was firm enough to test, but the soil was not in the same condition as the other tests; it was still slightly pliable and any minor pressure to

surface caused greater depressions than in other tests. The soil appeared to have swelled, reducing the bulk density from the original compaction density. One possible explanation for the draining problems was higher humidity during sample preparation. The test was conducted in mid-August, which usually has higher humidity than the previous summer months. The different soil conditions for clay loam Run 11 resulted in a deep (9.12 cm), narrow scour hole with the lowest τ_c, and highest $k_{d,}$ Since the goal of this study was to evaluate the jet test device without variability in initial soil conditions, clay loam Run 11 was removed from further data analysis.

The histograms, box plots, and 95% confidence intervals for the data showed there was low variance for both soils. The histograms show a distribution similar to a normal distribution, but the sample size was too small to determine the population distribution. Two clay loam parameters (Thomas method τ_c and water temperature) each had one outlier. The first clay loam jet test was conducted in the spring while the remainder of the tests were conducted throughout the summer. The lower temperature did not appear to affect test results. There were no soil condition outliers for any of the clay jet tests. Clay Run 8 had a higher ρ_b (1.53 g/cm^3) than the other nine tests (1.43 – 1.48 g/cm^3), but the bulk density value was not a statistical outlier.

The remolded samples were prepared to minimize variability of moisture content and bulk density between tests. The clay loam was compacted with an average gravimetric soil moisture content of 0.12 (σ = 0.01; SE of mean = 0.00, median = 0.12) to a bulk density of 1.53 g/cm^3 (σ = 0.01 g/cm^3; SE of mean = 0.00; median = 1.53 g/cm^3), and jet tested with an average soil moisture content of 0.23 (σ = 0.01; SE of mean = 0.00; median = 0.23) (Figure 4.1). The remolded clay was compacted and tested with a higher average gravimetric soil moisture content than the clay loam at 0.16 (σ = 0.01; SE of mean = 0.00; median = 0.16) and 0.26 (σ = 0.01; SE of mean = 0.00; median = 0.26), respectively, and compacted to a bulk density of 1.46 g/cm^3 (σ

= 0.03 g/cm^3; SE of mean = 0.01; median = 1.45 g/cm^3). Compacting moisture contents varied by 13.9% for clay loam, and 7.1% for clay, while the testing moisture contents for clay loam and clay varied by 9.3% and 5.0%, respectively. The bulk density varied by 1.8% for clay loam and 4.7% for clay. The small range and standard deviation verified similar testing conditions for the runs of both soil types.

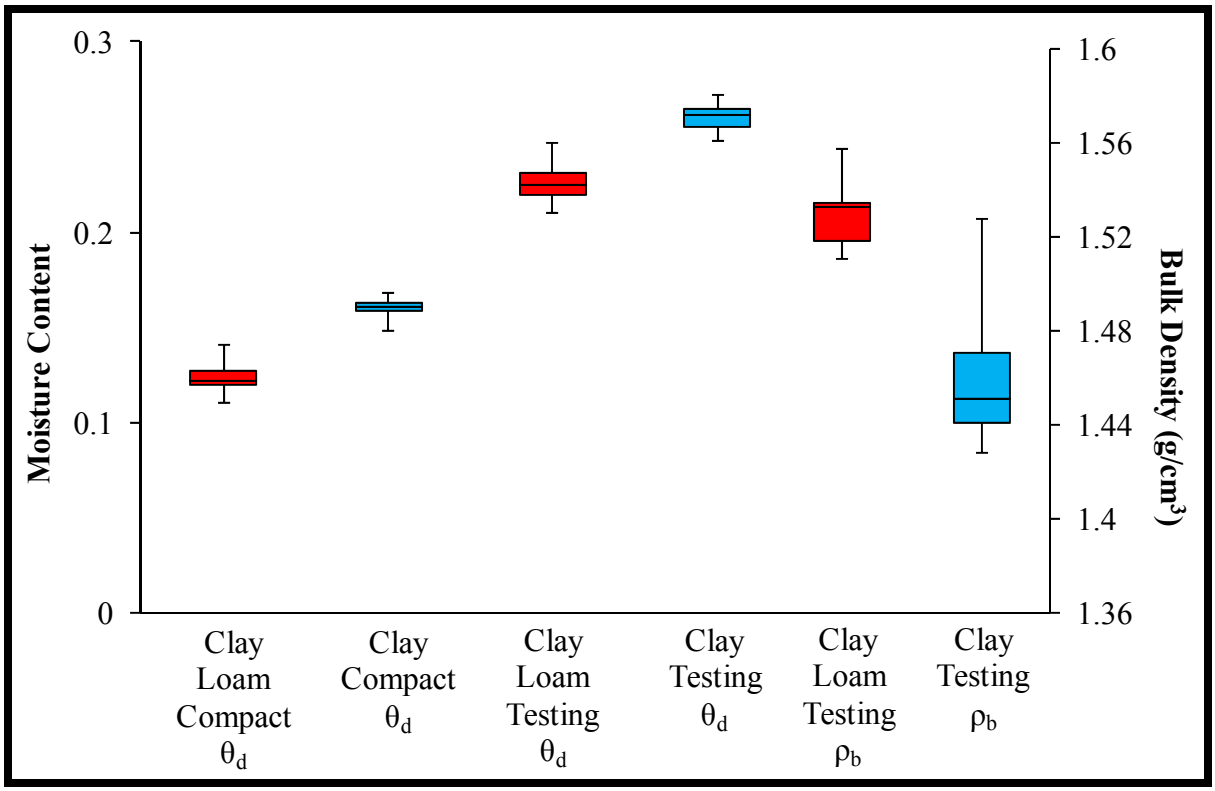

Figure 4.1. Box plots for clay loam and clay compacting moisture content, testing moisture content, and bulk density.

Using the Wilcoxon matched-pairs signed rank tests for related pairs, differences in test sample bulk density with depth or between inside and the outside of the jet tank were evaluated. For the clay loam, test results indicated no statistically significant differences in ρ_b of the compacted samples ($\alpha = 0.05$): 1) surface ρ_b inside and outside of the jet tank ($p = 0.142$; $n = 6$); 2) ρ_b inside and outside of the jet tank ($p = 0.076$; $n = 9$); 3) inside ρ_b at surface and below the surface ($p = 0.059$; $n = 5$); and, 4) ρ_b at surface and below the surface ($p = 0.176$; $n = 7$).

Overall, the clay loam soil bulk density inside the JTD base ring was slightly higher than outside of the ring. While the inside surface ρ_b was slightly lower than the inside below the surface ρ_b, the surface ρ_b was usually higher than the below the surface ρ_b (except clay loam Run 6 and 7), regardless of sampling location inside or outside the base ring.

For the clay, Wilcoxon test ($p = 0.019$; $n = 10$) results indicated a significant difference in ρ_b of the compacted samples ($\alpha = 0.05$). All of the runs, except clay Run 6 (inside and outside ρ_b equal) and Run 8 (inside ρ_b higher than outside ρ_b), had lower ρ_b inside the base ring than outside, suggesting the soil density changed during the test (i.e. swelling effects), assuming uniform compaction or there was non-uniform compaction. Observations of the clay soil before and after testing support the option that the bulk densities changed during testing due to effects such as soil swelling.

There were not enough clay loam runs ($n = 3$) with outside the base ring surface and below the surface testing θ_d measurements to determine if moisture content statistically varied with depth. The testing θ_d values outside the ring surface and below the surface were similar for clay loam Runs 1, 3, and 10, so no obvious differences were observed. A comparison of clay testing moisture content with depth could not be done, due to sampling problems with the clay. The testing θ_d values outside the ring surface and below the surface were similar for the five clay runs (Runs 2, 7, 8, 9, 10), so no obvious differences of moisture content were observed with soil depth.

The remolded samples for each soil type were prepared to ensure there was minimal variability due to soil structure, moisture content, bulk density, and subaerial processes, which are factors shown to impact cohesive soil erosion. Hanson and Robinson (1993) found bulk density and moisture content at the time of compaction had major influences on the erodibility of

cohesive soils. During that study, soil erodibility decreased when either bulk density (constant compaction moisture) or compaction moisture (constant bulk density) increased. The soil samples for this study were prepared with similar compacting moisture contents and bulk densities, and tested at consistent moisture contents to minimize these influences on erosion. However, experience during the study suggested τ_c and k_d were very sensitive to bulk density and moisture content.

Water temperature gradually increased over the time frame from spring through summer, in which the jet tests were conducted. Temperature varied by 25.7% for clay loam tests and 46.4% for clay. The large variation for clay tests was due to a test conducted earlier in the spring than the other tests. Conductivity is related to temperature, so it also increased gradually throughout the testing period. Conductivity varied by 9.6% for clay loam tests and 11.3% for clay. Eroding fluid chemistry influences cohesive soil erosion (Harder et al., 1976; Arulanandan et al., 1980; Kamphuis and Hall, 1983; Lawler et al., 1997; Wynn and Mostaghimi, 2006). The wide range of measured values for k_d and τ_c in natural stream tests confirms the importance of other factors in cohesive soil erosion, including soil moisture content, bulk density and structure, vegetation, and, subaerial processes (Allen et al., 1999; Hanson and Simon, 2001; Wynn and Mostaghimi, 2006; Wynn et al., 2008). However, temperature and conductivity did not appear to affect erosion results.

4.1.2. Jet Test Results for Remolded Clay Loam

The k_d and τ_c values calculated by the Blaisdell method (Blaisdell et al., 1981; Hanson and Cook, 2004) from ten jet tests (Run 11 was removed from analysis as discussed above) for the clay loam ranged from 1.68 to 2.81 cm^3/N-s (μ = 2.30 cm^3/N-s; σ = 0.35 cm^3/N-s; SE of mean = 0.11; median = 2.31 cm^3/N-s) and 0.28 to 0.78 Pa (μ = 0.48 Pa; σ = 0.16 Pa; SE of mean

= 0.05; median = 0.45 Pa), respectively (Table 4.1). Alternatively, the Thomas method resulted in k_d values ranging from 5.06 to 8.82 cm^3/N-s (μ = 6.73 cm^3/N-s; σ = 1.23 cm^3/N-s; SE of mean = 0.39; median = 6.57 cm^3/N-s) and τ_c values ranging from 6.55 to 10.13 Pa (μ = 7.88 Pa; σ = 0.94 Pa; SE of mean = 0.30; median = 7.73 Pa). The Blaisdell τ_c and k_d had a 95% confidence interval for the mean of 0.37Pa to 0.59 Pa, and 2.05 cm^3/N-s to 2.55 cm^3/N-s, respectively. Alternatively, the Thomas method had a 95% confidence interval for the τ_c mean of 7.21 Pa to 8.56 Pa, and for the k_d mean of 5.85 cm^3/N-s to 7.62 cm^3/N-s.

Table 4.1. Jet test conditions and results for remolded clay loam samples with the multiangle submerged jet test device.

Jet Test Clay Loam Run	Compact θ_d[a]	Initial Test θ_d	ρ_b[b] (g/cm^3)	*Blaisdell* τ_c (Pa)	*Blaisdell* k_d (cm^3/N-s)	*Thomas* τ_c (Pa)	*Thomas* k_d (cm^3/N-s)	Water Temp (°C)	Water Conductivity[c] (µS/cm)
1	0.11	0.22	1.52	0.57	1.68	10.13	5.06	15.2	143
2	0.13	0.21	1.51	0.40	2.13	7.62	6.00	19.4	154
3	0.11	0.23	1.54	0.78	2.31	8.36	7.67	20.0	160
4	0.12	0.25	1.54	0.55	2.42	7.26	7.70	20.5	160
5	0.12	0.22	1.52	0.48	1.99	8.01	5.73	21.3	154
6	0.13	0.23	1.53	0.33	2.69	7.32	8.82	21.0	156
7	0.12	0.23	1.52	0.42	2.59	7.81	7.72	21.3	153
8	0.13	0.22	1.56	0.35	2.31	7.66	6.00	21.6	172
9	0.12	0.22	1.53	0.28	2.81	6.55	7.14	21.2	157
10	0.14	0.23	1.54	0.63	2.03	8.13	5.50	23.2	171
11[d]	0.13	0.24	1.46	0.05	3.47	4.61	6.45	24.0	205
Mean[e]	*0.12*	*0.23*	*1.53*	*0.48*	*2.30*	*7.88*	*6.73*	*20.5*	*158*
Median[f]	*0.12*	*0.23*	*1.53*	*0.45*	*2.31*	*7.73*	*6.57*	*21.1*	*156*
SD[g]	*0.01*	*0.01*	*0.01*	*0.16*	*0.35*	*0.94*	*1.23*	*2.1*	*8*

[a] Gravimetric soil moisture content; [b] Bulk density; [c] Average of test start and end measurements; [d] Run 11 was an outlier for initial soil conditions and was removed from further analysis; [e] Mean for Runs 1 to 10 (excludes Run 11); [f] Median for Runs 1 to 10 (excludes Run 11); [g] Standard deviation for Runs 1 to 10 (excludes Run 11)

The remolded clay loam test samples eroded in a consistent manner. Most samples had a few cracks on the soil surface, usually around the edges, before testing. The scour holes were usually circular with average depth of 6.29 cm, similar to a bowl, although some tests had oval-

shaped holes, and some tests had possible erosion by compaction lifts (observed by smooth, flat surface) (Figure 4.2). See Appendix A for before and after pictures of all the jet tests.

Figure 4.2. Clay loam Run 8 before (left) and after (right) testing.

4.1.3. Jet Test Results for Remolded Clay

The k_d and τ_c values calculated by the Blaisdell method (Blaisdell et al., 1981; Hanson and Cook, 2004) from the ten clay jet tests ranged from 1.36 to 2.69 cm^3/N-s (μ = 2.11 cm^3/N-s; σ = 0.41 cm^3/N-s; SE of mean = 0.13; median = 2.18 cm^3/N-s) and 0.30 to 2.72 Pa (μ = 1.25 Pa; σ = 0.74 Pa; SE of mean = 0.23; median =1.10 Pa), respectively (Table 4.2). Alternatively, the Thomas method calculated k_d values ranged from 4.35 to 9.41 cm^3/N-s (μ = 6.89 cm^3/N-s; σ = 1.75 cm^3/N-s; SE of mean = 0.55; median = 6.99 cm^3/N-s) and τ_c values ranged from 7.32 to 12.82 Pa (μ = 9.58 Pa; σ = 1.56 Pa; SE of mean = 0.49; median = 9.75 Pa). The Blaisdell τ_c and k_d had a 95% confidence interval for the mean of 0.72Pa to 1.78 Pa, and 1.78 cm^3/N-s to 2.46 cm^3/N-s, respectively. Alternatively, the Thomas method had a 95% confidence interval for the τ_c mean of 8.46 Pa to 10.69 Pa, and for the k_d mean of 5.63 cm^3/N-s to 8.14 cm^3/N-s.Most remolded clay samples had tiny cracks on the soil before inserting the base ring; however, during insertion, large cracks formed in the soil along the inside and outside edges of the ring. The base ring was harder to hammer into the compacted clay soil than it was for the clay loam. Erosion

during the clay jet tests was more irregular than the clay loam tests. Most of the scour holes were wide with an average scour hole depth of 6.11 cm, similar to a dinner plate, with erosion over the entire area inside the base ring, including under the bentonite (Figure 4.3). Visual evidence of erosion by compaction lifts (flat, even, and smooth areas) was observed in most of the tests, but usually not in the hole. See Appendix A for before and after pictures of all the jet tests.

Table 4.2. Jet test conditions and results for remolded clay samples with the multiangle submerged jet test device.

				Blaisdell		*Thomas*			
Jet Test Clay Run	**Compact θ_d[a]**	**Initial Test θ_d[b]**	**ρ_b[c] (g/cm^3)**	**τ_c (Pa)**	**k_d (cm^3/N-s)**	**τ_c (Pa)**	**k_d (cm^3/N-s)**	**Water Temp[d] (°C)**	**Water Conductivity[e] (µS/cm)**
1	0.16	0.26	1.43	0.57	2.69	7.66	8.22	9.1	154
2	0.17	0.25	1.48	1.13	1.78	10.39	5.96	13.1	170
3	0.16	0.26	1.45	1.19	1.86	10.20	6.80	13.6	164
4	0.16	0.27	1.46	0.30	2.23	7.32	5.12	16.8	153
5	0.17	0.27	1.47	0.88	1.79	8.50	4.35	16.9	164
6	0.16	0.27	1.46	1.06	2.13	9.68	7.18	17.9	150
7	0.16	0.26	1.45	1.32	2.29	9.81	8.47	18.7	163
8	0.16	0.26	1.53	2.72	1.36	12.82	4.90	21.2	171
9	0.15	0.26	1.44	1.05	2.43	9.30	8.45	21.2	183
10	0.15	0.27	1.44	2.30	2.53	10.07	9.41	21.5	171
Mean	*0.16*	*0.26*	*1.46*	*1.25*	*2.11*	*9.58*	*6.89*	*17.0*	*164*
Median	*0.16*	*0.26*	*1.45*	*1.10*	*2.18*	*9.75*	*6.99*	*17.4*	*164*
SD[f]	*0.01*	*0.01*	*0.03*	*0.74*	*0.41*	*1.56*	*1.75*	*4.1*	*10*

[a] Gravimetric soil moisture content at compaction; [b] Gravimetric soil moisture content at testing, average of two or three measurements (except Runs 3 and 5 with only one measurement); [c] Bulk density, average of two measurements (except Runs 4 and 6 with only one measurement); [d]Average of pre-test and post-test; [e]Average of four measurements (pre-test, post-test, start, and end); [f]Standard deviation

Figure 4.3. Clay Run 3 before (left) and after (right) testing.

4.1.4. Critical Shear Stress and Soil Erodibility Relationship

There was no significant relationship between τ_c and k_d for either soil (Figure 4.4). Although the observed inverse relationship was similar to the results of Arulanandan et al. (1980), Hanson and Cook (1997), Hanson and Simon (2001) and Wynn (2004), the insignificance of the relationship supported conclusions by Knapen et al. (2007) that τ_c and k_d were not related.

Hanson and Simon (2001) observed an inverse power relationship ($R^2 = 0.64$) between τ_c and k_d data from 83 submerged jet tests on highly erodible loess streambeds in the Midwestern United States. The typically silt-bedded streams (50 to 80% silt-sized material) had τ_c values ranging from 0.00 to 400 Pa and k_d values between 0.001 to 3.75 cm^3/N-s. Wynn (2004) also observed an inverse relationship ($R^2 = 0.263$; $p = 0.0000$) from 142 jet tests on vegetated streambanks. The lack of statistically significant relationships between τ_c and k_d values for the remolded soils in this study supports the conclusion that natural soil structure plays a major role in cohesive soil erosion.

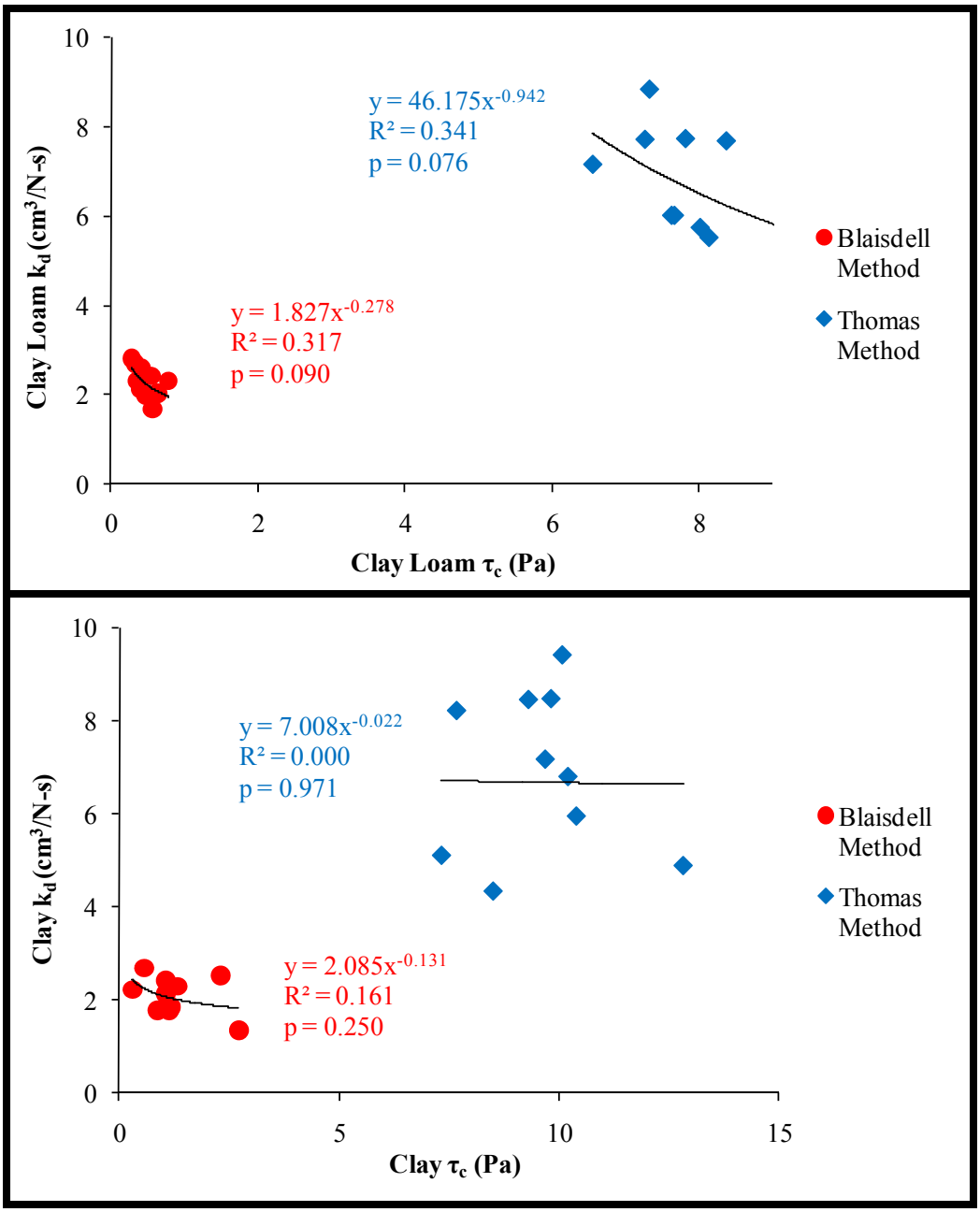

Figure 4.4. Clay loam (top) and clay (bottom) τ_c versus k_d relationship for the Blaisdell and Thomas methods.

4.1.5. Traditional Blaisdell and Thomas Method Comparison

The results of the Wilcoxon matched-pairs signed rank test indicate there were significant differences for the clay loam and the clay between the two calculation methods for k_d ($p = 0.006$) and τ_c ($p = 0.006$). The traditional Blaisdell method was chosen as the best calculation method for τ_c and k_d for this study, because the Thomas method results were questionable, and the

Blaisdell τ_c and k_d values were generally closer to the flume results than the Thomas τ_c and k_d (except for the Thomas clay average k_d), suggesting the Thomas method was not appropriate for these tests.

During jet test data analysis, several issues with the Thomas method were identified. The Thomas method was designed to be applicable for jet tests with dimensionless time (T*) to reach the equilibrium depth (H_e) either less than 0.2 or very close to 1.0 (Blaisdell et al., 1981; Stein and Nett, 1997; R. Thomas, personal communication, 3 November 2009). The Blaisdell method estimates the equilibrium scour depth with a hyperbolic asymptote, and then calculates a critical shear stress based on the equilibrium depth and time to reach that depth. Soil erodibility is iteratively calculated to minimize error from the critical shear stress and dimensionless time function (Hanson and Cook, 1997). Unlike the traditional Blaisdell method, the Thomas method does not use the hyperbolic asymptote to estimate τ_c. The Thomas method constrains the critical shear stress value to a minimum value of 0.062 and a maximum value, which depends on test conditions, and then iteratively calculates both τ_c and k_d to minimize the error. The predicted time to reach equilibrium scour depth (reference time, T_r) and equilibrium depth are calculated based on τ_c.

Theoretically, the calculation method with the minimum least squares error (usually with maximum T^*) should be used estimate τ_c and k_d. A comparison of the solver sum of squares error (Table 4.3) for each method shows the Thomas method has smaller errors than the Blaisdell method. However, there were inconsistencies in the results from the Thomas method, even though the jet tests were in the region that the method should be applicable. For most of the jet tests, the estimated T_r to reach equilibrium depth were less than the actual test duration of 2700 sec resulting in dimensionless time greater than 1.0 and indicating the equilibrium scour depth

was reached during the test, even though the actual scour depth was still increasing. However, many of the jet tests did not actually reach H_e during the test. Due to these issues, the Blaisdell solution method was utilized. Additional research is needed to determine the best methods for analyzing the scour data from the jet tests, and further evaluation of Thomas' iterative method for jet test τ_c and k_d estimation is needed to address the concerns.

Table 4.3. Solver errors and parameters for the Blaisdell and Thomas methods.

	Blaisdell Method				Thomas Method				Test H^d
Run	Σ Err²	T_r[a] (s)	H_e[b] (m)	T^*[c]	Σ Err²	T_r (s)	H_e (m)	T^*	(m)
Clay Loam 1	1.24	664988	0.634	0.005	0.11	2927	0.150	1.014	0.145
Clay Loam 2	0.83	900696	0.756	0.004	0.08	3762	0.172	0.822	0.162
Clay Loam 3	1.57	292387	0.528	0.012	0.18	2521	0.162	1.178	0.158
Clay Loam 4	1.14	474436	0.629	0.008	0.13	3094	0.173	0.996	0.167
Clay Loam 5	0.93	698827	0.667	0.005	0.10	3561	0.163	0.865	0.155
Clay Loam 6	1.19	935052	0.825	0.004	0.06	2700	0.174	1.096	0.169
Clay Loam 7	1.23	691457	0.751	0.005	0.10	2887	0.174	1.013	0.168
Clay Loam 8	0.98	1006878	0.813	0.003	0.13	3776	0.173	0.788	0.163
Clay Loam 9	0.94	1121621	0.892	0.003	0.15	3961	0.185	0.753	0.174
Clay Loam 10	1.06	476490	0.608	0.007	0.27	3780	0.169	0.815	0.160
Clay 1	1.43	410057	0.625	0.008	0.14	2699	0.170	1.081	0.165
Clay 2	1.55	231638	0.466	0.015	0.16	2487	0.154	1.199	0.150
Clay 3	1.72	201711	0.444	0.017	0.12	2179	0.151	1.360	0.149
Clay 4	0.86	1335375	0.881	0.002	0.21	4726	0.177	0.634	0.163
Clay 5	1.12	328119	0.514	0.011	0.40	4465	0.165	0.699	0.153
Clay 6	1.78	210235	0.474	0.016	0.17	2253	0.157	1.291	0.154
Clay 7	2.17	140409	0.426	0.023	0.23	1883	0.157	1.527	0.155
Clay 8	2.09	80661	0.297	0.045	0.37	2179	0.137	1.398	0.135
Clay 9	2.02	186262	0.476	0.017	0.23	2036	0.160	1.408	0.157
Clay 10	2.56	55708	0.324	0.057	0.33	1636	0.155	1.741	0.154

[a]Reference time; [b]Equilbrium scour depth; [c]Dimensionless time; [d]Test scour depth at 2700 sec

4.1.6. Jet Test Repeatability Discussion

The variance for Blaisdell τ_c values significantly differed between the clay loam and the clay (n = 10; p = 0.00), based on a two-sided f-test for variances (α = 0.05). However, there was

no significant difference in the variance for Blaisdell k_d for the two soils (n = 10; 0.648). The jet test device repeatability may vary with soil type.

The vast difference in k_d and τ_c variability between field and controlled laboratory jet test data can be observed in Figure 4.5. Wynn et al. (2008) jet tested streambanks along Stroubles Creek, near Blacksburg, Virginia, USA, and the resulting k_d measurements (calculated from Blaisdell method) ranged from 0.01 to 8.59 cm^3/N-s (n = 72; μ = 0.71 cm^3/N-s; σ = 1.14 cm^3/N-s; median = 0.37 cm^3/N-s), and τ_c ranged from 0.00 to 43.32 Pa (n = 71; μ = 10.55 Pa; σ = 11.14 Pa; median = 7.08 Pa). Jet tests along the East Fork of the Little River, near Pilot, Virginia measured k_d values between 1.17 and 8.36 cm^3/N-s (n = 19; μ = 3.96 cm^3/N-s; σ = 2.09 cm^3/N-s; median = 3.94 cm^3/N-s) and τ_c values between 0.01 and 12.23 Pa (n = 19; μ = 1.57 Pa; σ = 2.71 Pa; median = 0.34 Pa) (Wynn and Mostaghimi, 2006). The standard deviation of critical shear stress for the remolded samples was low, but τ_c from field data had a range of four orders of magnitude (Wynn and Mostaghimi, 2006).

The modest variation of the two soil parameters, compared to the large range of values observed in the field at a single site, indicates the multiangle submerged jet test is repeatable with similar soil conditions. These results also indicate there are other significant factors influencing cohesive soil erodibility and critical shear stress in the field. The large variability of τ_c values measured in the field, compared with results from this study, suggests that variability in streambank surface soils due to subaerial processes and/or soil structure play a significant role in determining the minimum shear stress required to initiate sediment movement for cohesive soils. All the remolded samples used in this study had the same surface condition, a smooth, flat soil surface with no vegetation, or surface weathering. These results indicate that the jet test device

could be a useful tool for evaluating cohesive erosion and the natural factors that influence the erodibility of soils.

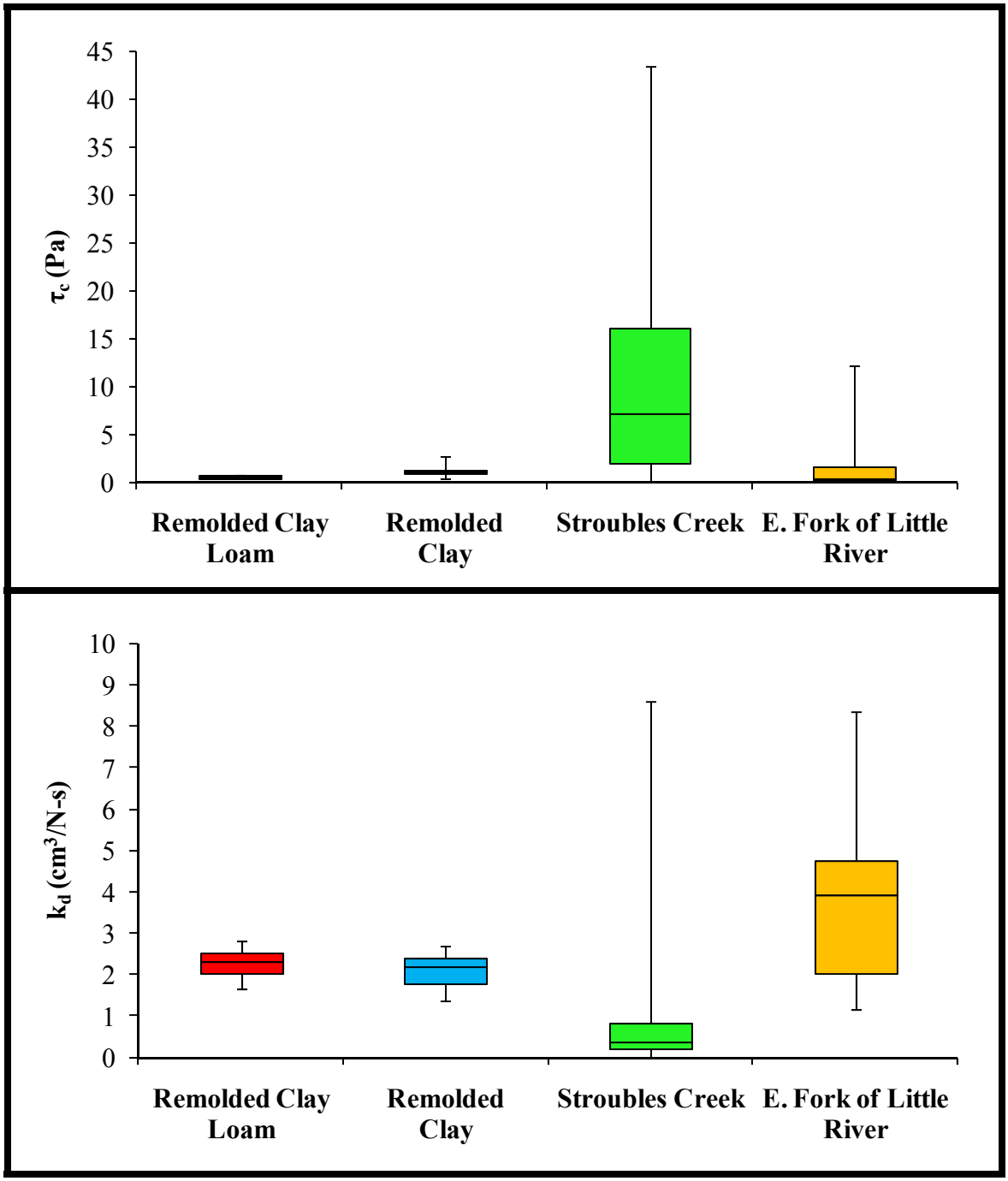

Figure 4.5. Box plots of critical shear stress (τ_c) (top) and soil erodibility (k_d) (bottom) measurements with the multiangle submerged jet test device for remolded clay loam and clay soils, Stroubles Creek streambanks near Blacksburg, VA (Wynn et al., 2008) and East Fork of the Little River streambanks near Pilot, VA (Wynn and Mostaghimi, 2006).

The grainy clay soil consisted mostly of aggregates, which remained as aggregates throughout the compaction, wetting, and testing. The aggregate sizes varied slightly, with the largest close to 0.64 cm, which was size of the sieving screen openings. After compaction, individual aggregates were visible, compacted next to other aggregates. After wetting and draining the clay, the individual aggregates were not as noticeable, but the soil did erode by the aggregates during the test. These eroded aggregates settled at the bottom of the JTD base ring instead of suspending in the water. The amount of eroded material deposited in the base ring was more than the clay loam, and the eroded aggregates were almost level with the scour hole for clay Runs 4 and 5. This deposition of material may have influenced the jet diffusion hydraulics due to the deposition's close proximity to the hole and affect the erosion.

The cumulative scour depth for clay loam ranged from 5.6 to 7.3 cm (maximum depth for clay loam Run 11 = 9.12 cm), and from 4.3 to 7.1 cm for clay. All tests for each soil type, except for clay loam Run 11, eroded in similar manner, as seen by the similar shapes of the scour curves in Figure 4.6. The initial high erosion rate decreased after the first 5 min. and then slowly decreased throughout the test. The scour curves of the clay soil usually leveled out more than the clay loam soil during the 45-min. jet tests. The erosion during the first 5 min. of the tests usually influenced the scour depth throughout the remaining duration of the test. There was a greater range in initial scour depth for the clay than the clay loam, which explains the greater variance in critical shear stress values. Since the erosion during the start of the test influenced the remaining scour depth, the scour curves were collapsed to a single initial scour depth, as seen in Figure 4.7. Even with remolded soil, differences were observed in the erosion rates between tests. The clay loam soil eroded very similarly after the first measurement point, except Run 11, which was removed from analysis due to lower bulk density. However, the erosion rates for the clay soil

were different for the tests, although some runs did collapse together with the same erosion pattern. These slight differences in the erosion rate were most likely due to erosion by aggregates, and differences in testing soil conditions.

The high erosion rate at the start of the test is typically attributed to weakening of the soil surface due to soil wet/dry or freeze/thaw cycling. However, prior to the jet tests, the samples were protected from surface weathering, so this initial high erosion rate was likely a characteristic of the jet test, and not the result of subaerial processes. The initial high erosion rate was instead likely the result of decreases in the applied shear stress as the scour hole deepened and the distance to the soil surface increased.

Additionally, the scour rates for both soils remained uniform throughout each test, as compared to the more variable rates observed during field studies (Wynn and Mostaghimi, 2006; Wynn et al., 2008) (Figure 4.8). Cumulative scour depth curves from jet tests on natural cohesive streambanks tend to be a series of steps, where the scour rates level off, and then quickly increase. Aggregate erosion, vegetation, animal burrows, soil conditions and composition, and other factors influencing cohesive erosion contribute to the fluctuations of scour rates during jet tests. As stated earlier, the clay loam and clay soils were sieved and thoroughly mixed, thus minimizing the presence of large aggregates, gravel, or roots.

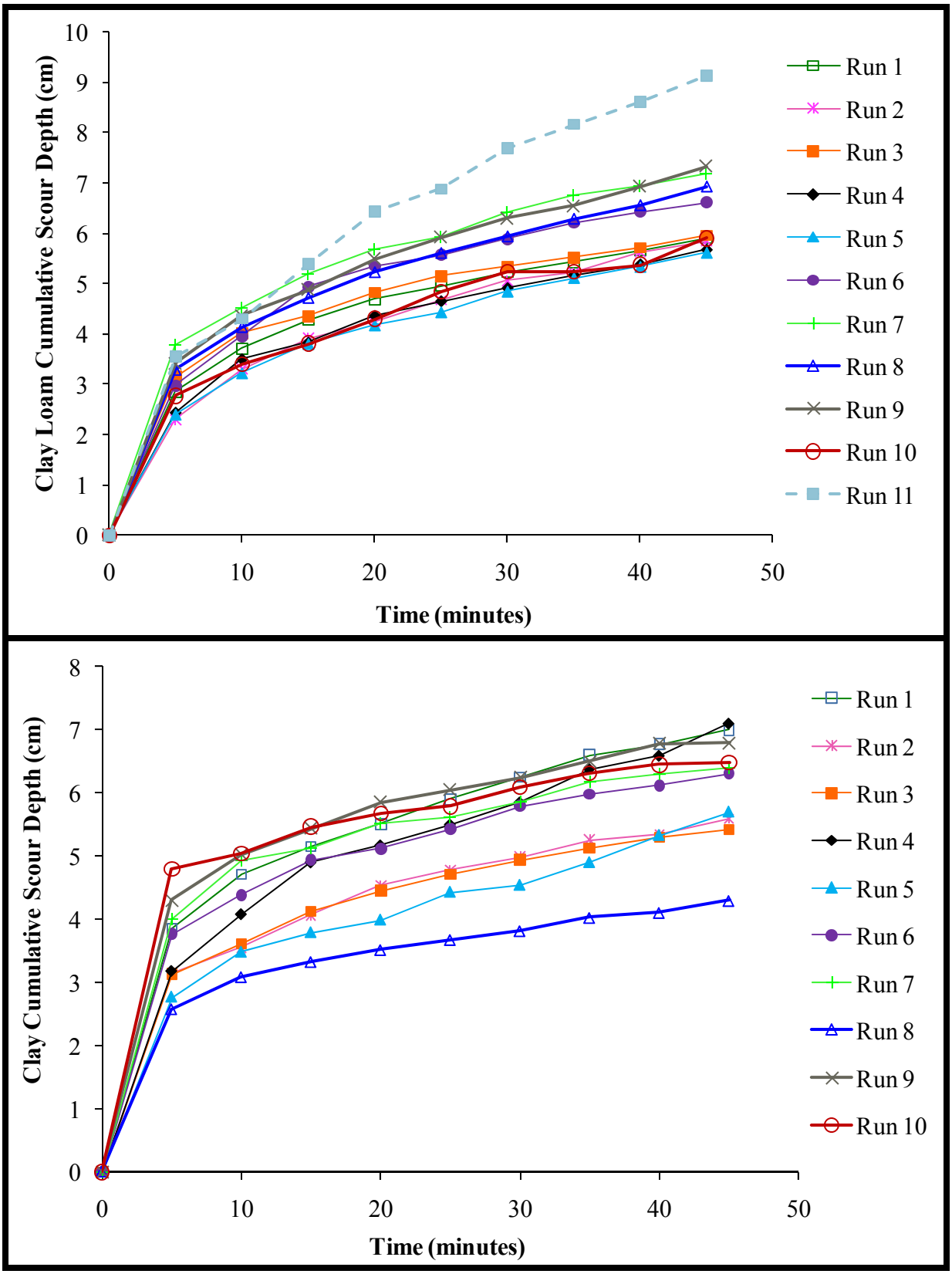

Figure 4.6. Cumulative scour depth clay loam (top) and clay (bottom) samples using the jet test device.

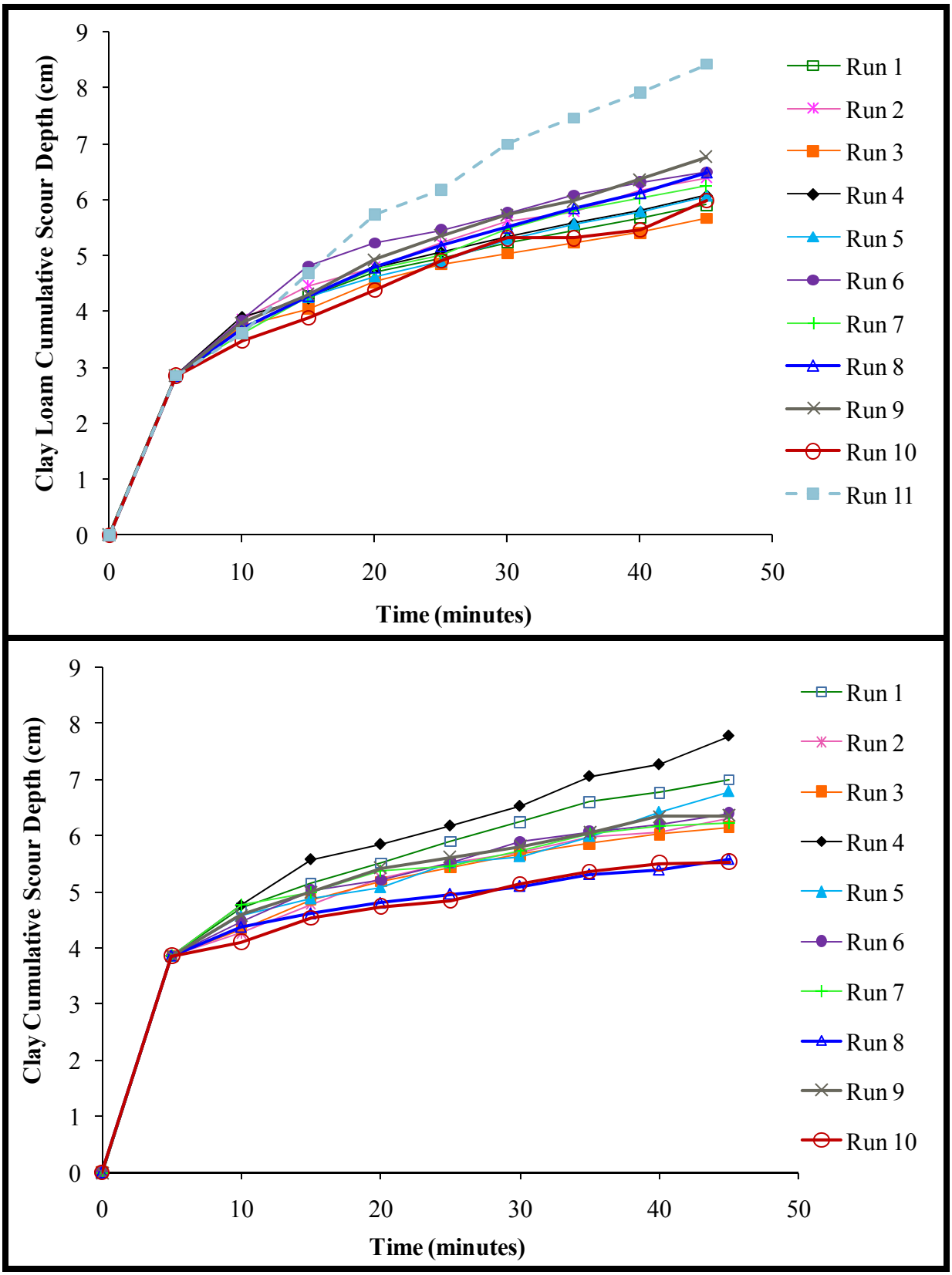

Figure 4.7. Cumulative scour depth clay loam (top) and clay (bottom) runs collapsed to same initial scour point (Run 1).

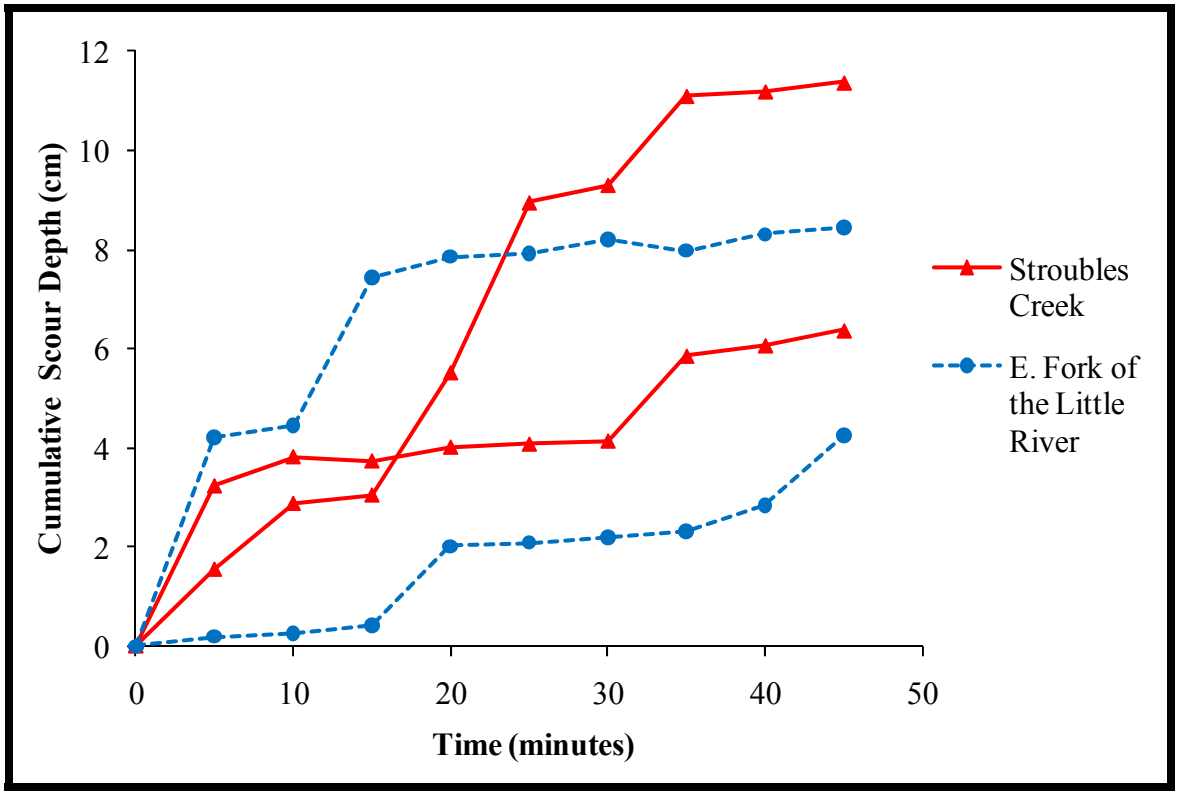

Figure 4.8. Cumulative scour depth for jet tests on streambanks of Stroubles Creek, near Blacksburg, VA (Wynn et al., 2008) and East Fork of the Little River, near Pilot, VA (Wynn and Mostaghimi, 2006).

Typically in the field, three jet tests are conducted to obtain average values of the erosion parameters (Hanson and Cook, 2004). Results from the laboratory tests suggest three tests may not be sufficient for estimating an average k_d and τ_c. The variance in erodibility coefficient leveled out with nine tests for both clay loam and clay soils, although the variance did increase after clay Run 8 (Figure 4.9). Critical shear stress variance leveled off following five tests for the clay loam; for the clay, it started to level out with seven tests and then peaked with run eight. The critical shear stress measured for clay Run 8 was the highest out of the ten jet tests, and k_d was the lowest measured value. If clay Run 8 was removed from the data set, the Blaisdell critical shear stress mean changed from 1.25 Pa to 1.09 Pa (σ = 0.56 Pa; median = 1.06 Pa) with a 95% confidence interval for the mean of 0.66 Pa to 1.52 Pa. The soil erodibility coefficient

changed from 2.11 cm^3/N-s to 2.19 cm^3/N-s (σ = 0.33 cm^3/N-s; median = 2.23 cm^3/N-s) with a 95% confidence interval for the mean of 1.94 cm^3/N-s to 2.45 cm^3/N-s. As stated earlier, compared with the rest of the nine clay tests, the compaction and testing moisture content of Run 8 were similar, but the bulk density of the soil tested was 0.05 g/cm^3 greater than the highest bulk density tested in the previous tests. This slight difference in bulk density impacted how the clay eroded, as seen in Figure 4.6, where Run 8 had the lowest scour depth. This sensitivity to small changes in initial conditions seen in the erosion of carefully prepared remolded soils implies that the differences in soil conditions of the same streambank could have an even larger influence on erosion parameter measurements in the field.

The calculated sample size for a sample to have a statistically significant mean varied for critical shear stress and soil erodibility. Assuming a standard deviation of 0.74 Pa for critical shear stress, a sample size of at least 36 (α = 0.05; β = 0.2) is needed to significantly determine τ_c mean at a measurement difference of 0.5 Pa, or a sample size of 10 (α = 0.05; β = 0.2) to determine τ_c mean at a measurement difference of 1.0 Pa. A sample size of at least12 and 4 (α = 0.05; β = 0.2) is needed to significantly determine k_d mean at a measurement difference of 0.5 cm^3/N-s and 1.0 cm^3/N-s, respectively, assuming a standard deviation of 0.41. These sample sizes are greater than current sample size of three jet tests, suggesting three tests may not be sufficient for estimating an average k_d and τ_c, especially since a larger variation in measurements is found in the field than in remolded soil.

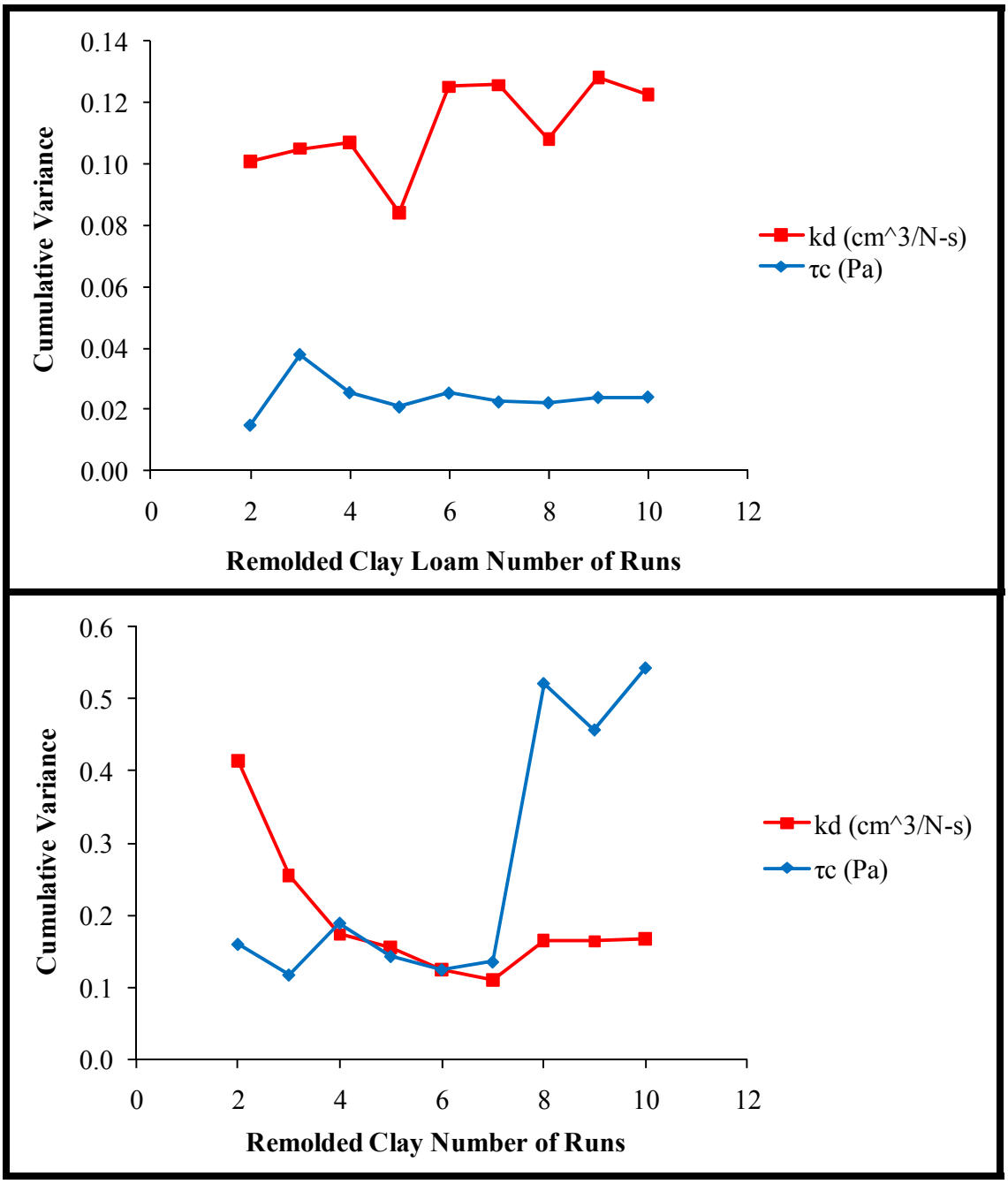

Figure 4.9. Variance change in critical shear stress (τ_c) and soil erodibility (k_d) with additional runs for clay loam (top) and clay (bottom).

Possible sources of error inherent to the jet test include differences in jet diffusion with difference in scour hole shape, soil swelling, and effects of pounding the base ring into the soil. Even with controlled compacted soil samples, the scour hole shape and size varied between tests

of the same soil type. The shape of the scour hole was not incorporated into the k_d and τ_c calculations; however, Hollick (1976) stated the scour hole shape will affect water dissipation in the hole and should be considered in jet test analysis. The effects of the scour hole shape on the jet hydraulics and test results should be further investigated. Swelling soils would cause the point gage to underestimate the scour depth measurements for jet testing, which would raise the τ_c and lower the k_d values. In this study, the clay loam did not appear to swell much during the jet tests, though the clay soil may have swelled during testing. The clay bulk densities inside and outside the jet test base ring were significantly different, with the inside bulk densities (average $\rho_b = 1.46$ g/cm^3) lower than the outside (average $\rho_b = 1.49$ g/cm^3), supporting the possibility of swelling during the test. This swelling of the clay would have affected the scour depth measurements and erodibility during the jet test duration. Sometimes the base ring was difficult to hammer into the soil. Pounding in one side sometimes caused the opposite side to rise slightly out of the soil, pulling on the surrounding soil. This action could break apart the soil profile, especially for weak soils, and influence the erodibility of the soil surface or the soil around the insertion point.

4.2. Multiangle Submerged Jet Test Device Comparison to Traditional Flume Studies

The clay loam and clay soils both eroded irregularly as aggregates during the flume tests. There were seven clay loam runs and five clay runs. Two additional clay loam runs were conducted to better define the erosion curve. Both soils visibly swelled during testing. An inverse relationship between compacted bulk density and the erodibility of the soils was observed.

4.2.1. Soil Condition Verification

The compacting θ_d, testing θ_d, and testing ρ_b were compared to ensure the testing soil conditions were similar among the soil types. There were no soil condition outliers for any of the clay loam or clay flume runs. Clay loam Run 4 had a higher bulk density (1.58 g/cm^3) than the other clay loam tests (1.51 to 1.55 g/cm^3), and clay Run 1 had a higher bulk density (1.48 g/cm^3) than the other clay tests (1.42 – 1.44 g/cm^3). The histograms, box plots, and 95% confidence intervals for all the data showed low variances and no outliers. The histograms suggest the data followed a normal distribution, but the sample size was too small to determine the population distribution.

The remolded samples for the flume tests was compacted and tested with similar average gravimetric soil moisture content as the samples tested with the jet test. The clay loam was compacted with an average soil moisture content of 0.12 (σ = 0.00; SE of mean = 0.00; median = 0.12) to an average bulk density of 1.54 g/cm^3 (σ = 0.02 g/cm^3; SE of mean = 0.01; median = 1.54 g/cm^3), and tested with an average moisture content of 0.18 (σ = 0.01; SE of mean = 0.00; median = 0.18) (Figure 4.10). The average post-bulk density for clay loam samples of 1.40 g/cm^3 (σ = 0.07 g/cm^3; SE of mean = 0.03; median = 1.36 g/cm^3) was lower than the calculated testing bulk density. The results from a Wilcoxon matched-pairs signed rank test for related pairs (n = 6; p = 0.036) indicate there was a significant difference between testing bulk density and post-test bulk density, and that significant swelling occurred during testing. This change in bulk density from soil swelling of the clay loam may have changed the erodibility of the soil during testing. Wynn and Mostaghimi (2006) showed a strong correlation between bulk density and soil erodibility.

The clay was compacted with an average soil moisture content of 0.15 (σ = 0.00; SE of mean = 0.00; median = 0.15) to an average bulk density of 1.44 g/cm^3 (σ = 0.02 g/cm^3; SE of mean = 0.01; median = 1.43 g/cm^3), and tested with an average moisture content of 0.21 (σ = 0.01; SE of mean = 0.00; median = 0.21) (Figure 4.11). Post-test bulk density samples for clay were not collected because of the difficulty to collect an accurate sample due to the crumbly and pliable nature of the moist soil and the small soil depth after erosion. The small range and standard deviation for both soils verified similar testing conditions for the runs.

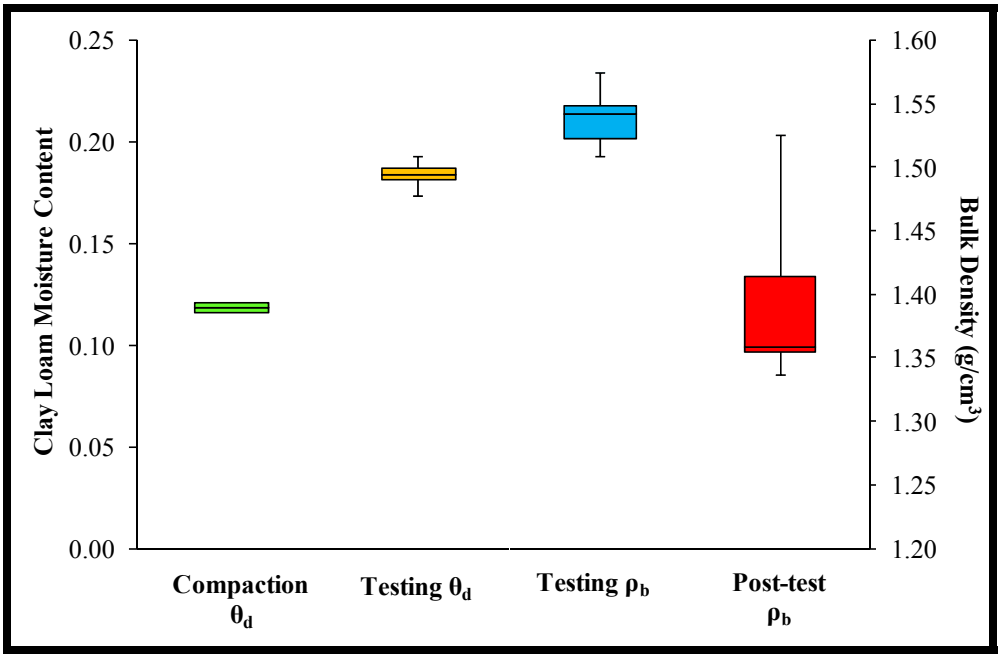

Figure 4.10. Box plot for clay loam compacting and testing moisture content, and testing and post-testing bulk density.

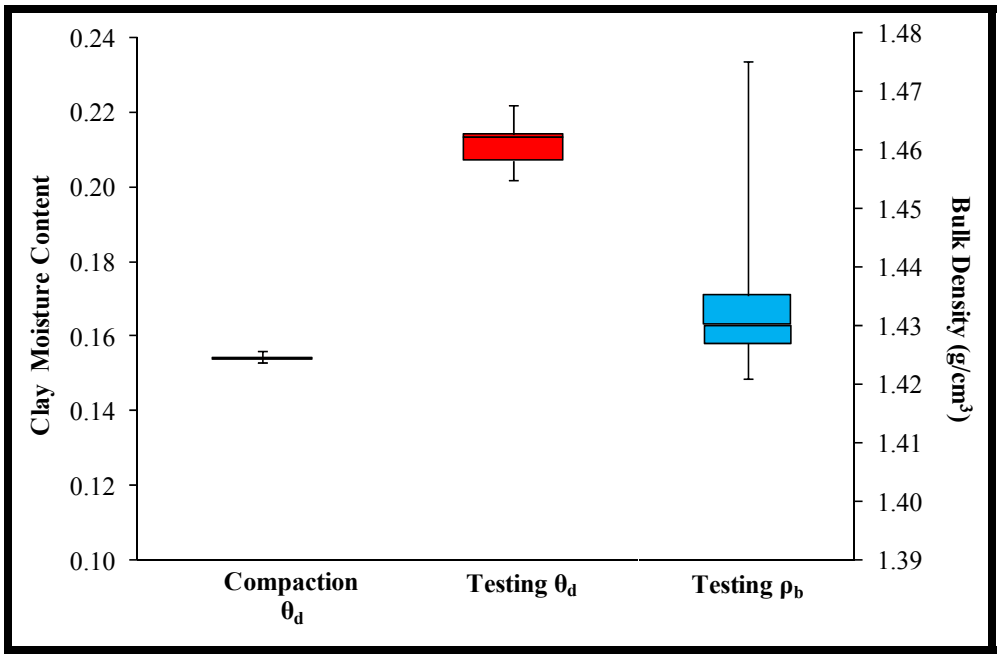

Figure 4.11. Box plot for clay compacting and testing moisture content, and testing bulk density. Post-test bulk density samples were not collected due to soil conditions.

Mann-Whitney tests compared the testing bulk density, the compacting moisture content, and the testing moisture content between the jet and the flume tests to verify the soil samples had similar testing conditions. Test results indicated no significant difference between clay loam compacting θ_d (JTD = 0.12; flume test = 0.12) (JTD n = 10; flume n = 7; p = 0.115 adjusted for ties) and testing ρ_b (JTD = 1.53 g/cm^3; flume test = 1.54 g/cm^3) (JTD n = 10; flume n = 7; p = 0.525 adjusted for ties). However, there was a significant difference for testing θ_d (JTD = 0.23; flume test = 0.18) (JTD n = 10; flume n = 7; p = 0.001 adjusted for ties). The clay soil conditions between jet test (ρ_b = 1.46 g/cm^3; compacting θ_d = 0.16; testing θ_d = 0.26) and the flume (ρ_b = 1.44 g/cm^3; compacting θ_d = 0.15; testing θ_d = 0.21) had similar results as the clay loam. Test results indicated no significant differences between compacting θ_d (JTD n = 10; flume n = 5; p = 0.074 adjusted for ties) and testing ρ_b (JTD n = 10; flume n = 5; p = 0.098), but there was a significant difference for testing θ_d (JTD n = 10; flume n = 5; p = 0.003 adjusted for ties). For both the clay loam and clay, the jet test testing moisture content was higher than the

flume. This difference was most likely due to the smaller sample size draining for the same 16-hour duration as the larger samples tested with the jet test device. In addition, there could have been moisture lost during the time (1.5 to 2 hours) needed for the silicone caulk to dry around the sample box before flume testing. During this time, the soil was covered with a plastic film, but moisture loss was still possible.

4.2.2. Flume Results from Remolded Clay Loam Tests

Flow conditions for the clay loam tests were subcritical and quasi-uniform (Table 4.4). However, the flow was approximated as uniform flow based on the logarithmic velocity profiles (Appendix B). Usually the erosion rate was higher for higher applied shear stress, except for Run 7 (Table 4.5).

Table 4.4. Flow properties during clay loam flume tests.

Flume Clay Loam Run	Average Discharge (m^3/s)	Flow Depth at Soil (cm)[a]	Reynolds Number	Froude Number	Applied τ (Pa)		
					LOW[b]	VDL[c]	Avg τ
1	0.0135	7.60	46000	0.21	0.18	0.17	0.02
2	0.0143	6.07	50000	0.31	0.25	0.25	0.34
3	0.0141	4.45	52000	0.48	0.47	0.63	0.50
4	0.0482	8.49	129000	0.62	1.92	2.08	2.65
5	0.0162	4.85	48000	0.48	0.36	0.52	0.57
6	0.0369	7.59	121000	0.56	1.52	1.74	4.48
7	0.0463	8.57	133000	0.59	1.28	1.61	1.78

[a]Average of water depth at 6.5 cm upstream and downstream of respective soil edge; [b]Law of the Wall; [c]Velocity defect law

Table 4.5. Flume test conditions and results for remolded clay loam samples.

Flume Clay Loam Run	Compact θ_d[a]	Initial Test θ_d	Test ρ_b[b] (g/cm^3)	% Soil Loss	Erosion Rate[c] (cm/day)	Water Temp[d] (°C)	Water Conductivity[e] (µS/cm)
1	0.12	0.18	1.55	0.6%	0.79	19.5	152
2	0.12	0.19	1.54	0.3%	0.44	19.5	152
3	0.12	0.18	1.55	5.9%	8.23	20.0	157
4	0.12	0.17	1.58	22.6%	30.65	11.2	178
5	0.12	0.19	1.51	1.7%	2.39	12.1	162
6	0.12	0.19	1.51	37.4%	53.41	18.1	163
7	0.12	0.18	1.53	33.4%	46.95	13.6	151
Mean	*0.12*	*0.18*	*1.54*	---	---	*16.3*	*159*
Median	*0.12*	*0.18*	*1.54*	---	---	*18.1*	*157*
SD[f]	*0.00*	*0.01*	*0.02*	---	---	*3.8*	*10*

[a] Gravimetric soil moisture content; [b] Bulk density; [c]Calculated from the test ρ_b and testing surface area; [d]Average of beginning, middle, and end measurements; [e]Average of beginning, middle, and end measurements; [f]Standard deviation

During the flume tests, the clay loam swelled upwards and outwards, filling the gaps left by the acrylic spacers. The clay loam also swelled slightly during the wetting and draining process before the test. During Run 2, which was set at a low applied shear stress, the soil surface increased 0.04 cm during the 45-minute test, even with some slight soil loss from erosion. In general, the soil eroded in irregular aggregates by saltation over the soil surface and downstream along the bed (Figure 4.12). During lower applied shear stress, the eroded aggregates would get caught on the silicone seal or on the bed roughness. At higher flow rates, the downstream corners sometimes eroded differently than the rest of the soil. One downstream corner eroded lower than the rest of the soil during Run 6, and during Run 7, one downstream corner eroded lower than the rest of the soil, while the opposite downstream corner was higher and eroded least compared to the rest of the sample. See Appendix A for before and after pictures of all the clay loam flume tests.

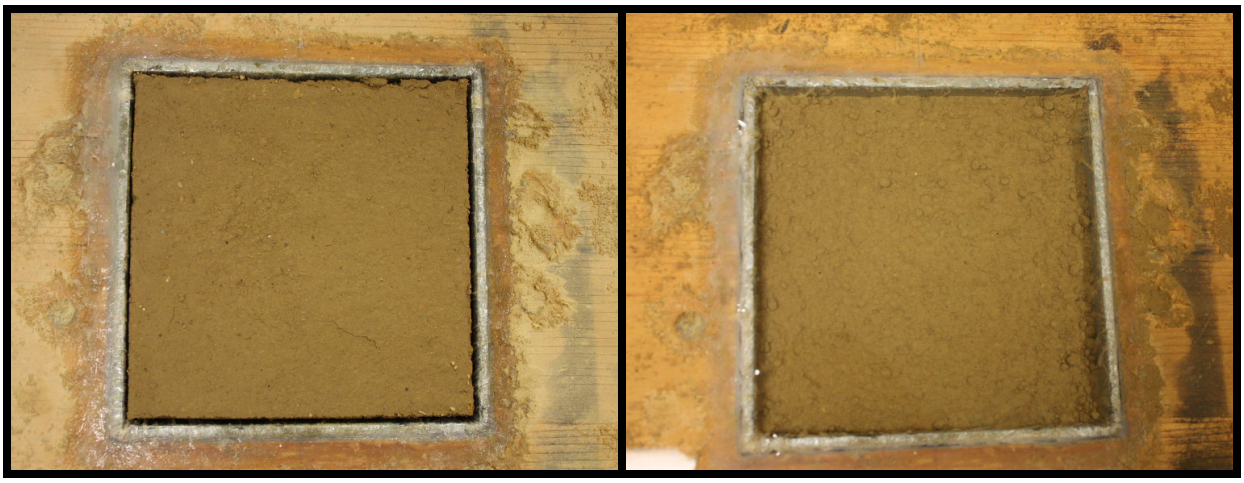

Figure 4.12. Before (left) and after (right) flume testing for clay loam Run 6.

Some aggregates disintegrated into individual particles and suspended into the recirculating water, which decreased the water clarity. Suspended sediment concentrations for samples collected before, during, and after the test showed how the sediment concentrations increased during test duration, especially during the higher flow rates (Table 4.6). The streamwise edges along the soil usually developed step-like edges. Since some of the soil near the surface around the box edge was removed with the acrylic pieces, the surface soil did not swell to the box sides like the lower soil did, which created a soil step. This edge usually remained during the duration of the test at low applied shear stresses.

Table 4.6. Suspended sediment concentration (SSC) during the clay loam flume runs

Flume Clay Loam Run	SSC (mg/L)		
	Pre-test	Mid-test	Post-test
1	4.9	6.6	5.1
2	7.2	6.3	5.1
3	10.0	11.6	12.4
4	12.2	34.3	49.0
5	6.7	8.6	6.8
6	15.6	35.9	57.9
7	26.2	53.7	87.5

Figure 4.13 shows the erosion rate (calculated from testing bulk density and testing surface area) and applied shear stress (from the velocity defect law) relationship. The approximate applied shear stress calculated from the velocity defect law (VDL) was considered the most accurate of the three applied shear stress calculations because this form of the law of the wall can be extended into the logarithmic transitional layer of uniform flow. The simple linear regression between the erosion rate and applied shear stress did not meet the assumption of a normal distribution of residuals and the intercept was not statistically different from zero, indicating the simple linear regression was not adequate. Instead, Theil-Sen non-parametric regression ($p = 0.02$) between the erosion rate (calculated by the testing bulk density and the testing surface area) and approximate applied shear stress from the velocity defect law was conducted, resulting in a τ_c of 0.23 Pa and k_d of 2.43 cm^3/N-s. The results from a one-sample Wilcoxon signed rank test indicate the JTD median critical shear stress was significantly different than the flume critical shear stress ($\alpha = 0.05$; $p = 0.01$); however, there was not a significant difference between JTD median k_d value and the flume measurement ($\alpha = 0.05$; $p = 0.26$).

The average critical shear stress and soil erodibility values from the JTD Blaisdell and Thomas method were used to determine the erosion rate line from the excess shear stress equation, which were plotted with the Theil-Sen regression line of the clay loam flume data (Figure 4.13). The Blaisdell and Theil-Sen flume lines were similar; however, the erosion line from the Thomas τ_c and k_d values was very different and not in the range of the measured flume data. As stated earlier, results from the Thomas method analysis were inconsistent

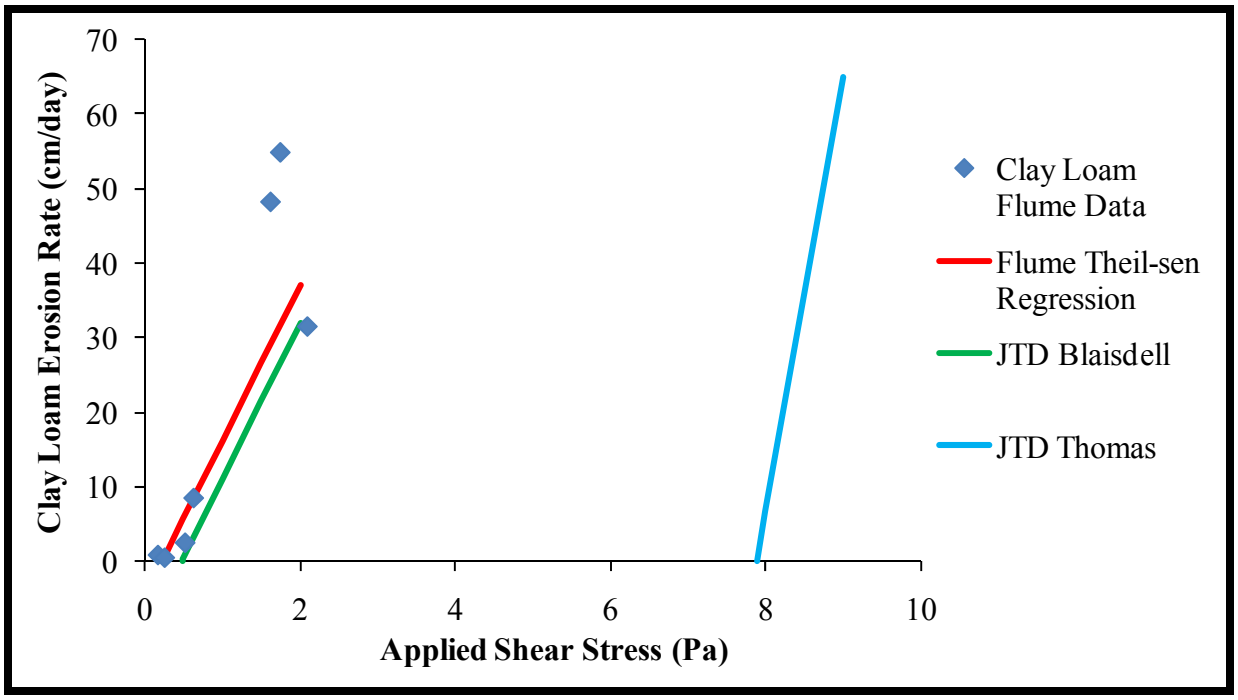

Figure 4.13. Clay loam flume data (erosion rate calculated by the testing bulk density and testing surface area versus the velocity defect law applied shear stress) with the linear excess shear stress equation lines using critical shear stress and soil erodibility values from flume Theil-Sen regression, and jet test device Blaisdell and Thomas methods.

To evaluate the sensitivity and the range of critical shear stress and soil erodibility values from the flume experiments, Theil-Sen regressions (p ranged from 0.02 to 0.04 for 12 regressions) between the four erosion rates (calculated from a combination of testing and post-test bulk densities, and pre-test and testing surface areas) and approximate applied shear stresses (basic law of the wall, velocity defect law, and average shear stress) were conducted, resulting in an average τ_c of 0.22 Pa (σ = 0.05 Pa; SE of mean = 0.01 Pa; median = 0.23 Pa) ranging from 0.16 Pa to 0.30 Pa, and an average k_d of 2.97 cm^3/N-s (σ = 1.30 cm^3/N-s; SE of mean = 0.38 cm^3/N-s; median = 2.82 cm^3/N-s) ranging from 1.44 cm^3/N-s to 4.82 cm^3/N-s (Table 4.7). Both testing and post-test bulk densities were included, because there would be error in the erosion rate measurement when calculating it based on the testing bulk density, because the density changed during the testing due to soil swelling. The testing bulk density represents the highest the bulk density of the soil was during testing, and the post-bulk density represents the lower

limit. During the test, the bulk density was probably between these two limits. Out of the three applied shear stress estimates, the average shear stress was considered the least accurate due to difficulties in measuring water depth and slope. Removing the values based on average shear stress calculation (p ranged from 0.01 to 0.04 for 8 regressions), the average τ_c changes to 0.23 Pa (σ = 0.05 Pa; SE of mean = 0.02 Pa; median = 0.23 Pa) ranging from 0.16 Pa to 0.30 Pa, and the average k_d changes to 3.68 cm^3/N-s (σ = 0.97 cm^3/N-s; SE of mean = 0.34 cm^3/N-s; median = 3.73 cm^3/N-s) ranging from 2.43 cm^3/N-s to 4.80 cm^3/N-s.

Mann-Whitney test compared the median τ_c and k_d values from the jet tests (τ_c = 0.45 Pa; k_d = 2.31 cm^3/N-s) to the flume test median values. Results indicated there was a significant difference between critical shear stress (JTD n = 10, flume n = 12; p = 0.00) median values from the jet test device and flume with results including all three applied shear stress calculation methods, but there was not a significant difference between soil erodibility (JTD n = 10, flume n = 12; p = 0.37). If the data based on the average applied shear stress were removed, the results indicated a significant difference between τ_c (JTD n = 10; flume n = 8; p = 0.00) and k_d (JTD n = 10; flume n = 8; p = 0.00) median values. Including the erosion rate calculated from the average shear stress method decreased the slope of the regression, decreasing k_d, which resulted in insignificant difference between the jet test and flume test median values.

Clay loam Run 4 had a lower erosion rate at a higher shear stress, most likely due to the higher bulk density of the soil compared to the other tests. The post-test bulk density of clay loam Run 4 was also higher than the rest of the tests, indicating less soil swelling occurred during the test. The average critical shear stress changes to 0.26 Pa (σ = 0.09 Pa; SE of mean = 0.02 Pa; median = 0.26 Pa) ranging from 0.13 Pa to 0.40 Pa and the average soil erodibility increased to 3.78 cm^3/N-s (σ = 1.69 cm^3/N-s; SE of mean = 0.49 cm^3/N-s; median = 4.45 cm^3/N-

s) ranging from 1.48 cm^3/N-s to 5.67 cm^3/N-s when clay loam Run 4 observation was removed from the Theil-Sen regressions (p ranged from 0.01 to 0.05 for 12 regressions), including all three applied shear stress calculations (Table 4.7). When the average shear stress was removed from the analysis (p = 0.01 for 8 regressions), the average τ_c changed to 0.29 Pa (σ = 0.07 Pa; SE of mean = 0.03 Pa; median = 0.26 Pa) ranging from 0.24 Pa to 0.40 Pa and k_d changed to 4.87 cm^3/N-s (σ = 0.61 cm^3/N-s; SE of mean = 0.21 cm^3/N-s; median = 4.93 cm^3/N-s) ranging from 3.97 cm^3/N-s to 5.67 cm^3/N-s.

Results from the Mann-Whitney tests with Run 4 observation removed indicated there was a significant difference between critical shear stress (JTD n = 10, flume n = 12; p = 0.00) median values from the jet test device and flume with results including all three applied shear stress calculation methods, but there was not a significant difference between soil erodibility (JTD n = 10, flume n = 12; p = 0.18). If the data based on the average applied shear stress was removed, the results indicated a significant difference between both τ_c (JTD n = 10; flume n = 8; p = 0.01) and k_d (JTD n = 10; flume n = 8; p = 0.00) median values.

If the applied shear stress (based on velocity defect law) and erosion rate (calculated with testing bulk density and testing surface area) were not linearly related, the clay loam data results in a power relationship (R^2 = 0.919; p = 0.001) with the excess shear stress exponent *a* as 1.9, instead of 1.0 (Figure 4.14). This power relationship slightly changed (R^2 = 0.931; p = 0.002) when clay loam Run 4 was removed. Without more flume runs, the form of the relationship between erosion rate and shear stress cannot be distinguished; however, the clay loam data fits a power relationship well indicating the possibility it could be a non-linear relationship. These power relationships would result in a k_d of 1.81 cm^3/N-s for all observations, and 1.52 cm^3/N-s if clay loam Run 4 was removed, with a corresponding τ_c of 0 Pa for both relationships.

Table 4.7. Flume clay loam critical shear stress and soil erodibility values using Theil-Sen regression depending on applied shear stress and erosion rate calculation method.

τ_a Calculation Method	Erosion Rate Calculation Method		Runs	k_d (cm^3/N-s)	τ_c (Pa)	p-value
	Bulk Density[a]	Surface Area[b]				
LOW[c]	Testing ρ_b	Pre-test area	All	3.23	0.16	0.02
LOW	Testing ρ_b	Testing area	All	3.14	0.16	0.02
LOW	Post-test ρ_b	Pre-test area	All	4.82	0.24	0.04
LOW	Post-test ρ_b	Testing area	All	4.69	0.24	0.04
LOW	Testing ρ_b	Pre-test area	w/o Run 4	4.95	0.24	0.01
LOW	Testing ρ_b	Testing area	w/o Run 4	4.82	0.24	0.01
LOW	Post-test ρ_b	Pre-test area	w/o Run 4	5.67	0.27	0.01
LOW	Post-test ρ_b	Testing area	w/o Run 4	5.52	0.27	0.01
VDL[d]	Testing ρ_b	Pre-test area	All	2.50	0.23	0.02
VDL	Testing ρ_b	Testing area	All	2.43	0.23	0.02
VDL	Post-test ρ_b	Pre-test area	All	4.35	0.31	0.04
VDL	Post-test ρ_b	Testing area	All	4.24	0.31	0.04
VDL	Testing ρ_b	Pre-test area	w/o Run 4	4.07	0.24	0.01
VDL	Testing ρ_b	Testing area	w/o Run 4	3.97	0.24	0.01
VDL[e]	Post-test ρ_b	Pre-test area	w/o Run 4	5.04	0.40	0.01
VDL	Post-test ρ_b	Testing area	w/o Run 4	4.91	0.40	0.01
Average shear stress	Testing ρ_b	Pre-test area	All	1.48	0.18	0.02
Average shear stress	Testing ρ_b	Testing area	All	1.44	0.18	0.02
Average shear stress	Post-test ρ_b	Pre-test area	All	1.65	0.26	0.04
Average shear stress	Post-test ρ_b	Testing area	All	1.61	0.26	0.04
Average shear stress	Testing ρ_b	Pre-test area	w/o Run 4	1.52	0.13	0.04
Average shear stress	Testing ρ_b	Testing area	w/o Run 4	1.48	0.13	0.04
Average shear stress	Post-test ρ_b	Pre-test area	w/o Run 4	1.71	0.30	0.05
Average shear stress	Post-test ρ_b	Testing area	w/o Run 4	1.66	0.30	0.05

[a]Bulk density used to calculate the erosion rate: testing ρ_b – calculated bulk density before test; and post-test ρ_b – bulk density after test; [b]Soil surface area used to calculate the erosion rate: pre-test area – soil area before swelling (14.8 cm x 14.8 cm); and testing area – soil area after swelling (15 cm x 15 cm); [c]Law of the Wall; [d]Velocity defect law

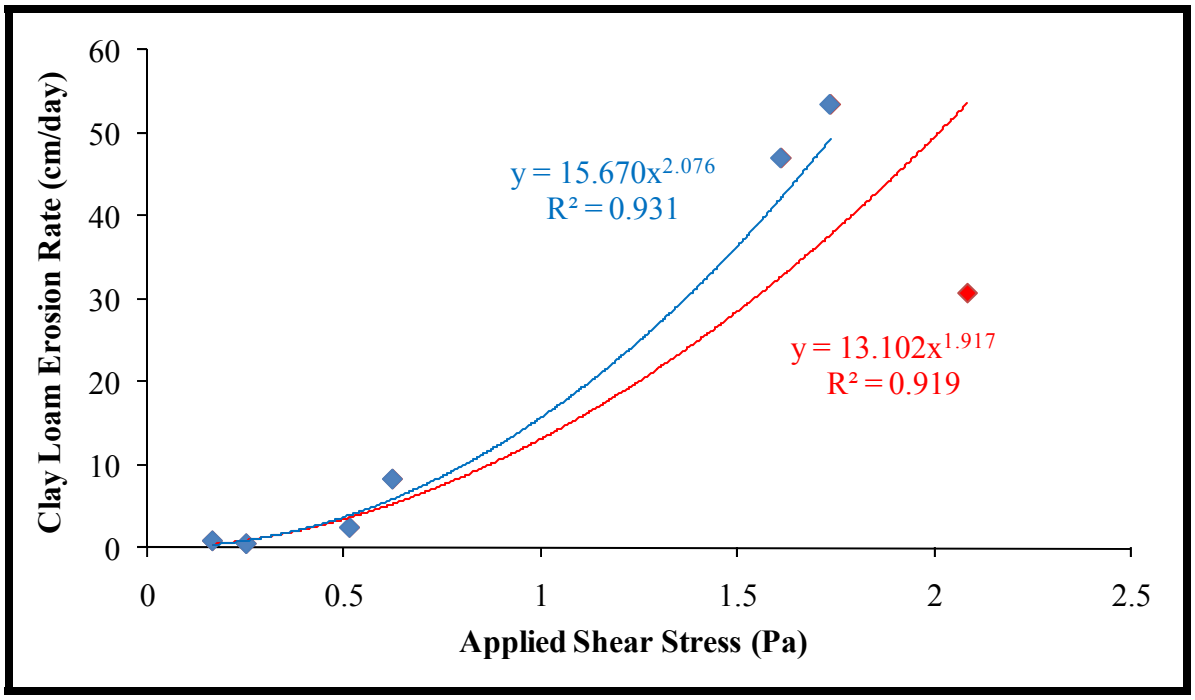

Figure 4.14. Clay loam flume erosion rate (calculated by the testing bulk density and testing surface area) versus the velocity defect law applied shear stress: for all runs (blue) and with Run 4 removed (red).

4.2.3. Flume Results from Remolded Clay Tests

Flow conditions for the clay loam tests were subcritical and not fully developed at different applied shear stresses (Table 4.8), and the erosion rate was higher for higher applied shear stress (Table 4.9). However, the flow was approximated as uniform flow based on the logarithmic velocity profiles (Appendix B).

Table 4.8. Flow properties during clay flume tests.

Flume Clay Loam Run	Average Discharge (m^3/s)	Flow Depth at Soil (cm)[a]	Reynolds Number	Froude Number	Applied τ (Pa)		
					LOW[b]	VDL[c]	Avg τ
1	0.0178	4.81	55000	0.54	0.33	0.42	0.49
2	0.0180	4.51	59000	0.60	0.51	0.43	0.58
3	0.0301	5.97	101000	0.66	0.75	0.81	1.43
4	0.0415	7.15	122000	0.69	1.16	1.38	3.21
5	0.0360	6.57	109000	0.68	0.84	1.03	0.58

[a]Average of water depth at 6.5 cm upstream and downstream of respective soil edge; [b]Law of the Wall; [c]Velocity defect law

Table 4.9. Flume test conditions and results for remolded clay samples.

Flume Clay Run	Compact θ_d[a]	Initial Test θ_d	Test ρ_b[b] (g/cm^3)	% Soil Loss	Erosion Rate[c] (cm/day)	Water Temp[d] (°C)	Water Conductivity[e] (µS/cm)
1	0.15	0.20	1.48	5.7%	7.72	13.5	163
2	0.15	0.21	1.43	10.2%	14.32	16.0	159
3	0.15	0.22	1.44	28.4%	39.59	17.8	167
4	0.16	0.21	1.43	33.9%	47.64	13.4	162
5	0.15	0.21	1.42	24.4%	34.54	14.3	158
Mean	*0.15*	*0.21*	*1.44*	---	---	*15.0*	*162*
Median	*0.15*	*0.21*	*1.43*	---	---	*14.3*	*162*
SD[f]	*0.00*	*0.01*	*0.02*	---	---	*1.9*	*3*

[a] Gravimetric soil moisture content; [b] Bulk density; [c]Calculated from the test ρ_b and testing surface area; [d]Average of beginning, middle, and end measurements; [e]Average of beginning, middle, and end measurements; [f]Standard deviation

The clay swelled overnight while draining and during the flume test. During testing, the soil swelled outward, filling in the gap left by the acrylic spacers; however, the vertical swelling was not as noticeable as it was for the clay loam samples. Similar to the jet test compacted boxes, the clay soil remained as aggregates throughout the compaction, wetting, and flume testing. There were usually small cracks on the surface before testing. The soil eroded as irregular aggregate bedload, where aggregates rolled and bounced over the soil surface and downstream along the bed (Figure 4.15). Sometimes, a large aggregate displaced other aggregates nearby when the large aggregate detached and rolled along the surface. During lower applied shear stress, the eroded aggregates would become lodged on the bed roughness, similar to the clay loam. At higher flow rates, the downstream corners sometimes eroded differently than the rest of the sample. During clay Runs 3 and 5, the downstream edge eroded lower than the rest of the soil. In Run 4, the downstream corners eroded lower and the downstream middle area was higher than the rest of the box, with the streamwise sides eroded lower than the middle.

Figure 4.15. Before (left) and after (right) flume testing for clay Run 3.

Some aggregates disintegrated into individual particles and suspended into the recirculating water, which decreased the water clarity. Suspended sediment concentrations before, during, and after the test showed how the concentrations changed during test duration, especially during the high flow rates (Table 4.10). The streamwise edges along the soil usually developed step-like edges, similar to the clay loam runs except smaller in form. The edge usually remained throughout the test at low applied shear stresses, while it eroded at higher flow rates.

Table 4.10. Suspended sediment concentration (SSC) during the clay flume runs

Flume Clay Run	SSC (mg/L)		
	Pre-test	Mid-test	Post-test
1	8.2	10.2	9.6
2	9.1	11.4	10.2
3	9.3	22.1	23.3
4	5.4	38.2	39.5
5	19.1	29.5	29.1

After testing, the clay was difficult to remove from the box and tools. Similar to the jet test, the surface soil would crumble and fall apart. Early attempts to collect a bulk density for the first two clay runs were unsuccessful. Bulk density samples could not be collected due to the

friable condition of the clay soil. In addition, the wet clay adhered to the tools, lining, and box, and was difficult to wash off the items.

Figure 4.16 shows the erosion rate (calculated from testing bulk density and testing surface area) and applied shear stress (from the velocity defect law) relationship. A Theil-Sen non-parametric regression (p = 0.05) between the erosion rate (calculated by the testing bulk density and the testing surface area) and approximate applied shear stress from the velocity defect law was conducted, resulting in a τ_c of 0.16 Pa and k_d of 4.59 cm^3/N-s. The results from a one-sample Wilcoxon signed rank test indicate the JTD median critical shear stress and soil erodibility were significantly different than the flume critical shear stress ($\alpha = 0.05$; p = 0.01)

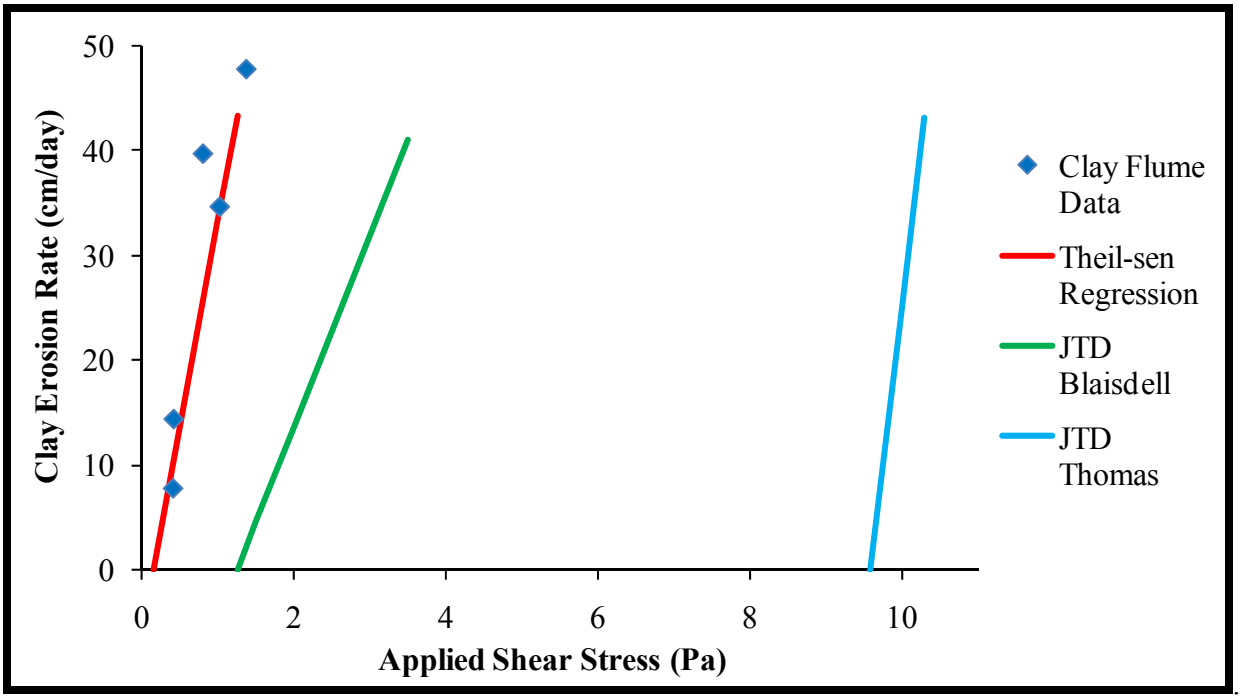

Figure 4.16. Clay flume data (erosion rate calculated by the testing bulk density and testing surface area versus the velocity defect law applied shear stress) with the linear excess shear stress equation lines using critical shear stress and soil erodibility values from flume Theil-Sen regression, and jet test device Blaisdell and Thomas methods.

The average critical shear stress and soil erodibility values from the JTD Blaisdell and Thomas method were used to determine the erosion rate line from the excess shear stress equation, which were plotted with the Theil-Sen regression line of the clay flume data (Figure

4.16). The Blaisdell line was to the right of the observed flume data and had a smaller slope (smaller k_d) than the Theil-Sen line; however, the erosion line from the Thomas τ_c and k_d values was not in the range of the measured flume data, although the slope was similar to the Theil-Sen line. As stated earlier, the Thomas method analysis produced inconsistent results, resulting in questionable calculated values.

To evaluate the sensitivity and the range of critical shear stress and soil erodibility values, Theil-Sen regressions (p ranged from 0.01 to 0.05 for 6 regressions) between the erosion rates (calculated from pre-test and testing surface areas) and approximate applied shear stresses (basic law of the wall, velocity defect law, and average shear stress) were conducted, resulting in an average τ_c of 0.11 Pa (σ = 0.09 Pa; SE of mean = 0.04 Pa; median = 0.17 Pa) ranging from 0 Pa to 0.17 Pa, and an average k_d of 4.35 cm^3/N-s (σ = 1.45 cm^3/N-s; SE of mean = 0.59 cm^3/N-s; median = 4.65 cm^3/N-s) ranging from 2.56 cm^3/N-s to 5.87 cm^3/N-s (Table 4.11). Out of the three applied shear stress estimates, the average shear stress was considered the least accurate due to difficulties in measuring water depth and slope. Removing the values based on average shear stress calculation (p =0.05 for 4 regressions), the average τ_c changes to 0.17 Pa (σ = 0.01 Pa; SE of mean = 0.00 Pa; median = 0.17 Pa) ranging from 0.16 Pa to 0.17 Pa, and the average k_d changes to 5.22 cm^3/N-s (σ = 0.67 cm^3/N-s; SE of mean = 0.33 cm^3/N-s; median = 5.21 cm^3/N-s) ranging from 4.59 cm^3/N-s to 5.87 cm^3/N-s.

Mann-Whitney test compared the median τ_c and k_d values from the jet tests (τ_c = 1.10 Pa; k_d = 2.18 cm^3/N-s) to the flume test median values. Results indicated there was a significant difference between critical shear stress (JTD n = 10, flume n = 6; p = 0.00) and soil erodibility (JTD n = 10, flume n = 6; p = 0.00) median values from the jet test device and flume with results including all three applied shear stress calculation methods. Even removing the data based on

the average applied shear stress, the results indicated a significant difference between τ_c (JTD n = 10; flume n = 4; p = 0.01) and k_d (JTD n = 10; flume n = 4; p = 0.01) median values.

Table 4.11. Flume clay critical shear stress and soil erodibility values using Theil-Sen regression depending on applied shear stress and erosion rate calculation method.

τ_a Calculation Method	Soil Surface Area[a]	k_d (cm^3/N-s)	τ_c (Pa)	p-value
Basic LOW[b]	Pre-test area	5.87	0.17	0.05
Basic LOW	Testing area	5.72	0.17	0.05
VDL[c]	Pre-test area	4.71	0.16	0.05
VDL	Testing area	4.59	0.16	0.05
Average shear stress	Pre-test area	2.63	0.00	0.01
Average shear stress	Testing area	2.56	0.00	0.01

[b]Soil surface area used to calculate the erosion rate: pre-test area – soil area before swelling (14.8 cm x 14.8 cm); and testing area – soil area after swelling (15 cm x 15 cm); [b]Law of the Wall; [c]Velocity defect law

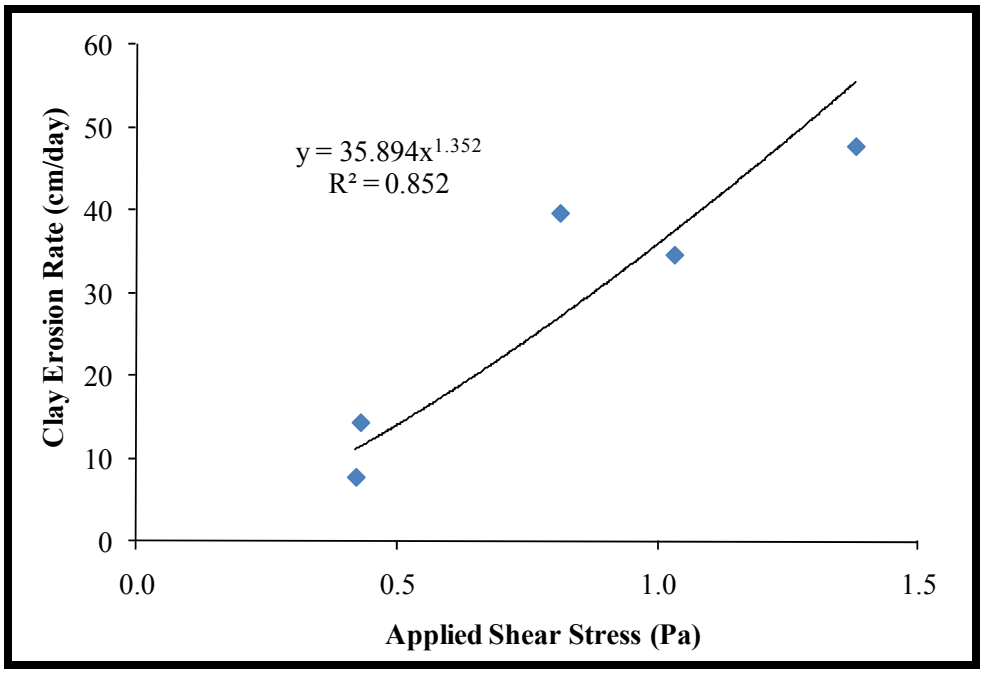

Figure 4.17. Clay flume erosion rate (calculated based on testing bulk density and testing surface area) versus the velocity defect law applied shear stress.

If the applied shear stress and erosion rate were not linearly related, the clay loam data results in a power relationship (R^2 = 0.852; p = 0.03) with the excess shear stress exponent *a* as 1.4, instead of 1.0 (Figure 4.17). This power relationship would result in a k_d of 4.15 cm^3/N-s

with a corresponding τ_c of 0 Pa. Without more flume runs, especially at lower applied shear stresses, the form of the relationship cannot be distinguished.

4.2.4. Jet Test Comparison to Traditional Flume Studies Discussion

The clay loam jet test average critical shear stress was 0.48 Pa and τ_c from the flume test was 0.23 Pa. The jet test average soil erodibility was 2.30 cm^3/N-s compared to a k_d value of 2.43cm^3/N-s from the flume test. There was a 70% difference between the jet test and flume test critical shear stress, while there was a 6% difference for the soil erodibility between the two testing methods. Assuming the flume results were accurate values resulted in a 109% error in the jet test critical shear stress, and a 5% error in the jet test soil erodibility. These jet test τ_c and k_d values would result in an under-estimation of 0.2 m of bank retreat from a 24-hr flood event for a second order stream (assuming slope = 0.1%, 1.5-m water depth).

The clay jet test average critical shear stress was 1.25 Pa, while the flume τ_c was 0.16 Pa. The jet test average k_d was 2.11 cm^3/N-s compared to a flume k_d value of 4.59 cm^3/N-s. There was a 155% difference between the jet test and flume test τ_c, and a 74% difference in k_d. Assuming the flume results were accurate values resulted in a 681% error in the jet test critical shear stress, and a 54% error in the jet test soil erodibility. These jet test erosion parameters would result in an under-estimation of 3.3 m of bank retreat from a one-day flood event for a second order stream (assuming slope = 0.1%, 1.5-m water depth).

For the clay loam and clay, the median critical shear stress and erodibility values (except clay loam k_d) from the jet test device were significantly different from the values obtained during the flume tests, which were assumed accurate, suggesting erosion results obtained using the multiangle submerged jet test device may not be as accurate as those from a traditional flume

study. However, several important factors may have influenced the final critical shear stress and soil erodibility values for both testing methods.

To evaluate the error and sensitivity in the flume test measurements, possible sources of error were identified that affected the outcome of the calculated critical shear stress and soil erodibility values:

- Soil loss in sample preparation and handling;
- Applied shear stress estimation method;
- Soil bulk density;
- Soil surface area; and
- The assumed linear relationship between erosion rate and applied shear stress.

Determining erosion rate by dry mass was difficult. Even with extra precautions, there was unaccounted soil loss. Sources of unaccounted for soil loss include box preparation (during compacting, on the compacting board, on hands, and on acrylic spacers that did not wash off), sealing the testing box in the flume bed, and soil removal after testing (on lining, on tools, on hands, and water leaks and splashes). For example, clay loam Run 1 had a larger soil loss (0.6%) than Run 2 (0.3%), although the applied shear stress was lower, and visually, Run 2 eroded slightly more than Run 1. However, the removal of soil after testing for Run 1 was unorganized and messy, resulting in more unaccounted loss of soil than the other tests (and thus errors in the erosion rate estimate), which may be why Run 1 had a higher soil loss. During the removal process of soil after clay Run 2, a small pin-size hole was found in the aluminum pan after water and a small amount of soil leaked out and was not recovered.

The extra unaccounted soil loss affects the estimated τ_c and k_d values from the flume. The soil loss would tend to shift the measured curve upwards compared to the true line. This

shift would move the intercept of the line to the left, which would decrease the measured τ_c from the true intercept. The extra soil loss may also increase the slope of the line, and increase the estimated k_d value compared to the true value.

To get an idea of the amount of soil lost during the preparation and soil removal, a control box for each soil type was prepared as though it would be tested (Table 4.12). The control boxes were also used to check calculated values of testing bulk density and moisture content to values obtained from a soil sample. The clay loam control box had a higher soil loss (0.4% soil loss) than clay loam Run 2 (0.3% soil loss) during testing. Overall, the soil loss calculated with these boxes represents the lower limit of error, especially for the clay, since handling the soil in the "error" boxes was easier, due to the low moisture content of those soils (since they were not tested in the flume). The low soil loss for the clay error box was due to the ease of removing the soil and rinsing soil off of tools and lining. Unlike the clay after testing, which was pliable, adhered to all the tools and in crevices, and was difficult to wash off, the clay from the control box was firm, drier, and easy to rinse off, and was in a condition for an accurate bulk density sample to be collected. From experience and observations, the clay error box had less soil loss than any of the tested boxes. However, these control boxes give a lower limit for possible error in the erosion rate.

Table 4.12. Control flume box conditions for clay loam and clay soils

Soil	Compact θ_d[a]	Initial Test θ_d[b]	Sample Test θ_d[c]	Test ρ_b[d] (g/cm^3)	Sample Test ρ_b[e] (g/cm^3)	Soil Loss (g)	% Soil Loss	ε[f] Error (cm/day)
Clay Loam	0.12	0.19	0.17	1.53	1.45	5.5	0.4 %	0.51
Clay	0.15	0.22	0.19	1.42	1.40	0.3	0.0 %	0.00

[a] Compaction gravimetric soil moisture content; [b]Gravimetric soil moisture content calculated from weight; [c]Gravimetric soil moisture content of sampled soil; [d]Bulk density calculated based on compacted soil volume; [e]Bulk density of sampled soil; [f]Erosion rate calculated from average test bulk density, test time = 2700 sec, and testing surface area

Using 5.5 g as the error in soil mass loss for both soil types, adjusted erosion rates were calculated to determine the change in critical shear stress and soil erodibility values. For each run, 5.5 g was subtracted from the measured soil loss, and the corresponding erosion rates were calculated based on the bulk density and surface area. Critical shear stress and soil erodibility were estimated from the combination of the adjusted erosion rate (calculated from testing and post-test bulk densities and pre-test and testing soil surface areas) and the approximate applied shear stress (law of the wall, velocity defect law, and average shear stress) by Theil-Sen regression. For the clay loam (p ranged from 0.01 to 0.05 for 24 regressions), τ_c ranged from 0.17 Pa to 0.42 and k_d ranged from 1.43 cm^3/N-s to 5.62 cm^3/N-s for the adjusted erosion rates (Table 4.13). The erosion rates for clay loam Runs 1 and 2 may be zero such that the measured soil loss could be from the preparation and soil removal processes, which would result in a higher critical shear stress value than the measured value. For clay (p ranged from 0.01 to 0.05 for 6 regressions), τ_c ranged from 0 Pa to 0.18 Pa, and k_d ranged from 2.56 cm^3/N-s to 5.87 cm^3/N-s (Table 4.14). An unaccounted for soil loss of 5.5 g during preparation and soil removal processes affect the overall flume critical shear stress and soil erodibility values slightly. Refer to Appendix D for erosion data and confidence intervals.

Overall, the calculated bulk densities and moisture contents were similar to the soil samples indicating the calculated values for the tested boxes were representative of the soil conditions. The initial testing moisture content was slightly lower than the sample moisture content. This difference was most likely due to moisture lost during the time needed for the silicone caulk to dry around the sample box before flume testing. During this time, the soil was covered with a plastic film, but moisture loss was still possible. The calculated bulk density and measured bulk densities were similar. The larger difference between values for the clay loam

was probably due to difficulties collecting an accurate sample, since the soil would not cut smoothly to ring volume, resulting in small amounts of soil falling out of the ring.

Table 4.13. Flume clay loam critical shear stress and soil erodibility values from the adjusted erosion rate using Theil-Sen regression depending on applied shear stress and erosion rate calculation method.

τ_a Calculation Method	Erosion Rate Calculation Method		Runs	k_d (cm^3/N-s)	τ_c (Pa)	p-value
	Bulk Density[a]	Surface Area[b]				
LOW[c]	Testing ρ_b	Pre-test area	All	3.23	0.18	0.02
LOW	Testing ρ_b	Testing area	All	3.15	0.18	0.02
LOW	Post-test ρ_b	Pre-test area	All	4.78	0.25	0.04
LOW	Post-test ρ_b	Testing area	All	4.65	0.25	0.04
LOW	Testing ρ_b	Pre-test area	w/o Run 4	4.94	0.25	0.01
LOW	Testing ρ_b	Testing area	w/o Run 4	4.81	0.25	0.01
LOW	Post-test ρ_b	Pre-test area	w/o Run 4	5.67	0.28	0.01
LOW	Post-test ρ_b	Testing area	w/o Run 4	5.52	0.28	0.01
VDL[d]	Testing ρ_b	Pre-test area	All	2.48	0.25	0.02
VDL	Testing ρ_b	Testing area	All	2.41	0.25	0.02
VDL	Post-test ρ_b	Pre-test area	All	4.35	0.32	0.04
VDL	Post-test ρ_b	Testing area	All	4.23	0.32	0.04
VDL	Testing ρ_b	Pre-test area	w/o Run 4	4.07	0.25	0.01
VDL	Testing ρ_b	Testing area	w/o Run 4	3.96	0.25	0.01
VDL	Post-test ρ_b	Pre-test area	w/o Run 4	5.04	0.42	0.01
VDL	Post-test ρ_b	Testing area	w/o Run 4	4.91	0.42	0.01
Average shear stress	Testing ρ_b	Pre-test area	All	1.48	0.22	0.02
Average shear stress	Testing ρ_b	Testing area	All	1.43	0.22	0.02
Average shear stress	Post-test ρ_b	Pre-test area	All	1.66	0.30	0.04
Average shear stress	Post-test ρ_b	Testing area	All	1.61	0.30	0.04
Average shear stress	Testing ρ_b	Pre-test area	w/o Run 4	1.52	0.17	0.04
Average shear stress	Testing ρ_b	Testing area	w/o Run 4	1.48	0.17	0.04
Average shear stress	Post-test ρ_b	Pre-test area	w/o Run 4	1.71	0.34	0.05
Average shear stress	Post-test ρ_b	Testing area	w/o Run 4	1.66	0.34	0.05

[a]Bulk density used to calculate the erosion rate: testing ρ_b – calculated bulk density before test; and post-test ρ_b – bulk density after test; [b]Soil surface area used to calculate the erosion rate: pre-test area – soil area before swelling (14.8 cm x 14.8 cm); and testing area – soil area after swelling (15 cm x 15 cm); [c]Law of the Wall; [d]Velocity defect law

Table 4.14. Flume clay critical shear stress and soil erodibility values from the adjusted erosion rate using Theil-Sen regression depending on applied shear stress and erosion rate calculation method.

τ_a Calculation Method	Soil Surface Area[a]	k_d (cm^3/N-s)	τ_c (Pa)	p-value
LOW[b]	Pre-test area	5.87	0.18	0.05
LOW	Testing area	5.71	0.18	0.05
VDL[c]	Pre-test area	4.71	0.17	0.05
VDL	Testing area	4.58	0.17	0.05
Average shear stress	Pre-test area	2.63	0.00	0.01
Average shear stress	Testing area	2.56	0.00	0.01

[a]Soil surface area used to calculate the erosion rate: pre-test area – soil area before swelling (14.8 cm x 14.8 cm); and testing area – soil area after swelling (15 cm x 15 cm); [b]Law of the Wall; [c]Velocity defect law

Box plots were constructed to evaluate the range of possible critical shear stress and soil erodibility values calculated from the flume data (Figure 4.18). Included in these box plots were 50 calculated clay loam critical shear stress and soil erodibility values for clay loam and 13 values for clay. Forty-eight of the clay loam values were calculated from the test erosion rates and the adjusted erosion rates (with and without clay loam Run 4 data), by a combination of the three applied shear stress calculation methods (basic law of the wall, velocity defect law, and average shear stress), testing and post-test bulk densities, and pre-testing and testing soil surface areas. The remaining two clay loam pairs were estimated from the power relationships between the test erosion rates (calculated from test bulk density and testing surface area) with and without clay loam Run 4 data, and velocity defect law. Twelve of the clay values were calculated from the test erosion rates and the adjusted erosion rates, by a combination of pre-testing and testing soil surface areas. The remaining one pair of values was estimated by the power relationship between the test erosion rates (calculated from the test bulk density and testing surface area) and the velocity defect law. The critical shear stress and soil erodibility values for the clay and clay loam can be found in Appendix D.

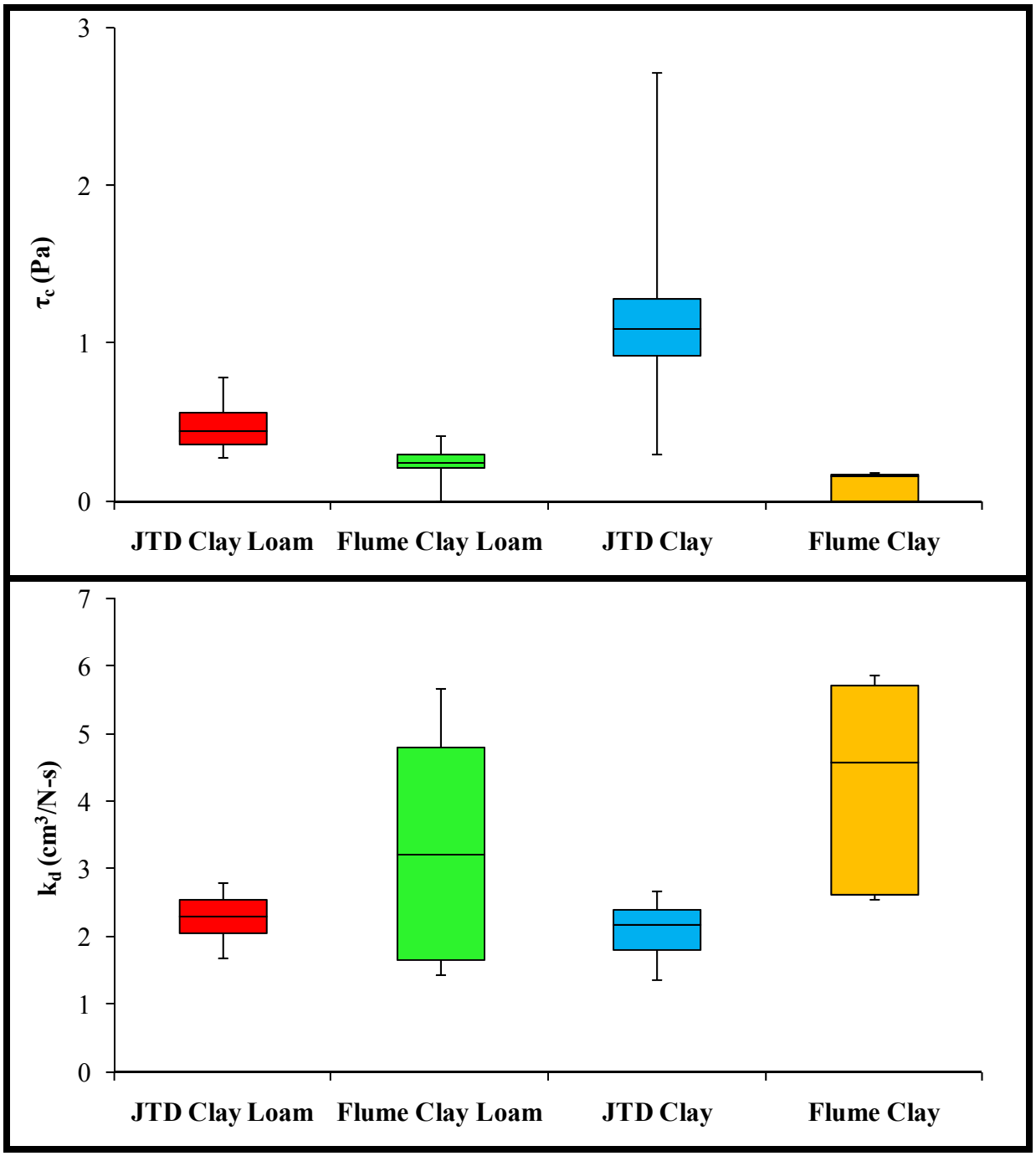

Figure 4.18. Box plots of critical shear stress (τ_c) (top) and soil erodibility (k_d) (bottom) measurements with the multiangle submerged jet test device and possible range of measurements with the flume for remolded clay loam and clay.

As seen in Figure 4.18, the median values from the jet test data were different than the median flume values. The flume critical shear stress varied less than the jet test critical shear stress. The greater variation in jet test critical shear stress was probably due to testing soil

conditions and soil swelling, as well as the τ_c was calculated for individual jet tests based on scour depth measurements, while the τ_c values for the flume were extrapolated based on the same data, resulting in values similar to each other. In contrast to the critical shear stress, the flume soil erodibility varied more than the jet test values. For the flume tests, the different soil erodibility values varied more than the critical shear stress values depending on the data used to calculate the parameters, indicating the k_d was more sensitive. Soil erodibility was calculated from the slope of the regression line, which changed depending on the calculation method used to estimate the data, especially the applied shear stress in the flume. This sensitivity shows the limitation in general flume studies, which are the traditional method for estimating critical shear stress and soil erodibility of soils. Since the flow was approximately uniform, all the applied shear stresses approximately represented the bed shear stress. The average shear stress was considered the least accurate of the applied shear stress values due to the difficulty in measuring water depth and slope during the tests because of the surface waves. Irregularities from roughening the bed changed 1 mm to 2 mm throughout the flume, and the artificial bed height varied along the flume. Although the bed slope along the full length of the flume was small (0.009%), the bed area around the test section was lower than upstream and downstream due to minimal support underneath the bed. The jet test k_d range did overlap with the possible flume values, especially the clay loam, indicating the jet test device may have potential in estimating the erosion parameters, and may .

The critical shear stress from the flume data was estimated by assuming the relationship between the erosion rate and the applied shear stress was linear. However, some research suggests that this relationship is not linear at low applied shear stresses. Paintal (1971) conducted flume studies with non-cohesive bedload (2.5 mm and 7.95 mm particles) and found

the data did not follow a straight line in the relationship between applied shear stress and bedload transport rate. Paintal (1971) concluded that there was no specific critical point for soil movement; to have no erosion there needs to be no flow, as turbulent velocity spikes can cause movement at any flow. Ariathurai and Arulanandan (1978) also observed a non-linear relationship between erosion rate and shear stress for a few of the undisturbed samples. Some erosion studies have found a power relationship fits better, with the excess shear stress exponent *a* varying 1.05 to 6.8 (Knapen et al., 2007). Zhu et al. (2001) found that at low to medium shear stresses, a power relationship fit the data better than the linear excess shear stress equation. With only seven flume tests for the clay loam and five for the clay, there were not enough data to definitively identify the form of the relationship. Examination of the clay plot (Figure 4.17) shows that if there was a non-linear relationship, a representative critical shear stress (power curve does not intersect applied shear stress axis) would be higher than the calculated 0.16 Pa. However, high erosion occurred at applied shear stresses similar to the jet test average critical shear stress value of 1.25 Pa, showing the jet test device over-estimated the parameter. Results suggest the variation in jet test device critical shear stress and soil erodibility measurements may vary with soil type.

Clay jet test Run 8 had a higher bulk density than the rest of the samples, which contributed to the highest τ_c (2.72 Pa) and lowest k_d (1.36 cm^3/N-s). If Run 8 data was removed, the resulting average Blaisdell τ_c would be lower at 1.09 Pa (σ = 0.56, median = 1.06 Pa) with a range of 0.30 Pa to 2.30 Pa, and the resulting average Blaisdell k_d would be 2.19 cm^3/N-s (σ = 0.33, median = 2.23 Pa) with a range of 1.78 to 2.69 cm^3/N-s. However, as mentioned above, the applied shear stress in the flume around 1 Pa resulted in high erosion rate, and was not the initiation point of detachment.

Soil swelling during the flume test was probably the most influential factor on the resulting critical shear stress and soil erodibility values. Soil swelling was observed for both soils, decreasing the bulk density of sample. The clay loam post-test bulk density median was 11.9% less than the calculated testing bulk density median, and the testing and post-test densities were significantly different. Previous research has shown that decreases in bulk density increase the erodibility of a soil (Hanson and Robinson, 1993; Allen et al., 1999; Wynn and Mostaghimi, 2006). In the clay loam flume tests, Run 4 testing bulk density was 2.5% more than the median testing bulk density of the other six runs, and this small difference appeared to affect the erosion rate of the run. In addition, a 5% difference in testing bulk density for a jet test run compared to the median of the other runs appeared to affect the critical shear stress and soil erodibility of the soil. The decrease in bulk density during the flume tests would decrease the critical shear stress and increase the soil erodibility of the soil. This effect was observed in the flume tests. The resulting critical shear stress and soil erodibility values from the flume may be accurate for the soil at the lower bulk density, but the values would not be accurate at the initial testing bulk density, which was the bulk density the soil was jet tested. The decrease in bulk density due to soil swelling explains the difference in critical shears stress and soil erodibility between the jet tests and the flume tests. Although the initial soil conditions were similar for the jet tests and flume tests, the actual testing soil conditions were not similar, so the assumption that the values from the flume tests represent accurate parameter measurements may not be correct. The multiangle submerged jet test device may be a good methodology for measuring erosion parameters, even though the critical shear stress and soil erodibility values were significantly different from the flume tests.

Swelling of the soils was observed more during the flume tests, than during the jet tests. The soil depth and area of the samples tested in the flume were much smaller than the jet test samples, so water would take less time to soak through the shorter depth. Also, since there were gaps between the box walls and the soil, water could seep around the soil cube allowing the water to be absorbed throughout the sample more quickly. In contrast, the area around the jet test walls was sealed with bentonite, preventing this water seepage around the insertion location. Future studies may need to measure erosion rates based on mass, because soil swelling makes scour depth and volume measurements inaccurate.

Other possible sources of error in the flume tests include the following: 1) soil aggregates detached from the soil surface due to erosion, but were not carried from the box; 2) soil surface not always flush with bed; 3) errors in estimating the applied shear stress from bed swelling and irregularities; 4) changes in the flow caused by the miniature propeller; 5) errors in water depth measurements due to surface waves; and 6) flow was not fully developed and non-uniform resulting in approximate shear stress values.

The jet test device and the flume have different flow characteristics, which influence the soil erosion. The jet test device water jet impacted the soil perpendicularly, while the flow in the flume was parallel to the surface. The submerged water jet for the JTD is similar to the vertical water force in a plunge pool (Stein and Nett, 1997; Hanson et al., 2002). The difference between flow from a submerged jet and typical channel flow could cause limitations because: 1) the jet has normal and tangential stress components; 2) jet turbulence is different than turbulence in a channel; 3) eroded particles must be transported horizontally and vertically out of the developed scour hole; 4) the eroded surface is not horizontal, which could be important for oriented or layered soil structures; and, 5) the soil samples must be uniform with depth (Hollick, 1976). In

addition, the JTD was used on an angled surface, and the flume tests were conducted with a horizontal soil surface. Gravitational forces on the soil could influence how aggregates erode, in addition to the flow mechanics of detachment versus fluvial entrainment. In the flume tests, the aggregates eroded like bedload, so this might change if the soil was tested at an angle, like a streambank.

Chapter 5: Conclusions

The overall goal of this research was to evaluate the *in situ* multiangle submerged jet test device in measuring streambank critical shear stress (τ_c) and soil erodibility (k_d). The first specific objective for this study was to determine the repeatability of the jet test device for measuring critical shear stress and soil erodibility, based on the standard deviation and 95% confidence interval A total of 21 jet tests were conducted on two locally available soil types, clay loam (11 tests) and clay (10 tests). Remolded soil samples were compacted at uniform moisture content to a constant bulk density.

Results from this study indicate the multiangle submerged jet test device is capable of determining the soil critical shear stress to within 0.74 Pa (59% of the mean) and soil erodibility to within 0.41 cm^3/N-s (19% of the mean) for the tested soils. Test repeatability varied with soil type, with lower repeatability for the more aggregated soil type. The lack of statistically significant relationships between τ_c and k_d values for the remolded soils in this study supports the conclusion that natural soil structure is a major factor in the variability observed in the erosion of undisturbed cohesive soils.

Compared with k_d and τ_c results from previous field jet testing (Hanson and Simon, 2001; Wynn and Mostaghimi, 2006; Wynn et al., 2008), the variation among the two erosion parameters for remolded soil was modest. Critical shear stress and soil erodibility measurements by the jet test device varied in the field by up to four orders of magnitude at a single site (Wynn and Mostaghimi, 2006; Wynn et al., 2008) Additionally, both remolded soils had uniform erosion rates during the duration of the test compared to the more variable stepped rates observed in natural soils (Wynn and Mostaghimi, 2006; Wynn et al., 2008). Tests on the uniform soils provided a contrast to field tests, indicating subaerial processes, bulk density, and other factors

play a significant role in the erodibility and critical shear stress of cohesive soils. The modest variation of the two soil parameters, compared to the large range of values observed in the field at a single site, suggests the multiangle submerged jet test device is repeatable with similar soil conditions. These results indicate that the jet test device could be a useful tool for evaluating cohesive erosion and the factors that influence the erodibility of soils.

The second objective for this study was to compare the critical shear stress and soil erodibility measured using the multiangle submerged jet test device to results from traditional flume studies. The similarity was statistically assessed ($\alpha = 0.05$) between the jet test device and flume measurements. The submerged jet test device measurements were compared with measurements derived from a total of 12 traditional flume tests for the clay loam (7 tests) and the clay (5 tests), assuming the critical shear stress and soil erodibility from the flume tests represented the true values. The remolded soil samples were prepared using the same conditions as for the jet tests, and inserted into the bottom of a recirculating flume, flush with the bed. Critical shear stress and soil erodibility were determined by fitting the data to the excess shear stress equation.

Comparing critical shear stress and soil erodibility measured using the multiangle submerged jet test device to parameters measured using traditional flume studies indicates there is a statistically significant difference between results from the two test methods ($\alpha = 0.05$). The resulting clay loam τ_c from the flume tests was 0.23 Pa and k_d was 2.43 cm^3/N-s, and the clay τ_c was 0.16 Pa and k_d was 4.59 cm^3/N-s. These values were determine from the relationship between the erosion rate, calculated by the testing bulk density and testing surface area, and applied shear, stress calculated from the velocity defect law. In comparison, for the jet tests the mean τ_c value was 0.48 Pa and k_d was 2.30 cm^3/N-s for the clay loam, and for the clay soil the

mean τ_c and k_d were 1.25 Pa and 2.11 cm^3/N-s, respectively. Despite the fact that the erosion parameters measured by the jet test device and the flume were statistically different, from an applied perspective, the parameters were close, especially considering the range of potential errors in both test methods. These findings indicate the multiangle submerged jet test provides reasonable measurement of erosion parameters in a field setting. Measurements of variability for the jet test device indicate a minimum sample size of ten jet tests is needed to have confidence ($\alpha = 0.05$; $\beta = 0.20$) in estimates of τ_c and k_d to within 1.0 Pa and 1.0 cm^3/N-s of the true values.

Although the values were significantly different, several factors may have influenced the final critical shear stress and soil erodibility values for both testing methods. One major possible factor was estimating the erosion parameters with the flume data by assuming the relationship between the erosion rate and the applied shear stress in the shear stress equation is linear. Some research suggests this relationship is not linear at low applied shear stresses, and the flume tests in this study were conducted at low shear stresses. Research addressing the non-linear relationship is limited, so the simple linear excess shear stress equation is still currently applied to cohesive erosion data.

Another major factor that had an important effect on the results was soil swelling during the jet tests. Decreases in bulk density were measured for both soils and test methods, with the clay loam during the jet test showing the least swelling. Soil swelling would have increased the soil erodibility by decreasing soil bulk density. Conversely, soil swelling would have influenced the erosion rate measurement for the jet test, making it appear that less material was removed, decreasing k_d and increasing τ_c. Other possible factors include unaccounted soil loss during the flume sample preparation and analysis, possible differences in erosion mechanics between the

two tests (detachment versus entrainment), and the sample orientation during testing (45^o angle for the jet tests and horizontal for the flume tests).

Critical shear stress and soil erodibility parameters are difficult to determine for cohesive soils, even in a controlled laboratory setting. The large variation of k_d values, based on different calculation methods, observed in this study indicates sensitivities in estimating erosion parameter values from the flume due to soil swelling, applied bed shear stress estimates, and the form of the erosion rate and applied shear stress relationship. Many methods for estimating the parameters exist due to this measurement difficult, including empirical equations, resulting in a wide range of measured values. In addition, numerous factors influence cohesive soil erodibility and not all of them are currently known.

This study provided the repeatability and statistical comparison to traditional flume results of the multiangle submerged jet test device for remolded clay loam and clay soil. Further investigations are needed to determine if there is a linear relationship between applied shear stress and erosion rate for cohesive soils. Additionally, the effects of the shape and size of the scour hole on the jet diffusion hydraulics need to be evaluated to determine if the hole dimensions should be included in the analysis. Since soil swelling is a potential complication with all cohesive soils, improved methods for estimating soil erosion rate that are not influenced by soil swelling should be developed. To further develop the traditional flume test for cohesive erosion, especially of streambanks, differences in the erosion mechanics and erosion rate between horizontal and angled soil samples should be determined.

Results of this research have potential implications for stream restoration, water quality management and erosion modeling, and evaluation of earthen dams and levees, all of which rely on accurate critical shear stress and soil erodibility parameters. Accurate parameter estimations

will help stream restoration design advance from empirical methods toward process-based analytical designs.

References

Aberle, J., V. Nikora, and R. Walters. 2002. In situ measurement of cohesive sediment dynamics with a straight benthic flume. In *HMEM 2002*, 110-109.

Albertson, M. L., Y. B. Dai, R. A. Jensen, and H. Rouse. 1950. Diffusion of submerged jets. *Transactions of the American Society of Civil Engineers*. 115 (2409): 639-664.

Allen, P. M., J. Arnold, and E. Jakubowski. 1997. Design and testing of a simple submerged-jet device for field determination of soil erodibility. *Environmental and Engineering Geoscience*. 3 (4): 579-584.

Allen, P. M., J. Arnold, and E. Jakubowski. 1999. Prediction of stream channel erosion potential. *Environmental & Engineering Geoscience*. 5 (3): 339-351.

Ariathurai, R., and K. Arulanandan. 1978. Erosion rates of cohesive soils. *Journal of the Hydraulics Division of the ASCE*. 104: 279-283.

Arulanandan, K., E. Gillogley, and R. Tully. 1980. Development of a quantitative method to predict critical shear stress and rate of erosion of natural undisturbed cohesive soils. Technical Report GL-80-5. Vicksburg, MS: U.S. Army Corps of Engineers.

ASCE. 1998. River width adjustment. I: Processes and mechanisms. *Journal of Hydraulic Engineering*. 124 (9): 881-902.

ASTM. 2005. Standard test methods for liquid limit, plastic limit, and plasticity index of soils, No. D4318-05. West Conshohocken, PA: American Society for Testing and Materials.

ASTM. 2007a. Standard practice for dry preparation of soil samples for particle-size analysis and determination of soil constants, No. D421-85(2007). In *Annual Book of ASTM Standards, Vol. 04.08*. West Conshohocken, PA: American Society for Testing and Materials.

ASTM. 2007b. Standard test method for erodibility determination of soil in the field or in the laboratory by the jet index method, No. D5852-00(2007). In *Annual Book of ASTM Standards, Vol. 04.08*. West Conshohocken, PA: American Society for Testing and Materials.

ASTM. 2007c. Standard test method for particle-size analysis of soils, No. D422-63(2007). In *Annual Book of ASTM Standards, Vol. 04.08*. West Conshohocken, PA: American Society for Testing and Materials.

ASTM. 2007d. Standard test methods for determining sediment concentration in water samples, No. D3977-97(2007). In *Annual Book of ASTM Standards, Vol. 11.02*. West Conshohocken, PA: American Society for Testing and Materials.

Beltaos, S., and N. Rajaratnam. 1974. Impinging circular turbulent jets. *Journal of the Hydraulics Division of the ASCE*. 100 (HY10): 1313-1328.

Bernhardt, E. S., K. Barnas, S. Brooks, J. Carr, S. Clayton, C. Dahm, J. Follstad-Shah, D. Galat, S. Gloss, P. Goodwin, D. Hart, B. Hassett, R. Jenkinson, S. Katz, G. M. Kondolf, P. S. Lake, R. Lave, J. L. Meyer, T. K. O'Donnell, L. Pagano, B. Powell, O. Sudduth, M. A. Palmer, J. D. Allan, and G. Alexander. 2005. Synthesizing U.S. river restoration efforts. *Science*. 308 (5722): 636-637.

Bicknell, B. R., J. C. Imhoff, J. L. Kittle, Jr., A. S. Donigian, Jr., and R. C. Johanson. 1997. Hydrological Simulation Program-Fortran, User's manual for version 11. EPA/600/R-97/080. Athens, Ga.: US EPA, National Exposure Research Laboratory.

Blaisdell, F. W., C. L. Anderson, and G. G. Hebaus. 1981. Ultimate dimensions of local scour. *Journal of the Hydraulics Division of the ASCE*. 107 (HY3): 327-337.

Charlton, R. 2008. *Fundamentals of Fluvial Geomorphology*. New York, NY: Routledge.

Clark, E. H. 1985. The off-site costs of soil erosion. *Journal of Soil and Water Conservation*. 40 (1): 19-22.

Clark, L. A., and T. M. Wynn. 2007. Methods for determining streambank critical shear stress and soil erodibility: Implications for erosion rate predictions. *Transactions of the ASABE*. 50 (1): 95-106.

Clesceri, L. S., A. D. Greenberg, and A. D. Eaton. 1998. 2540: Solids. In *Standard methods for the examination of water and wastewater*. 20th edition. Washington, D.C.: American Public Health Association, American Water Works Association, and Water Environment Federation.

Debnath, K., V. Nikora, J. Aberle, B. Westrich, and M. Muste. 2007. Erosion of cohesive sediments: Resuspension, bed load, and erosion patterns from field experiments. *Journal of Hydraulic Engineering*. 133 (5): 508-520.

Dunn, I. 1959. Tractive resistance of cohesive channels. *Journal of the Soil Mechanics and Foundations Division, ASCE*. 85 (SM 3): 1-24.

Einstein, H. A. 1942. Formulas for the transportation of bedload. *Transactions of the American Society of Civil Engineers*. 107: 561-577.

Foster, G. R., L. D. Meyer, and C. A. Onstad. 1977. An erosion equation derived from basic erosion principles. *Transactions of the ASAE*. 20 (4): 678-682.

Garcia, M., ed. 2008. *Sedimentation Engineering: Processes, Measurements, Modeling, and Practice*, *ASCE Manuals and Reports on Engineering Practice, No. 110*. Reston, VA: ASCE.

Graf, W. H. 1984. *Hydraulics of Sediment Transport*. Littleton, Colorado: Water Resources Publications.

Grass, A. J. 1970. Inital instability of fine bed sand. *Journal of the Hydraulics Division of the ASCE*. 96: 619-632.

Grissinger, E. H. 1982. Bank erosion of cohesive materials. In *Gravel-bed Rivers: fluvial processes, engineering, and management*, ed. R. D. Hey, J. C. Bathurst, and C. R. Thorne. New York: John Wiley & Sons, Ltd.

Hanson, G. J. 1989. Channel erosion study of two compacted soils. *Transactions of the ASAE*. 32 (2): 485-490.

Hanson, G. J. 1990a. Surface erodibility of earthen channels at high stresses. Part I - Open channel testing. *Transactions of the ASAE*. 33 (1): 127-131.

Hanson, G. J. 1990b. Surface erodibility of earthen channels at high stresses. Part II - Developing an in situ testing device. *Transactions of the ASAE*. 33 (1): 132-137.

Hanson, G. J. 1991. Development of a jet index to characterize erosion resistance of soils in earthen spillways. *Transactions of the ASAE*. 34 (5): 2015-2020.

Hanson, G. J., and K. R. Cook. 1997. Development of excess shear stress parameters for circular jet testing. ASAE Paper No. 97-2227. St. Joseph, MI: ASAE.

Hanson, G. J., and K. R. Cook. 2004. Apparatus, test procedures, and analytical methods to measure soil erodibility in situ. *Applied Engineering in Agriculture*. 20 (4): 455-462.

Hanson, G. J., K. R. Cook, and A. Simon. 1999. Determining erosion resistance of cohesive materials. In *Proceedings of the ASCE International Water Resources Engineering Conference*. Seattle, WA: ASCE.

Hanson, G. J., and K. M. Robinson. 1993. The influence of soil moisture and compaction on spillway erosion. *Transactions of the ASAE*. 36 (5): 1349-1352.

Hanson, G. J., K. M. Robinson, and D. M. Temple. 1990. Pressure and stress distributions due to a submerged impinging jet. In *Proceedings of the 1990 National Conference, Hydraulic Engineering, ASCE*, 525-530: ASCE.

Hanson, G. J., and A. Simon. 2001. Erodibility of cohesive streambeds in the loess area of the midwestern USA. *Hydrological Processes*. 15: 23-38.

Hanson, G. J., A. Simon, and K. R. Cook. 2002. Non-vertical jet testing of cohesive streambank materials. ASAE Paper No. 02-2119. St. Joseph, MI: ASAE.

Harder, L., K. Arulanandan, P. Rabbon, R. Green, and M. Wahler. 1976. Laboratory Techniques in the Prediction of Soil Erodibility. *PB-263 093 - National Technical Information Service*. 29.

Heinzen, R. T. 1976. Erodibility Criteria for Soil. MS thesis. University of CA, Davis.

Hollick, M. 1976. Towards a routine test for the assessment of the critical tractive forces of cohesive soils. *Transactions of the ASAE*. 19 (6): 1076-1081.

Houwing, E. J., and L. C. van Rijn. 1998. In Situ Erosion Flume (ISEF): determination of bed-shear stress and erosion of a kaolinite bed. *Journal of Sea Research*. 39 (3-4): 243-253.

Julian, J. P., and R. Torres. 2006. Hydraulic erosion of cohesive riverbanks. *Geomorphology*. 76 (1-2): 193-206.

Kamphuis, J. W., and K. R. Hall. 1983. Cohesive material erosion by unidirectional current. *Journal of Hydraulic Engineering*. 109 (1): 49-61.

Knapen, A., J. Poesen, G. Govers, G. Gyssels, and J. Nachtergaele. 2007. Resistance of soils to concentrated flow erosion: A review. *Earth-Science Reviews*. 80 (1-2): 75-109.

Knighton, D. 1998. *Fluvial Forms and Processes: A New Perspective*. New York: Oxford University Press, Inc.

Langendoen, E. 2000. CONCEPTS - Conservational Channel Evolution and Pollutant Transport System: Stream corridor version 1.0. Research Report No. 16. Oxford, MS: USDA-ARS.

Lavelle, W., and H. O. Mofjeld. 1987. Do critical stresses for incipient motion and erosion really exist? *Journal of Hydraulic Engineering*. 113 (9): 370-385.

Lawler, D. M. 1995. The impact of scale on the processes of channel-side sediment supply: a conceptual model. In *Effects of Scale on Interpretation and Management of Sediment and Water Quality. IAHS Pub. 226*. Wallingford, U.K.: International Association of Hydrological Sciences.

Lawler, D. M., C. R. Thorne, and J. M. Hooke. 1997. Chapter 6: Bank erosion and instability. In *Applied Fluvial Geomorphology for River Engineering and Management*, ed. C. R. Thorne, R. D. Hey and M. D. Newson. New York, N.Y.: John Wiley & Sons.

Lyle, W. M., and E. T. Smerdon. 1965. Relation of compaction and other soil properties to erosion resistance of soils. *Transactions of the ASAE*. 8: 419-422.

Mallison, T. 2008. Comparing In Situ Submerged Jet Test Device and Laboratory Flume Methods to Estimate Erosional Properties of Cohesive Soils for Bank Stability Models. M.S., Civil and Environmental Engineering, Knoxville, Tennessee: University of Tennessee.

Mazurek, K. A., N. Rajaratnam, and D. C. Sego. 2001. Scour of cohesive soil by submerged circular turbulent impinging jets. *Journal of Hydraulic Engineering*. 127 (7): 598-606.

Moldwin, M. B., and S. Rose. 2009. Documenting precision and accuracy in the open data policy era. *EOS, Transactions of the American Geophysical Union*. 9 (32).

Moody, J. A., J. D. Smith, and B. W. Ragan. 2005. Critical shear stress for erosion of cohesive soils subjected to temperatures typical of wildfires. *Journal of Geophysical Research-Earth Surface*. 110 (F1): 13.

Moore, W. L., and F. D. J. Masch. 1962. Experiments on the scour resistance of cohesive sediments. *Journal of Geophysical Research*. 67 (4): 1437-1446.

Nearing, M. A., G. R. Foster, L. J. Lane, and S. C. Finkner. 1989. A process-based soil erosion model for USDA-water erosion prediction project technology. *Transactions of the ASAE*. 32 (5): 1587-1593.

Osman, A. M., and C. R. Thorne. 1988. Riverbank stability analysis I: Theory. *Journal of Hydraulic Engineering*. 114: 134-150.

Ott, R. L., and M. Longnecker. 2001. *An Introduction to Statistical Methods and Data Analysis*. Fifth edition. Pacific Grove, CA: Thomson Learning, Inc. (Duxbury).

Owoputi, L. O., and W. J. Stolte. 1995. Soil detachment in the physically based soil erosion process: A review. *Transactions of the ASAE*. 38 (4): 1099-1110.

Paintal, A. S. 1971. Concept Of Critical Shear Stress In Loose Boundary Open Channels. *Journal of Hydraulic Research*. 9 (1): 91-113.

Partheniades, E. 1965. Erosion and deposition of cohesive soils. *Journal of the Hydraulics Division of the ASCE*. 91 (HY1): 105-139.

Partheniades, E., and R. E. Paaswell. 1968. Erosion of cohesive soil and channel stabilization. In *Civil Engineering Report vol. 19*. Buffalo, N.Y.: New York State University.

Pons, L. 2003. Helping states slow sediment movement: A high-tech approach to Clean Water Act sediment requirements. *Agricultural Research Magazine*. 51 (12): 12-14.

Poreh, M., and J. E. Cermak. 1959. Flow characteristics of a circular submerged jet impinging normally on a smooth boundary. In *Proceedings of the Sixth Annual Conference on Fluid Mechanics*, 198-212. University of Texas, Austin.

Potter, K. N., J. d. J. Velazquez-Garcia, and H. A. Torbert. 2002. Use of a submerged jet device to determine channel erodibility coefficients of selected soils of Mexico. *Journal of Soil and Water Conservation*. 57 (5): 272-277.

Ravens, T. M., and P. M. Gschwend. 1999. Flume measurements of sediment erodibility in Boston Harbor. *Journal of Hydraulic Engineering*. 125 (10): 998-1005.

Robert, A. 2003. *River Processes An introduction to fluvial dynamics*. New York: Oxford University Press, Inc.

Shields, A. 1936. *Application of similarity principles and turbulence research to bed-load movement*. Translated by W. P. Ott and J. C. van Uchelen. Pasadena, CA: USDA Soil Conservation Service Laboratory, California Institute of Technology.

Simon, A., A. Curini, S. E. Darby, and E. J. Langendoen. 2000. Bank and near-bank processes in an incised channel. *Geomorphology*. 35 (3-4): 193-217.

Smerdon, E. T. 1964. Effect of rainfall on critical tractive forces in channels with shallow flow. *Transactions of the ASAE*. 7: 287-290.

Smerdon, E. T., and R. P. Beasley. 1961. Critical tractive forces in cohesive soils. *Agricultural Engineering Research*. 42 (1): 26-29.

Stein, O. R., C. V. Alonso, and P. Y. Julien. 1993. Mechanics of jet scour downstream of a headcut. *Journal of Hydraulic Research*. 31 (6): 723-738.

Stein, O. R., and D. D. Nett. 1997. Impinging jet calibration of excess shear sediment detachment parameters. *Transactions of the ASAE*. 40 (6): 1573-1580.

Sturm, T. W. 2010. *Open Channel Hydraulics*. 2nd edition. New York, NY: McGraw-Hill Companies, Inc.

Temple, D. M., and G. J. Hanson. 1994. Headcut development in vegetated earth spillways. *Applied Engineering in Agriculture*. 10 (5): 677-682.

Thoman, R. W., and S. L. Niezgoda. 2008. Determining erodibility, critical shear stress, and allowable discharge estimates for cohesive channels: case study in the Powder River Basin of Wyoming. *Journal of Hydraulic Engineering*. 134 (12): 1677-1687.

Thomas, R. 2009. Personal communication, 3 November, 2009.

Thorne, C. R. 1982. Processes and mechanisms of river bank erosion. In *Gravel-bed Rivers*, ed. R. D. Hey, J. C. Bathurst and C. R. Thorne. New York: John Wiley & Sons, Ltd.

Thorne, C. R., and A. M. Osman. 1988. Riverbank stability analysis. II. Applications. *Journal of Hydraulic Engineering*. 114: 151-173.

USACE. 1993. *HEC-6: Scour and Deposition in Rivers and Resevoirs, User's Manual, Version 4.1*. Alexandria, VA: U.S. Army Corp of Engineers, Hydrologic Engineering Center.

USDA. 1996. Soil Survey Laboratory Methods Manual. Soil Survey Investigations Report No. 42. Lincoln, NE: USDA-NRCS National Soil Survey Center.

USEPA. 2002. National Water Quality Inventory: 2002 Report (305(b) report). Washington, D.C.

Vanoni, V. A. 1977. *Sedimentation Engineering*. New York: ASCE.

Viegas, D. X., and A. R. J. Borges. 1986. An erosion technique for the measurement of the shear stress field on a flat plate. *Journal of Physics E: Scientific Instruments*. 19 (8): 625-630.

Wan, C. F., and R. Fell. 2004. Investigation of rate of erosion of soils in embankment dams. *Journal of Geotechnical and Geoenvironmental Engineering*. 130 (4): 373-380.

Wilcock, P. R. 1996. Estimating local bed shear stress from velocity observations. *Water Resources Research*. 32 (11): 3361-3366.

Wynn, T. M. 2004. The effects of vegetation on stream bank erosion. PhD, Biological Systems Engineering, Blacksburg: Virginia Polytechnic Institute and State University.

Wynn, T. M., M. B. Henderson, and D. H. Vaughan. 2008. Changes in streambank erodibility and critical shear stress due to subaerial processes along a headwater stream, southwestern Virginia, USA. *Geomorphology*. 97 (3-4): 260-273.

Wynn, T. M., and S. Mostaghimi. 2006. The effects of vegetation and soil type on streambank erosion, Southwestern Virginia, USA *Journal of the American Water Resources Association*. 42 (1): 69-82.

Zhu, J. C., C. J. Gantzer, S. H. Anderson, R. L. Peyton, and E. E. Alberts. 2001. Comparison of concerntrated flow-detachment equations for low shear stress. *Soil and Tillage Research*. 61: 203-212.

Appendix A: Before and After Testing Pictures

A.2. Jet Testing

A.2.1. Clay Loam

Figure A.1. Clay loam Run 1 before (left) and after (right) jet testing.

Figure A.2. Clay loam Run 2 before (left) and after (right) jet testing.

Figure A.3. Clay loam Run 3 before (left) and after (right) jet testing.

Figure A.4. Clay loam Run 4 before (left) and after (right) jet testing.

Figure A.5. Clay loam Run 5 before (left) and after (right) jet testing.

Figure A.6. Clay loam Run 6 before (left) and after (right) jet testing.

Figure A.7. Clay loam Run 7 before (left) and after (right) jet testing.

Figure A.8. Clay loam Run 8 before (left) and after (right) jet testing.

Figure A.9. Clay loam Run 9 before (left) and after (right) jet testing.

Figure A.10. Clay loam Run 10 before (left) and after (right) jet testing.

Figure A.11. Clay loam Run 11 before (left) and after (right) jet testing.

A.2.2. Clay

Figure A.12. Clay Run 1 before (left) and after (right) jet testing.

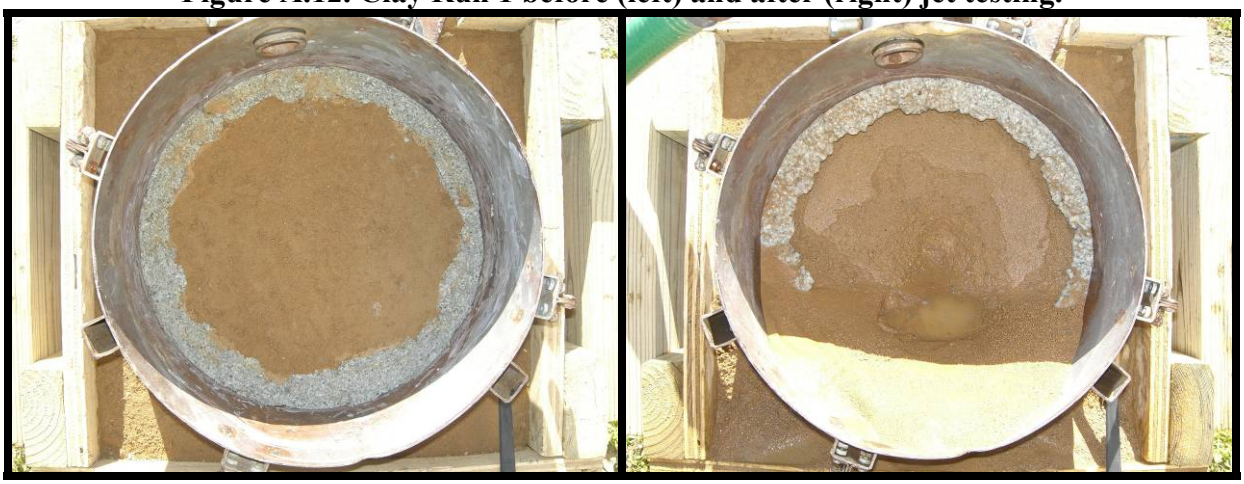

Figure A.13. Clay Run 2 before (left) and after (right) jet testing.

Figure A.14. Clay Run 3 before (left) and after (right) jet testing.

Figure A.15. Clay Run 4 before (left) and after (right) jet testing.

Figure A.16. Clay Run 5 before (left) and after (right) jet testing.

Figure A.17. Clay Run 6 before (left) and after (right) jet testing.

Figure A.18. Clay Run 7 before (left) and after (right) jet testing.

Figure A.19. Clay Run 8 before (left) and after (right) jet testing.

Figure A.20. Clay Run 9 before (left) and after (right) jet testing.

Figure A.21. Clay Run 10 before (left) and after (right) jet testing.

A.3. Flume Testing

A.3.1. Clay Loam

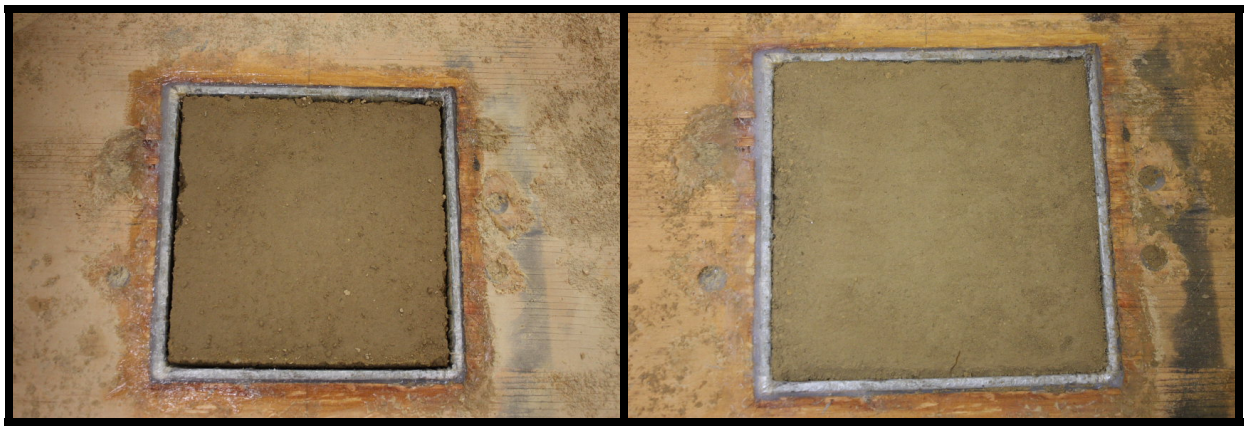

Figure A.22. Clay loam Run 1 before (left) and after (right) flume testing.

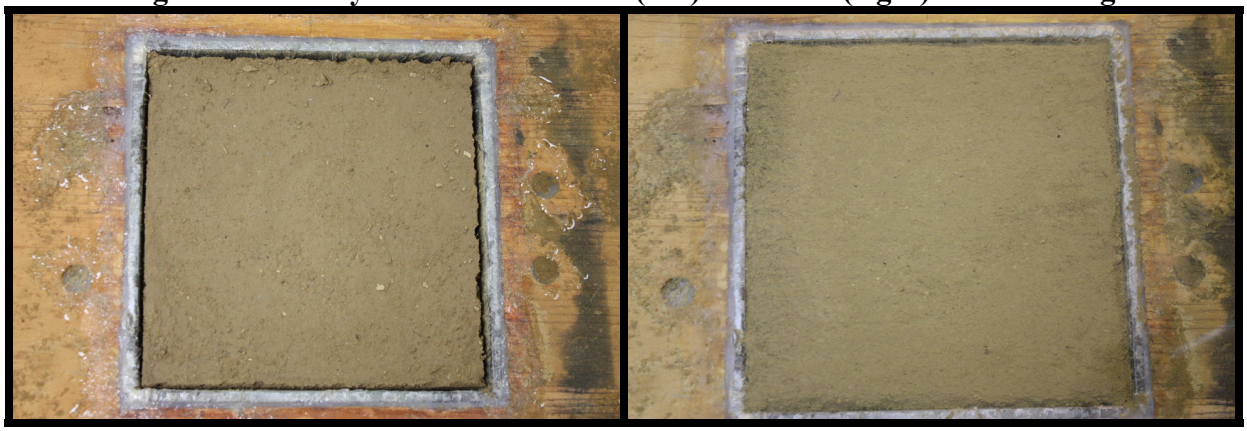

Figure A.23. Clay loam Run 2 before (left) and after (right) flume testing.

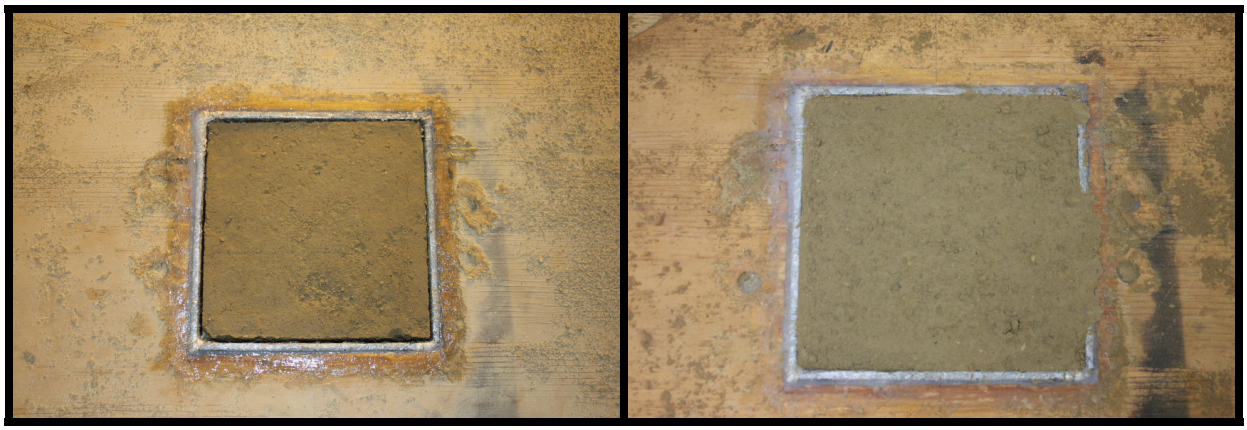

Figure A.24. Clay loam Run 3 before (left) and after (right) flume testing.

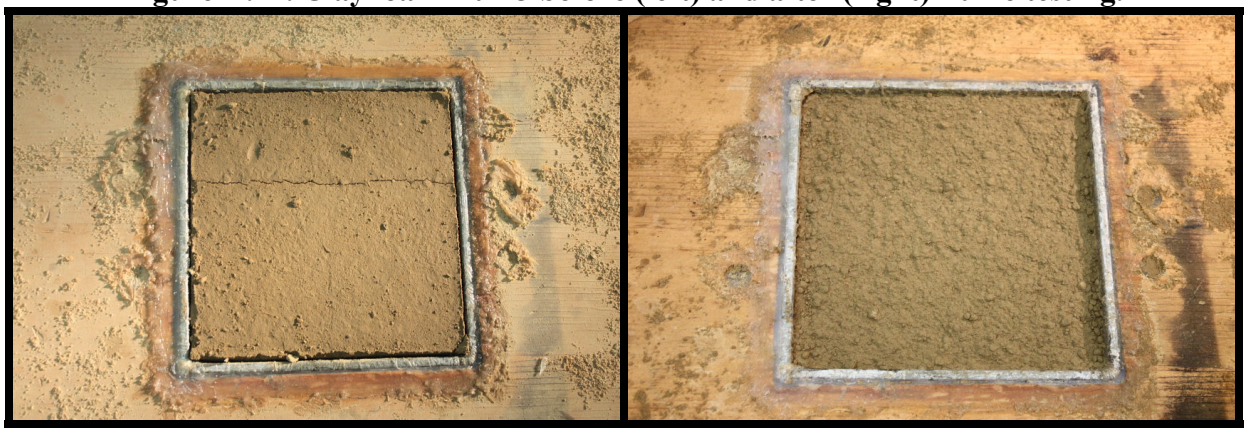

Figure A.25 Clay loam Run 4 before (left) and after (right) flume testing.

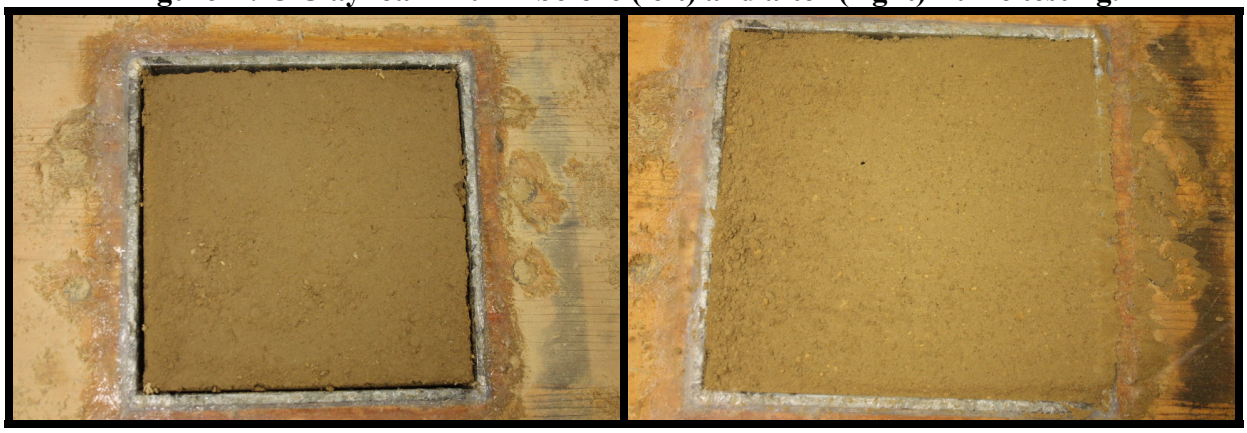

Figure A.26. Clay loam Run 5 before (left) and after (right) flume testing.

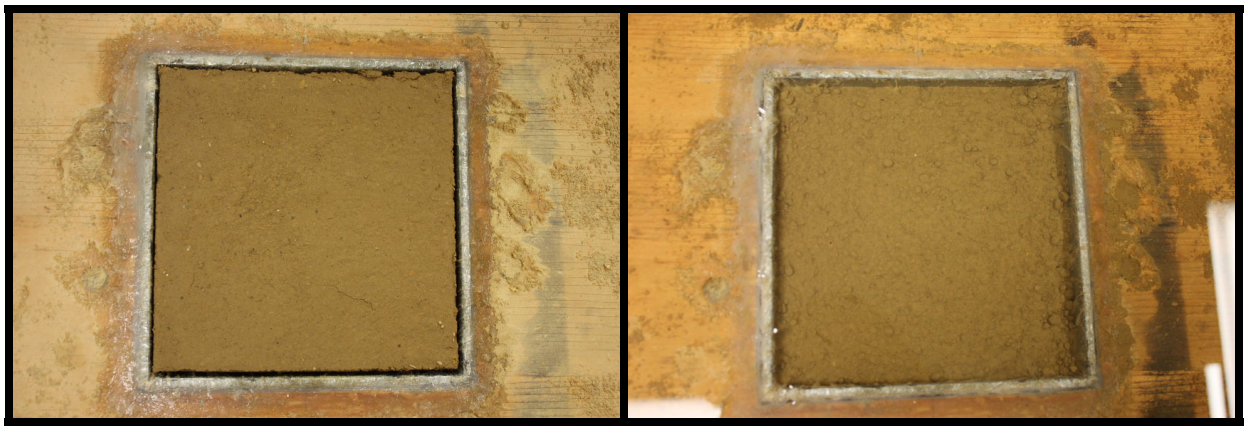

Figure A.27. Clay loam Run 6 before (left) and after (right) flume testing.

Figure A.28. Clay loam Run 7 before (left) and after (right) flume testing.

A.3.2. Clay

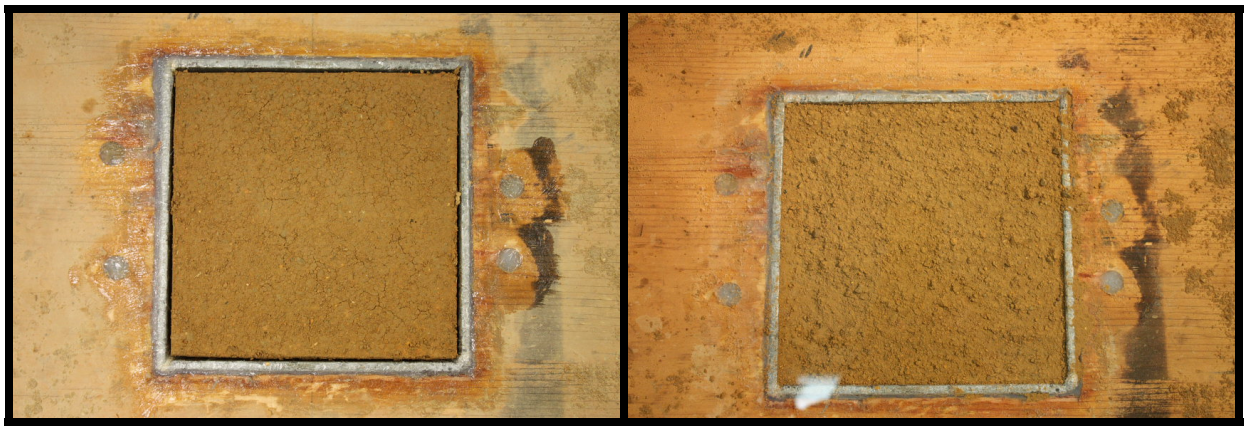

Figure A.29. Clay Run 1 before (left) and after (right) flume testing.

Figure A.30. Clay Run 2 before (left) and after (right) flume testing.

Figure A.31. Clay Run 3 before (left) and after (right) flume testing.

Figure A.32. Clay Run 4 before (left) and after (right) flume testing.

Figure A.33. Clay Run 5 before (left) and after (right) flume testing.

Appendix B: Flume Test Velocity Profiles

B.2. Clay Loam Measurements

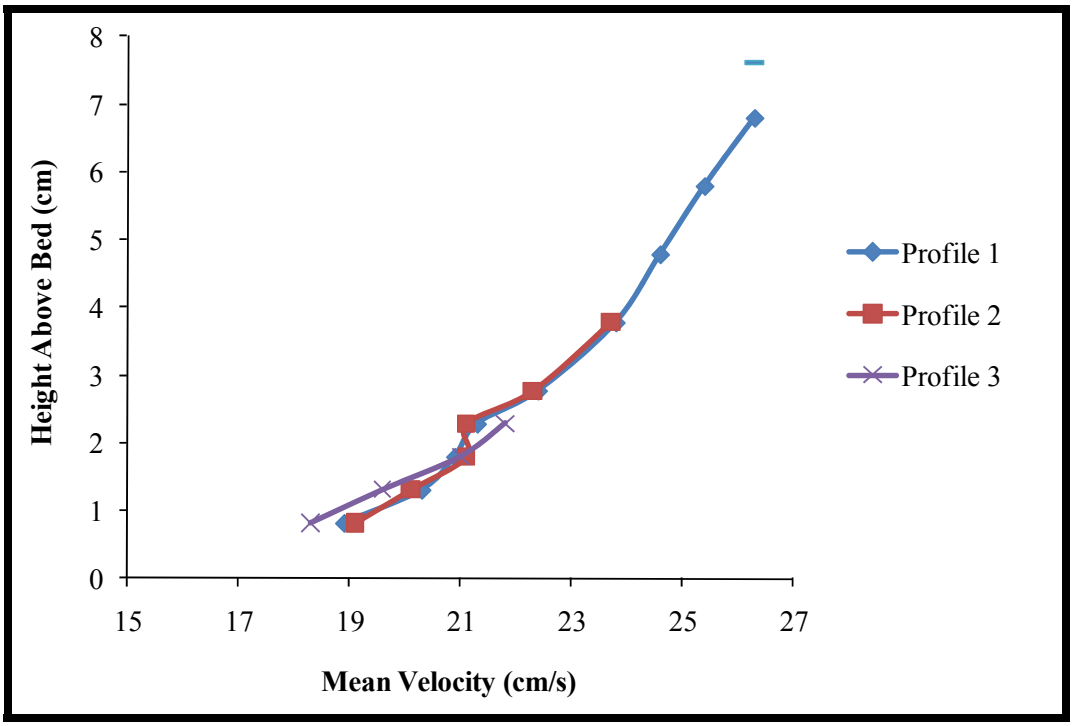

Figure B.1. Velocity profiles for clay loam Run 1.

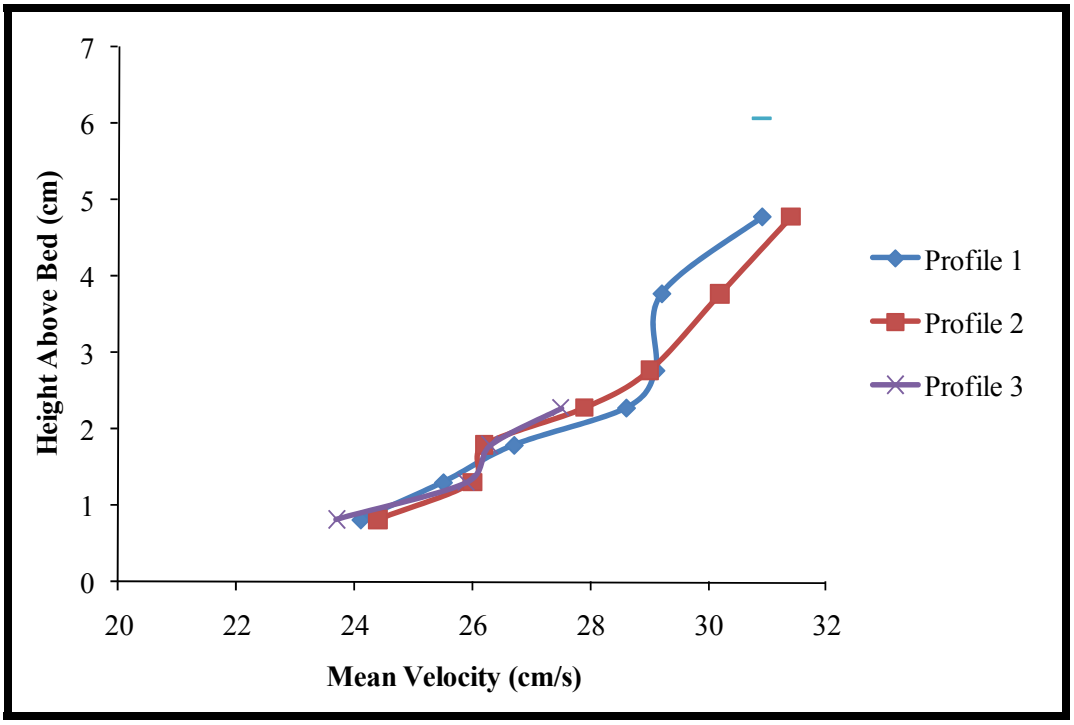

Figure B.2. Velocity profiles for clay loam Run 2.

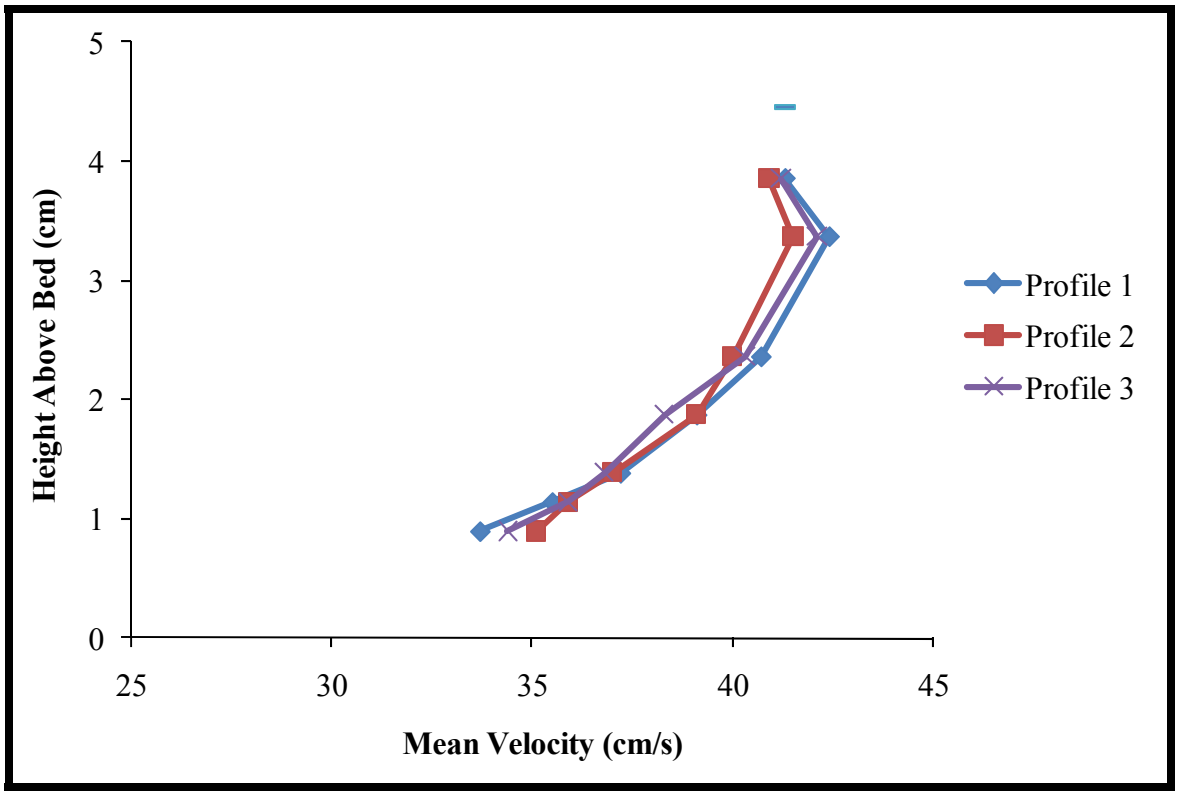

Figure B.3. Velocity profiles for clay loam Run 3.

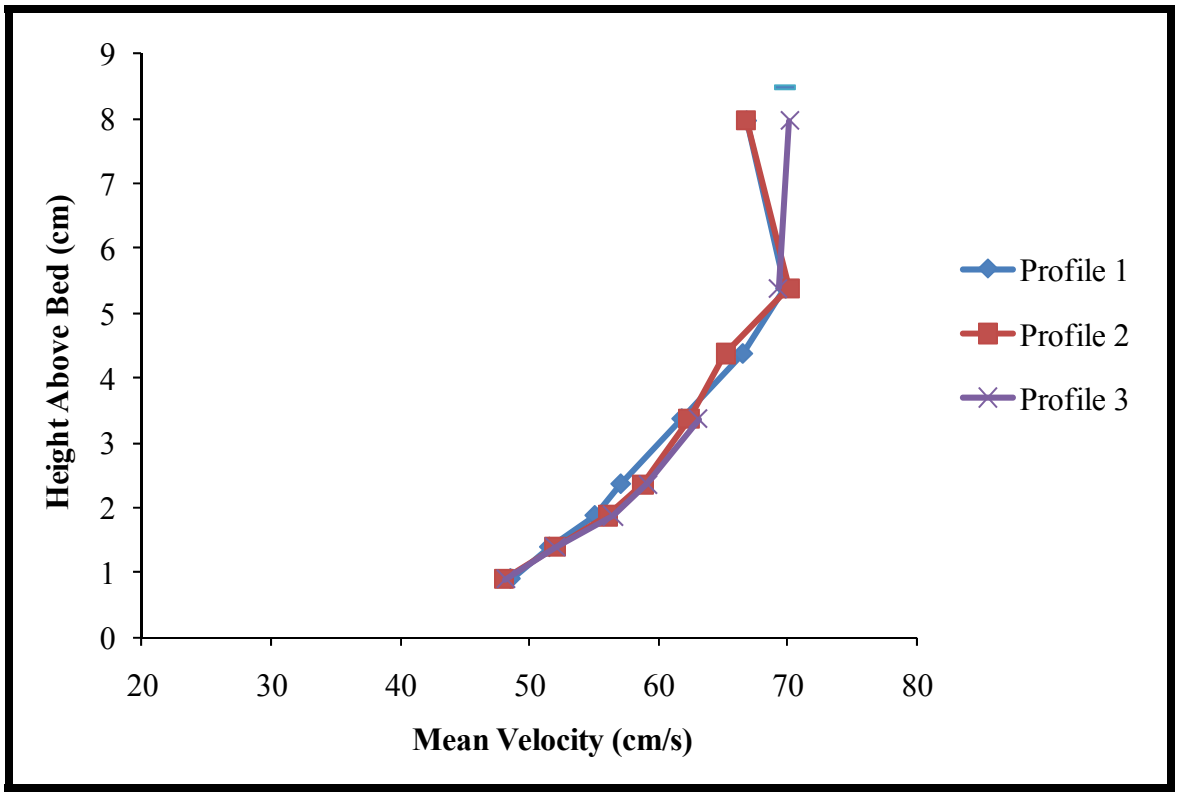

Figure B.4. Velocity profiles for clay loam Run 4.

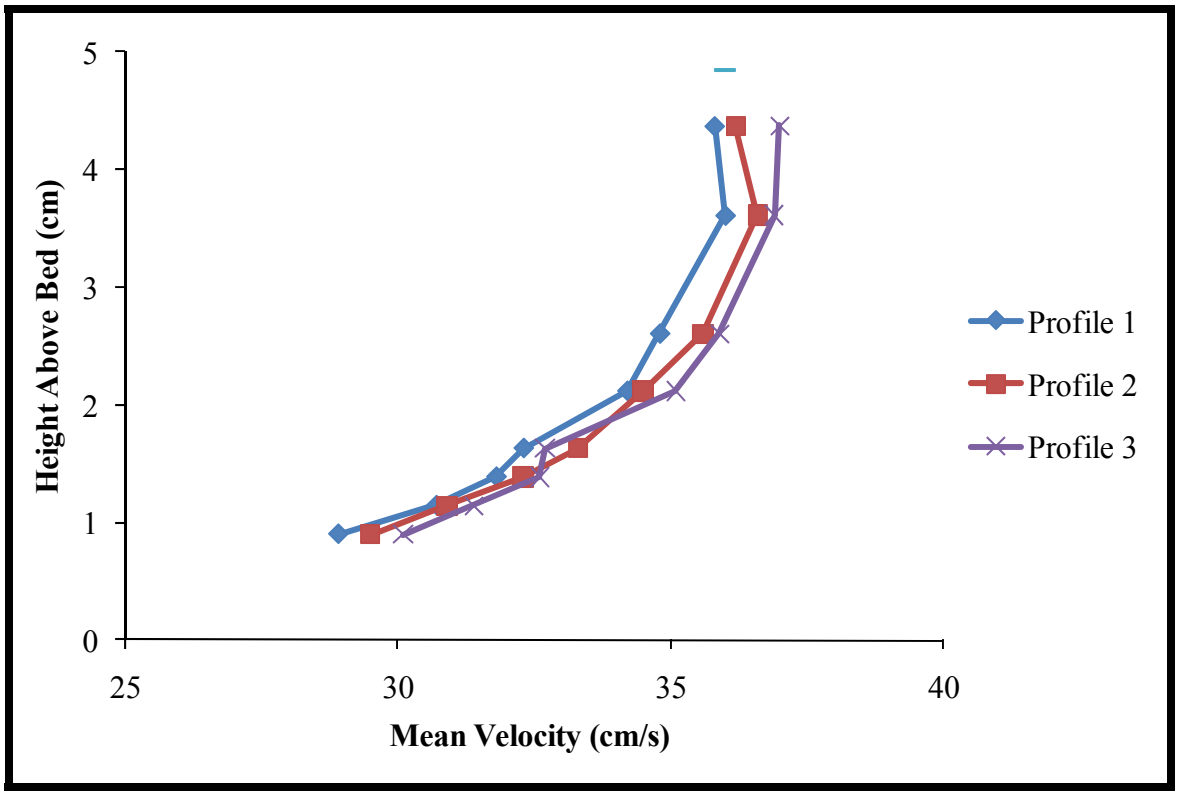

Figure B.5. Velocity profiles for clay loam Run 5.

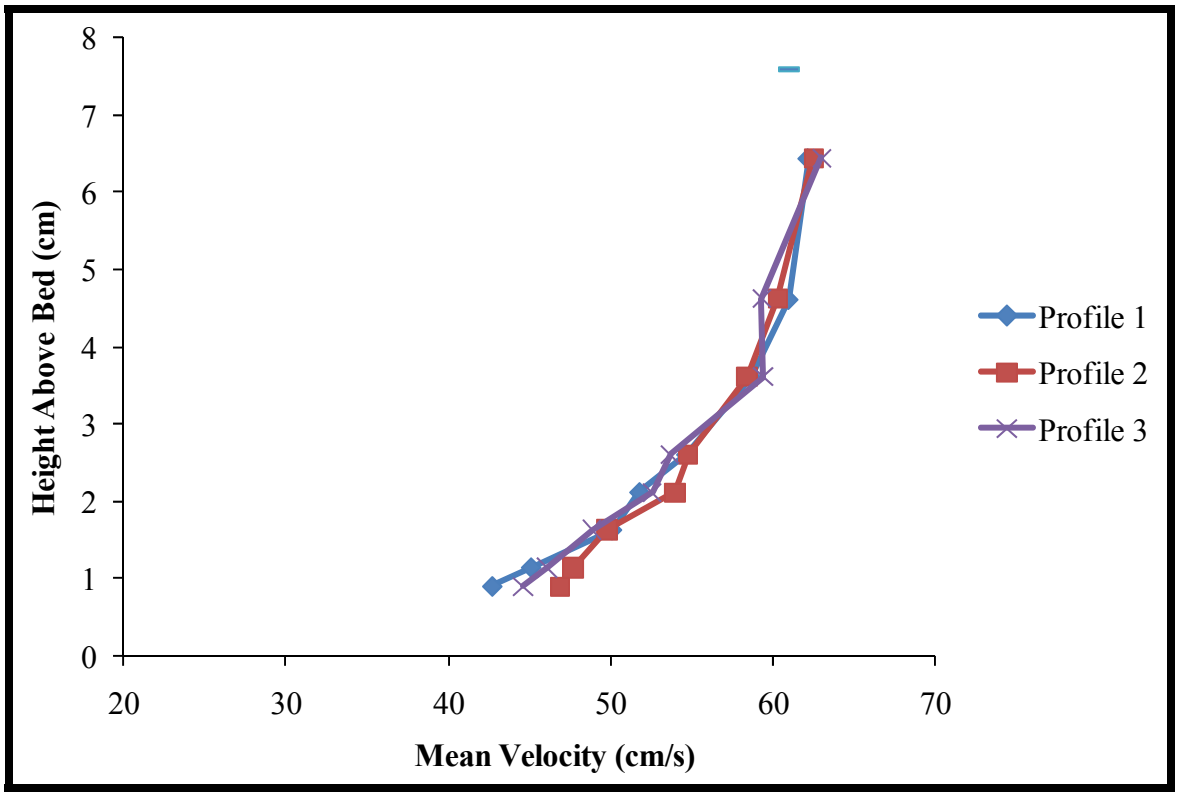

Figure B.6. Velocity profiles for clay loam Run 6.

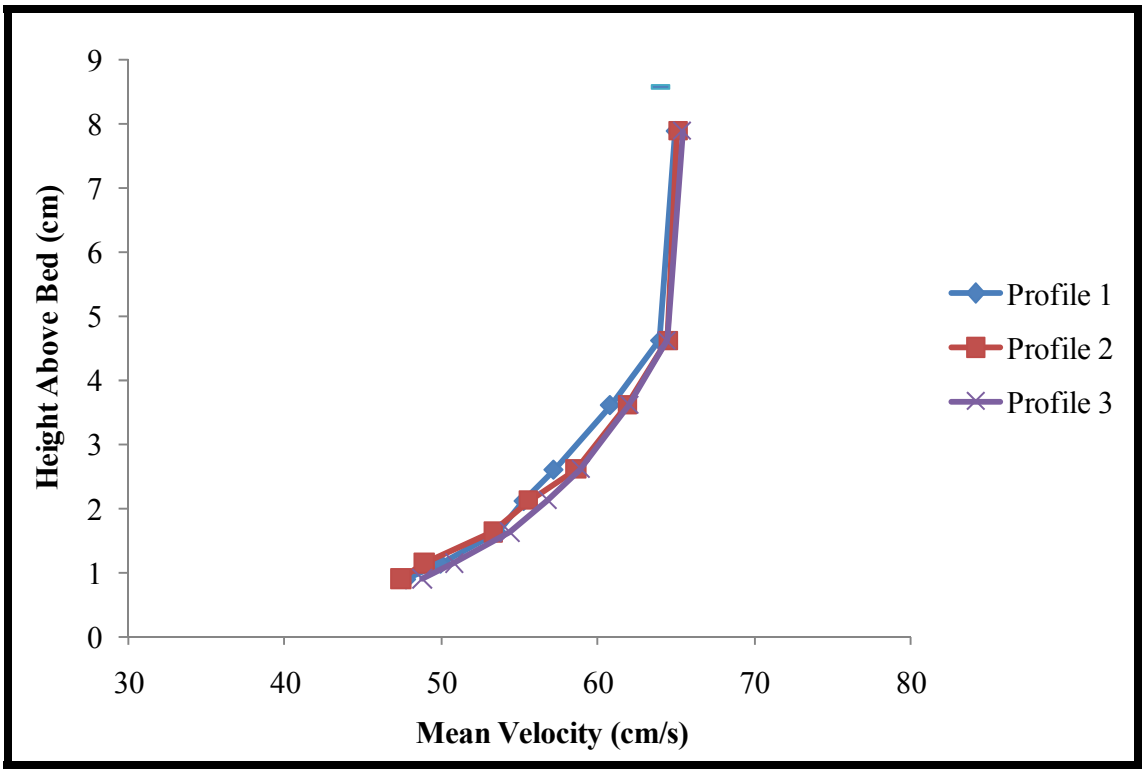

Figure B.7. Velocity profiles for clay loam Run 7.

B.3. Clay Measurements

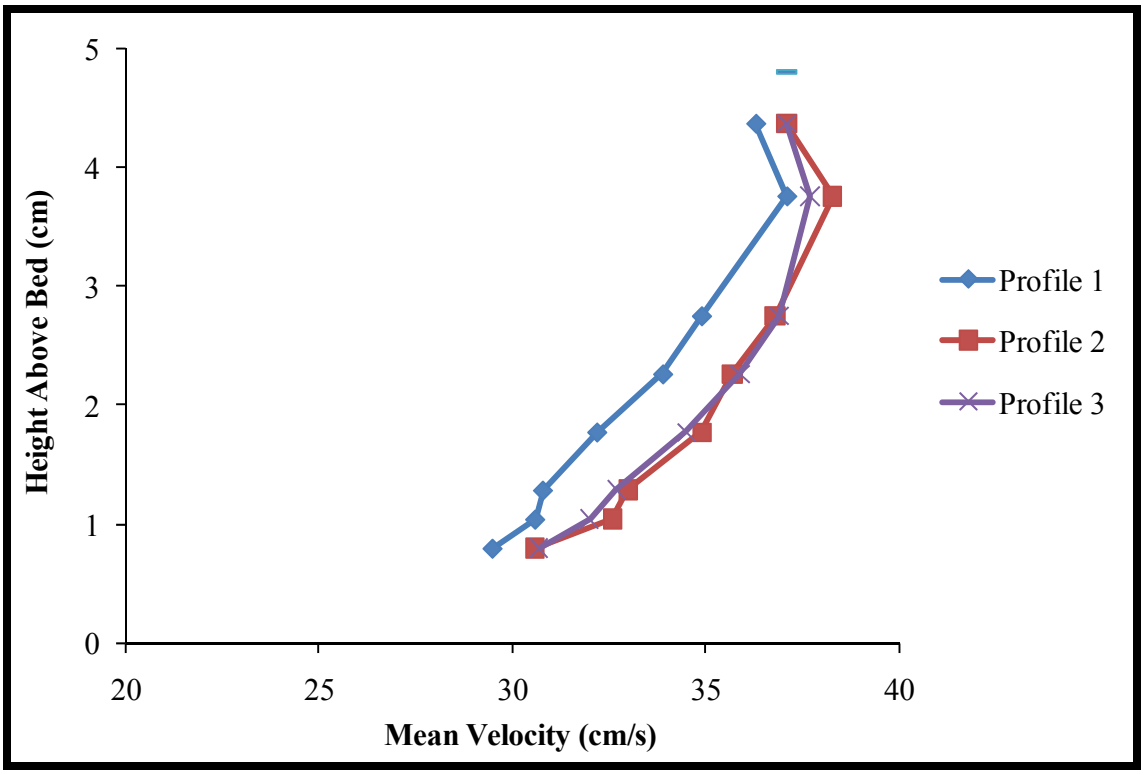

Figure B.8. Velocity profiles for clay Run 1.

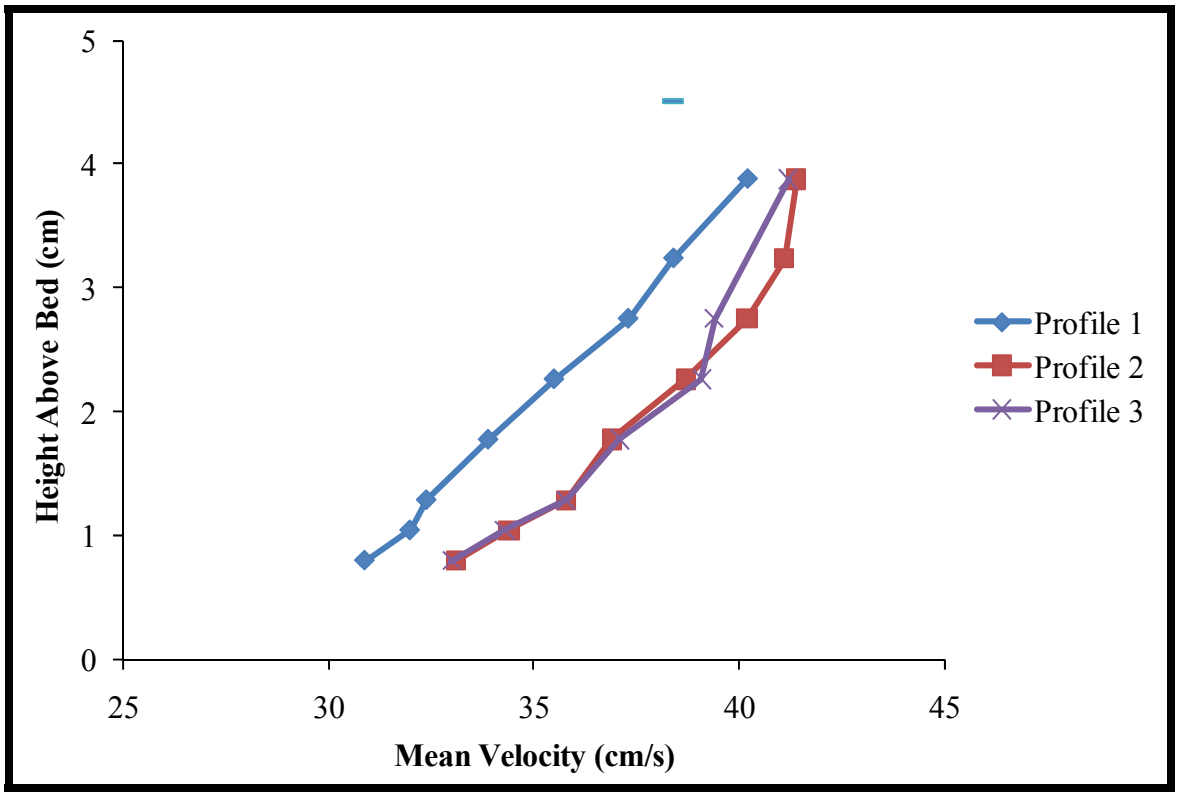

Figure B.9. Velocity profiles for clay Run 2.

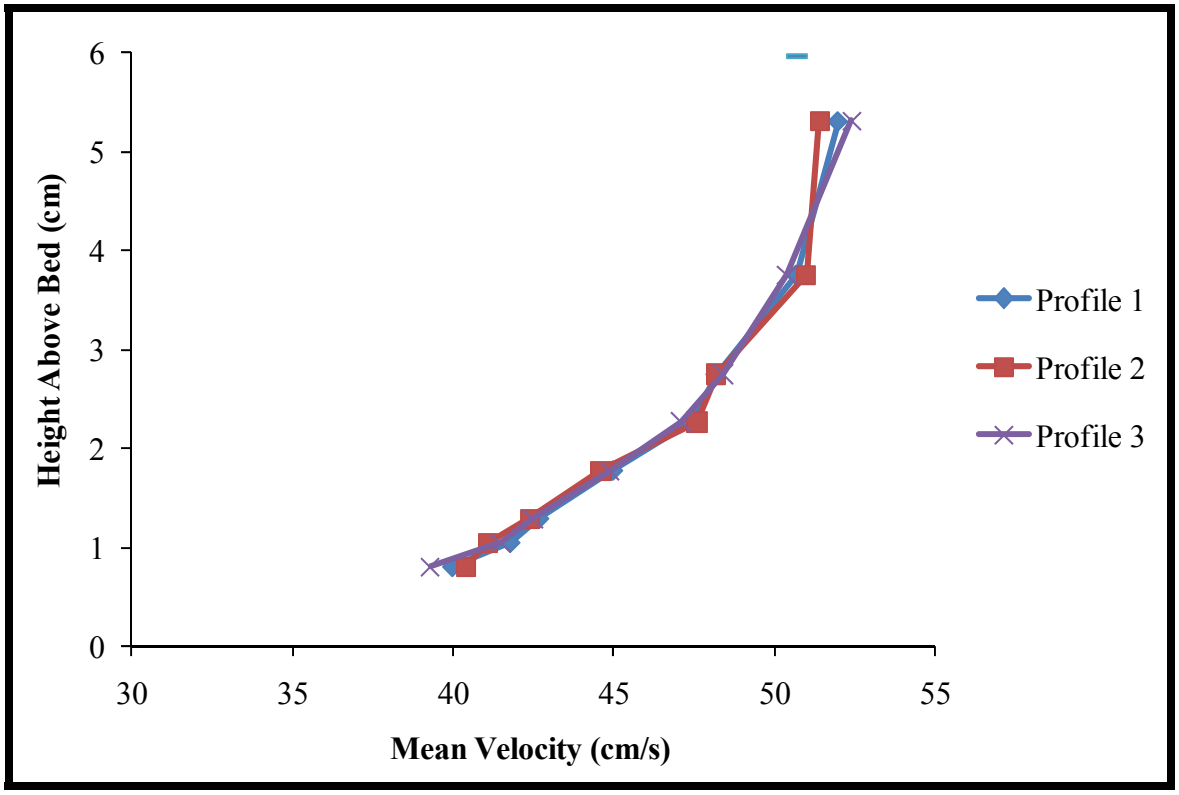

Figure B.10. Velocity profiles for clay Run 3.

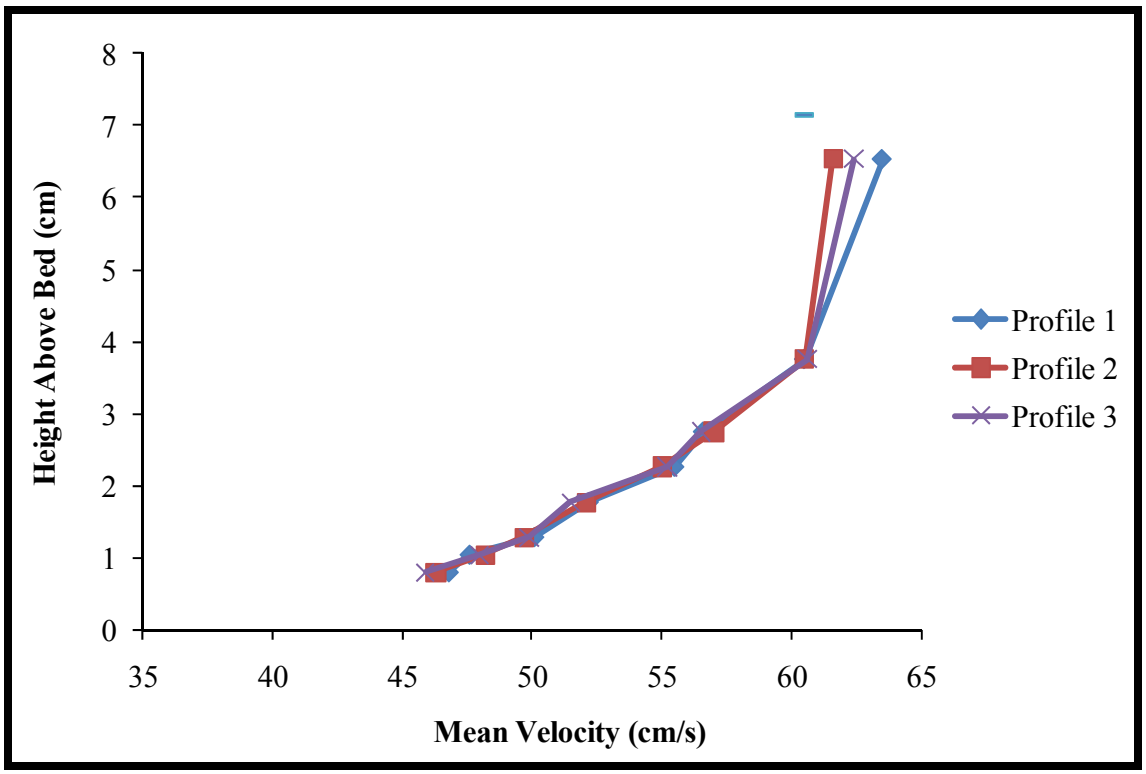

Figure B.11. Velocity profiles for clay Run 4.

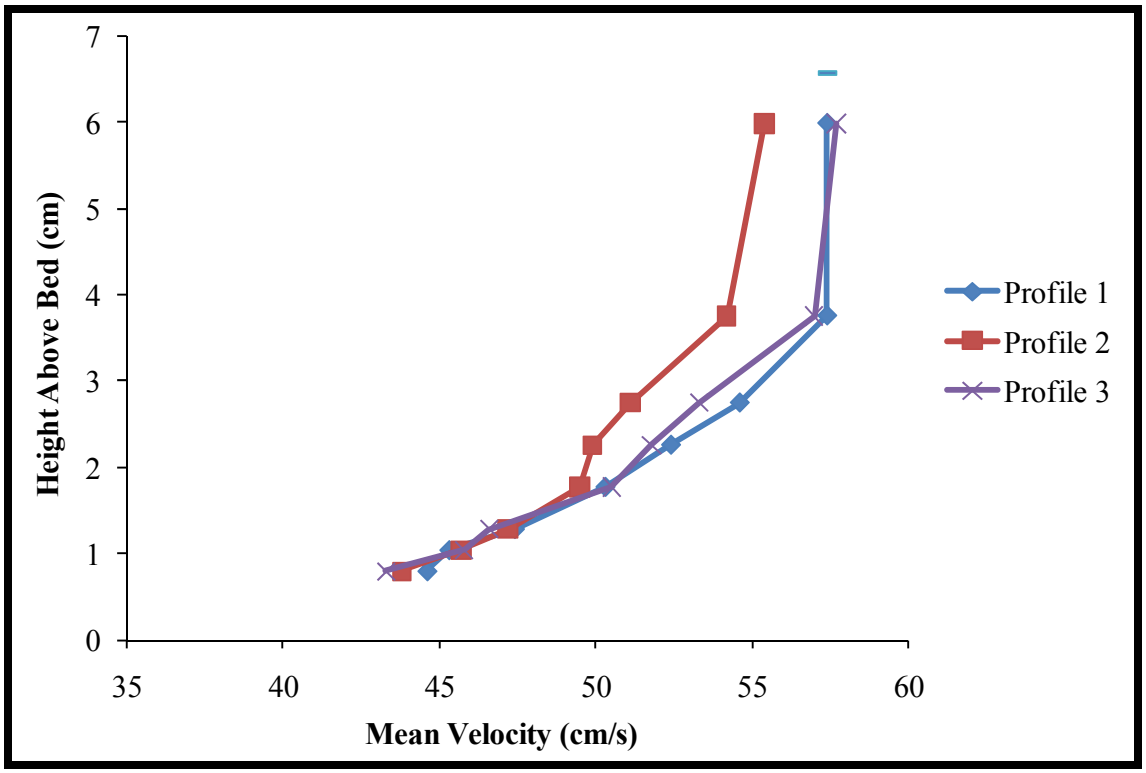

Figure B.12. Velocity profiles for clay Run 5

Appendix C: Jet Test Device Tests Raw Data

C.1. Clay Loam Measurements

Table C.1. JTD clay loam soil moisture content and water conditions.

		Water Temp (°C)				Conductivity (µS/cm)			
Run Number	Compacting θ_d	Pre-test	Test beginning[a]	Test end[b]	Post-test	Pre-test	Test beginning[a]	Test end[b]	Post-test
Clay Loam 1	0.111	---	15.2	---	---	---	143	142	---
Clay Loam 2	0.134	---	19.4	---	---	---	151	156	---
Clay Loam 3	0.112	---	20.0	---	---	---	155	165	---
Clay Loam 4	0.120	---	20.5	---	---	---	158	162	---
Clay Loam 5	0.121	---	21.3	---	---	---	156	152	---
Clay Loam 6	0.128	---	21.0	---	---	---	160	151	---
Clay Loam 7	0.122	---	21.3	---	---	---	153	---	---
Clay Loam 8	0.126	---	21.6	21.6	---	---	172	171	---
Clay Loam 9	0.123	---	21.2	---	---	---	155	158	---
Clay Loam 10	0.141	22.6	23.2	---	22.7	173	165	176	184
Clay Loam 11*	0.126	23.5	24.0	24.1	23.7	197	210	200	200

[a]Usually taken after 5 or 10 minutes; [b]Taken at end of test at 45 minutes; *Excluded from statistics

Table C.2. JTD clay loam post-test soil properties.

Run	Sample Location: Inside or Outside Ring	Sample #	Surface or Bottom	ρ_b (g/cm^3)	θ_d (g/g)
Clay Loam 1	Inside	1	Bottom	1.483	0.227
Clay Loam 1	Inside	2	Surface	1.515	0.227
Clay Loam 1	Inside	2	Bottom	1.576	0.213
Clay Loam 1	Outside	1	Surface	1.509**	0.215
Clay Loam 1	Outside	1	Bottom	---	0.207
Clay Loam 2	Inside	1	Surface	1.511	0.228
Clay Loam 2	Inside	1	Bottom	1.587	0.218
Clay Loam 2	Outside	1	Bottom	1.559	0.211
Clay Loam 3	Inside	1	Surface	1.535	0.235
Clay Loam 3	Inside	1	Bottom	1.550	0.225
Clay Loam 3	Outside	1	Surface	1.489	0.228
Clay Loam 3	Outside	1	Bottom	---	0.224
Clay Loam 4	Inside	1	Surface	1.542	0.243
Clay Loam 4	Outside	1	Surface	1.412	0.247
Clay Loam 5	Inside	1	Surface	1.518	0.234
Clay Loam 5	Outside	1	Surface	1.541	0.222
Clay Loam 6	Inside	1	Surface	1.534	0.238
Clay Loam 6	Inside	1	Bottom	---	0.227
Clay Loam 6	Outside	1	Bottom	1.460	0.237
Clay Loam 6	Outside	2	Bottom	1.534	0.229
Clay Loam 7	Inside	1	Surface	1.521	0.237
Clay Loam 7	Outside	1	Bottom	1.510	0.232
Clay Loam 8	Inside	1	Surface	1.558	0.229
Clay Loam 8	Inside	1	Bottom	1.568**	0.215
Clay Loam 8	Outside	1	Surface	1.480	0.219
Clay Loam 9	Inside	1	Surface	1.532	0.241
Clay Loam 9	Inside	1	Bottom	1.543	0.226
Clay Loam 9	Outside	1	Surface	---	0.222
Clay Loam 10	Inside	1	Surface	1.535	0.240
Clay Loam 10	Outside	1	Surface	1.530	0.231
Clay Loam 10	Outside	1	Bottom	---	0.243
Clay Loam 11*	Inside	1	Surface	1.460	0.259
Clay Loam 11*	Inside	1	Bottom	1.519**	0.244
Clay Loam 11*	Outside	1	Surface	1.436	0.252
Clay Loam 11*	Outside	2	Surface	1.508	0.243
Clay Loam 11*	Outside	2	Bottom	---	0.238

*Excluded from statistics; **Ring not completely filled, but very close

Table C.3. JTD clay loam scour depth history.

	Clay Loam Cumulative Scour Depth (cm)										
Time (min)	*Run 1*	*Run 2*	*Run 3*	*Run 4*	*Run 5*	*Run 6*	*Run 7*	*Run 8*	*Run 9*	*Run 10*	*Run 11**
0	0.00	0.00	0.00	0.00	0.00	0.00	0.00	0.00	0.00	0.00	0.00
5	2.85	2.30	3.15	2.44	2.40	2.97	3.78	3.29	3.42	2.77	3.55
10	3.71	3.30	4.02	3.50	3.22	3.95	4.52	4.14	4.37	3.40	4.30
15	4.27	3.91	4.35	3.83	3.80	4.93	5.19	4.72	4.88	3.81	5.38
20	4.69	4.24	4.82	4.36	4.17	5.34	5.68	5.23	5.49	4.30	6.43
25	4.96	4.67	5.15	4.65	4.43	5.57	5.93	5.61	5.92	4.83	6.88
30	5.22	5.06	5.33	4.91	4.84	5.88	6.41	5.94	6.30	5.23	7.69
35	5.43	5.22	5.52	5.17	5.11	6.20	6.74	6.29	6.54	5.23	8.16
40	5.66	5.62	5.71	5.38	5.33	6.43	6.95	6.56	6.93	5.37	8.61
45	5.90	5.84	5.96	5.67	5.61	6.61	7.17	6.93	7.33	5.90	9.12

*Excluded from statistics

Table C.4. JTD clay loam calculated erosion parameters.

	τ_c (Pa)		k_d (cm^3/N-s)	
Jet Test Run	Blaisdell Method	Thomas	Blaisdell Method	Thomas
Clay Loam 1	0.568	10.130	1.678	5.064
Clay Loam 2	0.395	7.620	2.127	6.000
Clay Loam 3	0.783	8.364	2.307	7.666
Clay Loam 4	0.548	7.258	2.421	7.700
Clay Loam 5	0.480	8.008	1.989	5.728
Clay Loam 6	0.327	7.319	2.693	8.823
Clay Loam 7	0.419	7.809	2.589	7.718
Clay Loam 8	0.349	7.658	2.313	5.999
Clay Loam 9	0.283	6.547	2.813	7.141
Clay Loam 10	0.629	8.128	2.028	5.503
Clay Loam 11*	0.051	4.612	3.466	6.446

*Excluded from statistics

Table C.5. JTD clay loam 95% confidence intervals.

	95% CI for the Mean		95% CI for the Median	
Calculation Method	Lower CI	Upper CI	Lower CI	Upper CI
Blaisdell τ_c (Pa)	0.367	0.589	0.341	0.589
Blaisdell k_d (cm^3/N-s)	2.045	2.546	2.015	2.625
Thomas τ_c (Pa)	7.211	8.558	7.298	8.209
Thomas k_d (cm^3/N-s)	5.852	7.617	5.651	7.706

C.2. Clay Measurements

Table C.6. JTD clay soil moisture content and water conditions.

Run Number	Compacting θ_d	Water Temp (°C)				Conductivity (µS/cm)			
		Pre-test	Test beginning[a]	Test end[b]	Post-test	Pre-test	Test beginning[a]	Test end[b]	Post-test
Clay 1	0.163	9.1	9.5	9.3	9.1	151	152	153	161
Clay 2	0.168	13.1	13.7	13.6	13.1	166	172	168	172
Clay 3	0.161	13.6	13.8	13.9	13.6	164	165	164	164
Clay 4	0.162	16.9	17.0	16.9	16.7	153	152	153	153
Clay 5	0.167	16.5	17.7	17.7	17.3	163	161	162	169
Clay 6	0.162	17.9	18.1	18.1	17.9	149	150	150	152
Clay 7	0.159	18.5	19.0	19.0	18.8	163	163	162	164
Clay 8	0.161	21.1	21.1	21.5	21.2	172	172	169	169
Clay 9	0.151	20.9	21.4	21.5	21.5	183	182	182	184
Clay 10	0.149	21.3	21.5	21.7	21.7	172	169	170	174

[a]Usually taken after 5 or 10 minutes; [b]Taken at end of test at 45 minutes

Table C.7. JTD clay post-test soil properties.

Run	Sample Location: Inside or Outside Ring	Sample #	Surface or Bottom	ρ_b (g/cm^3)	θ_d (g/g)
Clay 1	Inside	1	Bottom	1.398	0.288
Clay 1	Inside	2	Bottom	1.459	0.281
Clay 1	Outside	1	Bottom	1.474	0.257
Clay 1	Outside	2	Bottom	1.474	0.271
Clay 2	Inside	1	Bottom	1.463	0.268
Clay 2	Inside	2	Surface	---	0.269
Clay 2	Inside	2	Bottom	1.490	0.259
Clay 2	Outside	1	Surface	---	0.251
Clay 2	Outside	1	Bottom	1.567	0.241
Clay 2	Outside	2	Bottom	1.534*	0.254
Clay 3	Inside	1	Bottom	1.454*	0.274
Clay 3	Inside	2	Bottom	1.439	0.277
Clay 3	Outside	1	Bottom	1.492	0.255
Clay 4	Inside	1	Bottom	1.455	0.270
Clay 4	Outside	1	Bottom	1.490	0.265
Clay 4	Outside	2	Bottom	---	0.265
Clay 5	Inside	1	Surface	---	0.282
Clay 5	Inside	1	Bottom	1.448*	0.267
Clay 5	Inside	2	Bottom	1.499	0.265
Clay 5	Outside	1	Bottom	1.502*	0.265
Clay 6	Inside	1	Bottom	1.461	0.277
Clay 6	Inside	2	Surface	---	0.281
Clay 6	Inside	2	Bottom	---	0.282
Clay 6	Outside	1	Bottom	1.439	0.277
Clay 6	Outside	2	Bottom	1.484	0.268
Clay 7	Inside	1	Bottom	1.448	0.272
Clay 7	Inside	2	Bottom	1.446	0.276
Clay 7	Outside	1	Surface	---	0.250
Clay 7	Outside	1	Bottom	1.483	0.262
Clay 7	Outside	2	Bottom	1.495	0.265
Clay 8	Inside	1	Bottom	1.518	0.256
Clay 8	Inside	2	Bottom	1.537	0.250
Clay 8	Outside	1	Surface	---	0.268
Clay 8	Outside	1	Bottom	1.525	0.255
Clay 8	Outside	2	Bottom	1.459*	0.255
Clay 9	Inside	1	Bottom	1.430	0.280
Clay 9	Inside	2	Bottom	1.439	0.279
Clay 9	Outside	1	Surface	---	0.253
Clay 9	Outside	1	Bottom	1.490	0.251
Clay 9	Outside	2	Bottom	1.481	0.261
Clay 10	Inside	1	Bottom	1.443	0.272
Clay 10	Inside	2	Bottom	1.436*	0.273
Clay 10	Outside	1	Surface	---	0.291
Clay 10	Outside	1	Bottom	1.476	0.264
Clay 10	Outside	2	Bottom	1.478*	0.263

*Ring not completely filled, but very close

Table C.8. JTD clay scour depth history.

	Clay Cumulative Scour Depth (cm)									
Time (min)	*Run 1*	*Run 2*	*Run 3*	*Run 4*	*Run 5*	*Run 6*	*Run 7*	*Run 8*	*Run 9*	*Run 10*
0	0.00	0.00	0.00	0.00	0.00	0.00	0.00	0.00	0.00	0.00
5	3.86	3.15	3.13	3.18	2.77	3.77	4.01	2.58	4.30	4.80
10	4.71	3.56	3.61	4.08	3.48	4.39	4.93	3.09	5.02	5.05
15	5.15	4.07	4.13	4.90	3.79	4.94	5.13	3.33	5.44	5.47
20	5.51	4.54	4.45	5.17	3.99	5.12	5.52	3.52	5.86	5.68
25	5.90	4.79	4.71	5.50	4.43	5.43	5.61	3.68	6.05	5.79
30	6.25	4.99	4.94	5.85	4.54	5.80	5.87	3.82	6.25	6.09
35	6.60	5.26	5.13	6.38	4.90	5.98	6.18	4.03	6.50	6.31
40	6.77	5.35	5.30	6.59	5.33	6.12	6.31	4.11	6.78	6.45
45	7.00	5.59	5.42	7.10	5.70	6.31	6.39	4.30	6.80	6.48

Table C.9. JTD clay calculated erosion parameters.

	τ_c (Pa)		k_d (cm^3/N-s)	
Jet Test Run	Blaisdell Method	Thomas	Blaisdell Method	Thomas
Clay 1	0.567	7.664	2.688	8.217
Clay 2	1.133	10.390	1.777	5.958
Clay 3	1.186	10.200	1.856	6.804
Clay 4	0.296	7.321	2.229	5.117
Clay 5	0.877	8.496	1.786	4.351
Clay 6	1.058	9.682	2.129	7.176
Clay 7	1.324	9.813	2.293	8.471
Clay 8	2.720	12.820	1.355	4.898
Clay 9	1.052	9.301	2.429	8.453
Clay 10	2.303	10.070	2.529	9.408

Table C.10. JTD clay 95% confidence intervals.

	95% CI for the Mean		95% CI for the Median	
Calculation Method	Lower CI	Upper CI	Lower CI	Upper CI
Blaisdell τ_c (Pa)	0.725	1.779	0.771	1.659
Blaisdell k_d (cm^3/N-s)	1.814	2.400	1.783	2.463
Thomas τ_c (Pa)	8.461	10.691	8.211	10.265
Thomas k_d (cm^3/N-s)	5.634	8.137	5.042	8.459
Blaisdell τ_c (Pa) (w/o Run 8)	0.660	1.517	0.638	1.293
Blaisdell k_d (cm^3/N-s) (w/o Run 8)	1.936	2.446	1.802	2.506

Appendix D: Flume Tests Raw Data

D.1. Clay Loam Measurements

Table D.1. Flume clay loam settings and conditions.

Run Number	Flume Rate (Hz)	Tailgate Height (mm)	Discharge (m^3/s)			Reynolds Number	Froude Number	Applied Shear Stress (Pa)			Test Duration (s)
			Test Start	Test Middle	Test End			LOW[a]	VDL[b]	Average τ	
Clay Loam 1	15	35	0.0129	0.0137	0.0139	46144	0.206	0.184	0.168	0.020	2705
Clay Loam 2	15	25	0.0139	0.0143	0.0147	50201	0.305	0.248	0.254	0.335	2710
Clay Loam 3	15	0	0.0138	0.0141	0.0145	51649	0.480	0.467	0.625	0.497	2700
Clay Loam 4	45	0	0.0463	0.0487	0.0495	129919	0.622	1.917	2.083	2.647	2706
Clay Loam 5	15	10	0.0148	0.0164	0.0172	47621	0.484	0.364	0.516	0.565	2700
Clay Loam 6	35	0	0.0355	0.0372	0.0379	121470	0.564	1.521	1.736	4.479	2701
Clay Loam 7	45	0	0.0454	0.0464	0.0473	133475	0.590	1.283	1.611	1.781	2704

[a]Law of the Wall; [b]Velocity defect law

Table D.2. Flume clay loam erosion data.

Run Number	Soil loss (g)	% Soil loss	Erosion rate (g/s)	Erosion rate (cm/day)[a]	SSC[b] (mg/L)		
					Pre-test	Middle	Post-Test
Clay Loam 1	8.60	0.57%	0.0032	0.79	4.91	6.60	5.09
Clay Loam 2	4.79	0.32%	0.0018	0.44	7.20	6.33	5.10
Clay Loam 3	89.60	5.93%	0.0332	8.23	10.00	11.64	12.36
Clay Loam 4	340.16	22.57%	0.1257	30.65	12.25	34.34	48.96
Clay Loam 5	25.46	1.69%	0.0094	2.39	6.67	8.57	6.79
Clay Loam 6	565.51	37.45%	0.2094	53.41	15.56	35.93	57.90
Clay Loam 7	506.40	33.45%	0.1873	46.95	26.21	53.68	87.54

[a]Calculated from the test ρ_b and testing surface area; [b]Suspended sediment concentration

Table D.3. Flume clay loam soil conditions and water temperature and conductivity data.

Run Number	Compact θ_d[a]	Initial Test θ_d[b]	After Test θ_d[c]	Test ρ_b[d] (g/cm^3)	After Test ρ_b[e] (g/cm^3)	Water Temperature (°C)				Water Conductivity (µS/cm)			
						Pre-test	Test Start	Test Middle	Test End	Pre-test	Test Start	Test Middle	Test End
Clay Loam 1	0.121	0.181	---	1.550	---	19.4	19.5	19.5	19.5	150	151	151	153
Clay Loam 2	0.121	0.193	0.199	1.542	1.359	19.5	19.5	19.5	19.5	152	151	152	153
Clay Loam 3	0.116	0.182	0.228	1.548	1.359	19.9	19.9	20.0	20.0	156	157	158	157
Clay Loam 4	0.121	0.174	0.216	1.575	1.525	10.0	10.2	11.5	12.0	177	177	180	178
Clay Loam 5	0.116	0.187	0.217	1.514	1.346	11.5	11.9	12.1	12.2	155	161	161	164
Clay Loam 6	0.119	0.188	0.224	1.505	1.354	17.6	17.8	18.1	18.4	175	156	159	174
Clay Loam 7	0.116	0.184	0.212	1.532	1.433	12.3	12.7	13.7	14.5	141	150	150	152

[a]Gravimetric moisture content at compaction; [b]Calculated testing gravimetric moisture content; [c]Gravimetric moisture content after testing determined from sample; [d]Calculated bulk density; [e]Bulk density after testing from sample

Table D.4. Flume clay loam water depth measurements.

Run Number	Water Depth (cm)												Water Slope
	Upstream[a]			Upstream of box[b]			Downstream of box[c]			Downstream[d]			
	Test Start	Test Middle	Test End	Test Start	Test Middle	Test End	Test Start	Test Middle	Test End	Test Start	Test Middle	Test End	
Clay Loam 1[e]	7.37*	7.54	7.61	7.67	7.60	7.63	7.59	7.57	----	7.56	7.60	---	0.003%
Clay Loam 2	6.10	6.13	6.13	6.07	6.09	6.10	6.04	6.08	6.06	6.05	6.06	---	0.056%
Clay Loam 3	4.55	4.46	4.34	4.55	4.49	4.48	4.37	4.38	4.45	4.29	4.39	4.33	0.114%
Clay Loam 4	8.68	8.27	8.09	8.64	8.80	8.35	8.43	8.39	8.34	8.24	7.91	7.88	0.318%
Clay Loam 5	4.93	4.96	4.95	4.97	4.94	4.93	4.74	4.73	4.77	4.90	4.82	4.83	0.119%
Clay Loam 6	8.10	7.80	7.88	7.75	7.32	7.73	7.62	7.62	7.47	7.27	7.25	7.08	0.603%
Clay Loam 7	8.57	8.37	8.29	8.79	8.66	8.75	8.36	8.38	8.49	8.44	8.11	8.14	0.212%

[a]0.5 m upstream of upstream soil edge; [b]6.5 cm upstream of upstream soil edge; [c]6.5 cm downstream of downstream soil edge; [d]0.5 m downstream of downstream soil edge; [e]Different measurement method than other runs, zeroed point gage at bed and measured water surface; *measurement wrong, could not determine when reached bed

Table D.5. Flume clay loam applied shear stress from law of the wall and velocity defect law.

	Basic LOW						Velocity Defect Law					
	Profile 1		Profile 2		Profile 3		Profile 1		Profile 2		Profile 3	
Run Number	τ (Pa)	R^2	τ (Pa)	R^2	τ (Pa)	R^2	τ (Pa)	R^2	τ (Pa)	R^2	τ (Pa)	R^2
Clay Loam 1	0.207	0.977	0.148	0.942	0.197	0.991	0.160	0.960	0.148	0.942	0.197	0.991
Clay Loam 2	0.254	0.963	0.277	0.967	0.213	0.962	0.313	0.968	0.236	0.929	0.213	0.962
Clay Loam 3	0.587	0.940	0.462	0.963	0.352	0.958	0.839	0.997	0.477	0.986	0.559	0.988
Clay Loam 4	1.931	0.924	1.931	0.983	1.890	0.928	2.113	0.975	1.974	0.997	2.162	0.993
Clay Loam 5	0.356	0.953	0.370	0.964	0.366	0.943	0.505	0.986	0.534	0.994	0.510	0.978
Clay Loam 6	1.808	0.985	1.566	0.982	1.187	0.985	2.111	0.995	1.251	0.967	1.847	0.970
Clay Loam 7	1.230	0.974	1.168	0.968	1.450	0.957	1.507	0.994	1.849	0.996	1.478	>0.999

Table D.6. Flume clay loam Run 1 velocity data.

		Profile 1			Profile 2			Profile 3		
Point Gage Depth (cm)	Height above bed (cm)[a]	Average Velocity (cm/s)	Min Velocity (cm/s)	Max Velocity (cm/s)	Average Velocity (cm/s)	Min Velocity (cm/s)	Max Velocity (cm/s)	Average Velocity (cm/s)	Min Velocity (cm/s)	Max Velocity (cm/s)
43.769	0.82	18.9	14.0	24.7	19.1	14.5	100.5*	18.3	13.6	23.2
44.257	1.31	20.3	15.5	25.6	20.1	14.7	24.8	19.6	15.0	24.1
44.745	1.80	20.9	15.0	26.1	21.1	16.1	25.8	21.0	16.0	25.6
45.232	2.28	21.3	16.3	26.7	21.1	15.8	25.8	21.8	17.9	26.2
45.720	2.77	22.4	16.8	26.7	22.3	16.4	26.0	---	---	---
46.726	3.78	23.8	18.2	27.1	23.7	19.2	27.6	---	---	---
47.732	4.78	24.6	19.3	28.0	---	---	---	---	---	---
48.738	5.79	25.4	22.1	28.9	---	---	---	---	---	---
49.743	6.79	26.3	22.6	28.9	---	---	---	---	---	---

[a]Height above bed = point gage depth – (lowest measurement point gage depth – probe center above bed) ; *Velocity spike: 2nd to max = 45.8 cm/s, 3rd to max = 24.1 cm/s

Table D.7. Flume clay loam Run 2 velocity data.

		Profile 1			Profile 2			Profile 3		
Point Gage Depth (cm)	Height above bed (cm)	Average Velocity (cm/s)	Min Velocity (cm/s)	Max Velocity (cm/s)	Average Velocity (cm/s)	Min Velocity (cm/s)	Max Velocity (cm/s)	Average Velocity (cm/s)	Min Velocity (cm/s)	Max Velocity (cm/s)
43.891	0.82	24.1	17.2	29.5	24.4	18.0	31.2	23.7	18.3	52.9*
44.379	1.31	25.5	19.0	31.7	26.0	20.1	31.5	25.9	19.3	31.9
44.867	1.80	26.7	20.8	33.0	26.2	21.2	32.0	26.3	20.4	31.9
45.354	2.28	28.6	21.6	34.1	27.9	21.6	32.7	27.5	21.4	32.1
45.842	2.77	29.1	22.2	33.3	29.0	22.5	33.8	---	---	---
46.848	3.78	29.2	23.4	34.1	30.2	23.9	34.1	---	---	---
47.854	4.78	30.9	20.2	34.2	31.4	26.3	34.5	---	---	---

*Velocity spike: 2nd to max = 30.0 cm/s

Table D.8. Flume clay loam Run 3 velocity data.

		Profile 1			Profile 2			Profile 3		
Point Gage Depth (cm)	Height above bed (cm)	Average Velocity (cm/s)	Min Velocity (cm/s)	Max Velocity (cm/s)	Average Velocity (cm/s)	Min Velocity (cm/s)	Max Velocity (cm/s)	Average Velocity (cm/s)	Min Velocity (cm/s)	Max Velocity (cm/s)
43.769	0.90	33.7	25.6	41.6	35.1	27.8	43.1	34.4	25.9	42.9
44.013	1.14	35.5	26.7	44.6	35.9	27.5	44.6	35.9	28.4	43.5
44.257	1.39	37.2	29.1	45.2	37.0	28.7	44.3	36.8	29.2	43.9
44.745	1.88	39.1	30.5	45.9	39.1	31.1	46.1	38.3	30.1	46.2
45.232	2.36	40.7	32.5	47.0	40.0	46.2	32.4	40.3	32.8	46.6
46.238	3.37	42.4	34.3	47.1	41.5	34.9	47.9	42.1	33.9	48.6
46.726	3.86	41.3	35.1	46.6	40.9	33.6	46.1	41.2	33.7	73.8*

*Velocity spike: 2nd to max = 45.8 cm/s

Table D.9. Flume clay loam Run 4 velocity data.

		Profile 1			Profile 2			Profile 3		
Point Gage Depth (cm)	Height above bed (cm)	Average Velocity (cm/s)	Min Velocity (cm/s)	Max Velocity (cm/s)	Average Velocity (cm/s)	Min Velocity (cm/s)	Max Velocity (cm/s)	Average Velocity (cm/s)	Min Velocity (cm/s)	Max Velocity (cm/s)
43.769	0.90	48.6	32.8	67.5	48.0	34.2	78.0	48.2	32.0	63.4
44.257	1.39	51.6	37.0	66.0	52.0	37.9	63.9	52.0	38.1	67.9
44.745	1.88	55.1	38.7	70.7	56.1	40.1	69.7	56.5	39.9	71.1
45.232	2.36	57.1	41.5	71.1	58.8	37.3	74.6	59.2	43.4	72.2
46.238	3.37	61.8	45.0	74.8	62.4	44.8	76.6	63.1	47.5	76.5
47.244	4.37	66.5	50.0	79.0	65.2	49.7	76.3	---	---	---
48.250	5.38	69.8	51.9	83.3	70.2	55.0	83.7	69.3	49.3	83.6
50.841	7.97	66.8	54.1	75.4	66.8	55.5	78.0	70.2	59.9	80.2

Table D.10. Flume clay loam Run 5 velocity data.

		Profile 1			Profile 2			Profile 3		
Point Gage Depth (cm)	Height above bed (cm)	Average Velocity (cm/s)	Min Velocity (cm/s)	Max Velocity (cm/s)	Average Velocity (cm/s)	Min Velocity (cm/s)	Max Velocity (cm/s)	Average Velocity (cm/s)	Min Velocity (cm/s)	Max Velocity (cm/s)
43.769	0.90	28.9	21.1	37.0	29.5	22.8	37.5	30.1	23.0	37.8
44.013	1.14	30.7	24.7	38.9	30.9	21.4	40.0	31.4	21.9	91.2*
44.257	1.39	31.8	24.5	38.3	32.3	24.0	40.7	32.6	23.7	38.9
44.501	1.63	32.3	25.6	39.3	33.3	25.6	40.6	32.7	24.2	39.6
44.988	2.12	34.2	27.7	40.8	34.5	27.0	40.7	35.1	27.0	41.1
45.476	2.61	34.8	27.3	40.1	35.6	27.5	41.0	35.9	27.3	42.2
46.482	3.61	36.0	28.2	77.6	36.6	29.4	41.6	36.9	30.1	42.1
47.244	4.37	35.8	30.9	40.6	36.2	27.7	41.1	37.0	30.3	41.5

*Velocity spike: 2nd max = 41.2 cm/s, 3rd max = 38.0 cm/s

Table D.11. Flume clay loam Run 6 velocity data.

		Profile 1			Profile 2			Profile 3		
Point Gage Depth (cm)	Height above bed (cm)	Average Velocity (cm/s)	Min Velocity (cm/s)	Max Velocity (cm/s)	Average Velocity (cm/s)	Min Velocity (cm/s)	Max Velocity (cm/s)	Average Velocity (cm/s)	Min Velocity (cm/s)	Max Velocity (cm/s)
43.769	0.90	42.7	28.8	59.9	46.9	34.4	62.6	44.6	30.1	57.8
44.013	1.14	45.1	30.6	57.1	47.7	32.8	60.9	46.1	32.6	58.5
44.501	1.63	50.1	38.0	61.8	49.8	34.7	63.7	48.9	34.7	61.0
44.988	2.12	51.8	37.4	64.2	54.0	37.4	66.0	52.6	39.3	65.8
45.476	2.61	54.7	41.8	66.8	54.8	40.8	66.4	53.7	38.5	64.8
46.482	3.61	58.7	44.9	74.4	58.4	44.0	71.3	59.4	47.0	68.2
47.488	4.62	61.0	49.2	73.0	60.3	48.4	88.0	59.3	44.4	70.5
49.317	6.45	62.2	51.0	73.0	62.5	51.4	71.9	63.0*	53.2	72.6

*Ran out of time, only 26 seconds of measurements

Table D.12. Flume clay loam Run 7 velocity data.

		Profile 1			Profile 2			Profile 3		
Point Gage Depth (cm)	Height above bed (cm)	Average Velocity (cm/s)	Min Velocity (cm/s)	Max Velocity (cm/s)	Average Velocity (cm/s)	Min Velocity (cm/s)	Max Velocity (cm/s)	Average Velocity (cm/s)	Min Velocity (cm/s)	Max Velocity (cm/s)
43.769	0.90	47.8	34.5	62.0	47.4	33.0	62.3	48.8	35.1	65.1
44.013	1.14	50.0	37.0	64.0	48.9	34.4	63.7	50.8	33.8	68.2
44.501	1.63	53.6	39.3	71.3	53.3	39.6	66.9	54.4	39.9	69.3
44.988	2.12	55.3	39.4	68.3	55.6	41.4	69.7	56.8	40.9	69.6
45.476	2.61	57.2	42.5	70.2	58.6	44.2	72.4	58.9	44.3	72.7
46.482	3.61	60.8	46.4	72.0	61.9	45.5	71.8	62.0	47.8	73.3
47.488	4.62	64.0	49.7	74.0	64.5	50.3	75.2	64.4*	51.4	73.3
50.749	7.88	65.0	53.5	72.2	65.1	52.7	74.5	65.4**	54.9	72.7

*Short on time, only 47 seconds of measurements; **Short on time, only 40 seconds of measurements

Table D.13. Flume clay loam applied shear stresses and erosion rates for different calculation methods.

Flume Clay Loam Run	Applied Bed τ (Pa)			Erosion Rate from Data (mm/hr)				Erosion Rate Adjusted for 5.5g Less of Soil Loss (mm/hr)			
	LOW[a]	VDL[b]	Average Shear Stress	Erosion rate (testing ρ_b[c], pre-test area[d])	Erosion rate (testing ρ_b, testing area[e])	Erosion rate (post-test ρ_b[f], pre-test area)	Erosion rate (post-test ρ_b, testing area)	Erosion Rate (testing ρ_b, pre-testing area)	Erosion rate (testing ρ_b, testing area)	Erosion rate (post-test ρ_b, pre-test area)	Erosion rate (post-test ρ_b, testing area)
1	0.184	0.168	0.020	0.337	0.328	---	---	0.121	0.118	---	---
2	0.248	0.254	0.335	0.189	0.184	0.214	0.208	0.000	0.000	0.000	0.000
3	0.467	0.625	0.497	3.524	3.431	4.014	3.907	3.307	3.219	3.767	3.667
4	1.917	2.083	2.647	13.119	12.772	13.550	13.191	12.906	12.564	13.329	12.976
5	0.364	0.516	0.565	1.024	0.996	1.151	1.121	0.802	0.781	0.902	0.879
6	1.521	1.736	4.479	22.859	22.254	25.419	24.745	22.642	22.042	25.167	24.500
7	1.283	1.611	1.781	20.093	19.561	21.480	20.911	19.873	19.346	21.246	20.683

[a]Law of the Wall; [b]Velocity defect law; [c]Calculated testing bulk density before test; [d]Pre-testing soil surface area before swelling (14.8 cm x 14.8 cm); [e]Testing soil surface area after swelling (15 cm x 15 cm); [f]Bulk density after test

Table D.14. Flume clay loam critical shear stress and soil erodibility values using Theil-Sen regression depending on applied shear stress and erosion rate calculation method.

τ_a Calculation Method	Erosion Rate Calculation Method			Runs	k_d (cm^3/N-s)	τ_c (Pa)	p-value	95% CI for slope (cm^3/N-s)	
	Erosion Rate[a]	Bulk Density[b]	Soil Surface Area[c]					Lower Limit	Upper Limit
Basic LOW[d]	Test Erosion rate	Testing ρ_b	Pre-test area	All	3.229	0.164	0.0243	1.060	5.342
Basic LOW	Test Erosion rate	Testing ρ_b	Testing area	All	3.143	0.164	0.0243	1.031	5.201
Basic LOW	Test Erosion rate	Post-test ρ_b	Pre-test area	All	4.820	0.236	0.0388	0.0	6.145
Basic LOW	Test Erosion rate	Post-test ρ_b	Testing area	All	4.692	0.236	0.0388	0.0	5.982
Basic LOW	Adjusted Erosion rate	Testing ρ_b	Pre-test area	All	3.232	0.183	0.0243	1.051	5.334
Basic LOW	Adjusted Erosion rate	Testing ρ_b	Testing area	All	3.146	0.183	0.0243	1.023	5.192
Basic LOW	Adjusted Erosion rate	Post-test ρ_b	Pre-test area	All	4.778	0.248	0.0388	0.0	6.149
Basic LOW	Adjusted Erosion rate	Post-test ρ_b	Testing area	All	4.651	0.248	0.0388	0.0	5.986
Basic LOW	Test Erosion rate	Testing ρ_b	Pre-test area	w/o Run 4	4.947	0.237	0.0146	1.060	5.764
Basic LOW	Test Erosion rate	Testing ρ_b	Testing area	w/o Run 4	4.816	0.237	0.0146	1.031	5.611
Basic LOW	Test Erosion rate	Post-test ρ_b	Pre-test area	w/o Run 4	5.674	0.271	0.0143	2.245	7.720
Basic LOW	Test Erosion rate	Post-test ρ_b	Testing area	w/o Run 4	5.524	0.271	0.0143	2.185	7.516
Basic LOW	Adjusted Erosion rate	Testing ρ_b	Pre-test area	w/o Run 4	4.941	0.248	0.0146	1.051	5.764
Basic LOW	Adjusted Erosion rate	Testing ρ_b	Testing area	w/o Run 4	4.810	0.248	0.0146	1.023	5.612
Basic LOW	Adjusted Erosion rate	Post-test ρ_b	Pre-test area	w/o Run 4	5.671	0.282	0.0143	2.161	7.725
Basic LOW	Adjusted Erosion rate	Post-test ρ_b	Testing area	w/o Run 4	5.521	0.282	0.0143	2.104	7.521
VDL[e]	Test Erosion rate	Testing ρ_b	Pre-test area	All	2.498	0.233	0.0243	0.548	4.837
VDL	Test Erosion rate	Testing ρ_b	Testing area	All	2.431	0.233	0.0243	0.534	4.709
VDL	Test Erosion rate	Post-test ρ_b	Pre-test area	All	4.353	0.305	0.0388	0.0	7.295
VDL	Test Erosion rate	Post-test ρ_b	Testing area	All	4.238	0.305	0.0388	0.0	7.102
VDL	Adjusted Erosion rate	Testing ρ_b	Pre-test area	All	2.476	0.254	0.0243	0.543	4.838
VDL	Adjusted Erosion rate	Testing ρ_b	Testing area	All	2.411	0.254	0.0243	0.529	4.710
VDL	Adjusted Erosion rate	Post-test ρ_b	Pre-test area	All	4.349	0.319	0.0388	0.0	7.300
VDL	Adjusted Erosion rate	Post-test ρ_b	Testing area	All	4.234	0.319	0.0388	0.0	7.107
VDL	Test Erosion rate	Testing ρ_b	Pre-test area	w/o Run 4	4.074	0.241	0.0146	0.548	6.147
VDL	Test Erosion rate	Testing ρ_b	Testing area	w/o Run 4	3.967	0.241	0.0146	0.534	5.985

τ_a Calculation Method	Erosion Rate Calculation Method			Runs	k_d (cm^3/N-s)	τ_c (Pa)	p-value	95% CI for slope (cm^3/N-s)	
	Erosion Rate[a]	Bulk Density[b]	Soil Surface Area[c]					Lower Limit	Upper Limit
VDL[e]	Test Erosion rate	Post-test ρ_b	Pre-test area	w/o Run 4	5.039	0.404	0.0143	0.994	8.753
VDL	Test Erosion rate	Post-test ρ_b	Testing area	w/o Run 4	4.905	0.404	0.0143	0.967	8.521
VDL	Adjusted Erosion rate	Testing ρ_b	Pre-test area	w/o Run 4	4.068	0.254	0.0146	0.543	6.153
VDL	Adjusted Erosion rate	Testing ρ_b	Testing area	w/o Run 4	3.960	0.254	0.0146	0.529	5.990
VDL	Adjusted Erosion rate	Post-test ρ_b	Pre-test area	w/o Run 4	5.042	0.417	0.0143	0.957	8.714
VDL	Adjusted Erosion rate	Post-test ρ_b	Testing area	w/o Run 4	4.909	0.417	0.0143	0.931	8.483
Average shear stress	Test Erosion rate	Testing ρ_b	Pre-test area	All	1.477	0.179	0.0243	0.285	3.584
Average shear stress	Test Erosion rate	Testing ρ_b	Testing area	All	1.438	0.179	0.0243	0.277	3.490
Average shear stress	Test Erosion rate	Post-test ρ_b	Pre-test area	All	1.654	0.255	0.0388	0.0	4.644
Average shear stress	Test Erosion rate	Post-test ρ_b	Testing area	All	1.610	0.255	0.0388	0.0	4.521
Average shear stress	Adjusted Erosion rate	Testing ρ_b	Pre-test area	All	1.476	0.219	0.0243	0.285	3.584
Average shear stress	Adjusted Erosion rate	Testing ρ_b	Testing area	All	1.437	0.219	0.0243	0.278	3.489
Average shear stress	Adjusted Erosion rate	Post-test ρ_b	Pre-test area	All	1.658	0.299	0.0388	0.0	4.647
Average shear stress	Adjusted Erosion rate	Post-test ρ_b	Testing area	All	1.614	0.299	0.0388	0.0	4.524
Average shear stress	Test Erosion rate	Testing ρ_b	Pre-test area	w/o Run 4	1.520	0.129	0.0388	0.0	4.356
Average shear stress	Test Erosion rate	Testing ρ_b	Testing area	w/o Run 4	1.479	0.129	0.0388	0.0	4.241
Average shear stress	Test Erosion rate	Post-test ρ_b	Pre-test area	w/o Run 4	1.706	0.300	0.05	0.0	6.516
Average shear stress	Test Erosion rate	Post-test ρ_b	Testing area	w/o Run 4	1.661	0.300	0.05	0.0	6.343
Average shear stress	Adjusted Erosion rate	Testing ρ_b	Pre-test area	w/o Run 4	1.518	0.166	0.0388	0.0	4.356
Average shear stress	Adjusted Erosion rate	Testing ρ_b	Testing area	w/o Run 4	1.478	0.166	0.0388	0.0	4.241
Average shear stress	Adjusted Erosion rate	Post-test ρ_b	Pre-test area	w/o Run 4	1.705	0.335	0.05	0.0	6.459
Average shear stress	Adjusted Erosion rate	Post-test ρ_b	Testing area	w/o Run 4	1.659	0.335	0.05	0.0	6.288

[a]Erosion rate used in regression analysis: test erosion rate – calculated from the test data; and adjusted erosion rate – calculated from the test soil loss minus 5.5 g of soil; [b]Bulk density used to calculate the erosion rate: testing ρ_b – calculated bulk density before test; and post-test ρ_b – bulk density after test; [c]Soil surface area used to calculate the erosion rate: pre-test area – soil area before swelling (14.8 cm x 14.8 cm); and testing area – soil area after swelling (15 cm x 15 cm); [d]Law of the Wall; [e]Velocity defect law

D.2. Clay Measurements

Table D.15. Flume clay settings and conditions.

Run Number	Flume Rate (Hz)	Tailgate Height (mm)	Discharge (m^3/s)			Reynolds Number	Froude Number	Applied Shear Stress (Pa)			Test Duration (s)
			Test Start	Test Middle	Test End			LOW[a]	VDL[b]	Average τ	
Clay 1	15	10	0.0178	0.0178	0.0178	54641	0.540	0.327	0.421	0.485	2711
Clay 2	15	---	0.0179	0.0180	0.0180	59351	0.599	0.510	0.430	0.575	2700
Clay 3	25	---	0.0301	0.0301	0.0302	101264	0.659	0.747	0.813	1.427	2700
Clay 4	35	---	0.0414	0.0415	0.0415	121676	0.692	1.163	1.380	3.211	2697
Clay 5	30	---	0.0359	0.0360	0.0360	109364	0.682	0.842	1.032	0.578	2702

[a]Law of the Wall; [b]Velocity defect law

Table D.16. Flume clay erosion data.

Run Number	Soil loss (g)	% Soil loss	Erosion rate (g/s)	Erosion rate (cm/day)[a]	SSC[b] (mg/L)		
					Pre-test	Middle	Post-Test
Clay 1	80.43	5.71%	0.0297	7.72	8.20	10.20	9.62
Clay 2	143.99	10.20%	0.0533	14.32	9.06	11.37	10.18
Clay 3	399.53	28.35%	0.1480	39.59	9.29	22.14	23.33
Clay 4	477.36	33.89%	0.1770	47.64	5.44	38.21	39.47
Clay 5	345.32	24.45%	0.1278	34.54	19.09	29.46	29.12

[a]Calculated from the test ρ_b and testing surface area; [b]Suspended sediment concentration

Table D.17. Flume clay soil conditions and water temperature and conductivity data.

Run Number	Compact θ_d[a]	Initial Test θ_d[b]	Test ρ_b[c] (g/cm^3)	Water Temperature (°C)				Water Conductivity (µS/cm)			
				Pre-test	Test Start	Test Middle	Test End	Pre-test	Test Start	Test Middle	Test End
Clay 1	0.154	0.202	1.475	13.0	13.4	13.5	13.6	159	165	164	159
Clay 2	0.153	0.214	1.430	15.7	15.9	16.0	16.1	157	160	159	157
Clay 3	0.154	0.222	1.435	18.1	17.7	17.8	17.9	157	166	167	167
Clay 4	0.156	0.213	1.427	12.5	12.9	13.5	13.9	162	162	163	161
Clay 5	0.154	0.207	1.421	13.5	13.9	14.3	14.7	157	160	158	157

[a]Gravimetric moisture content at compaction; [b]Calculated testing gravimetric moisture content; [c]Calculated bulk density

Table D.18. Flume clay water depth measurements and water slope.

Run Number	Water Depth (cm)												Water Slope
	Upstream[a]			Upstream of box[b]			Downstream of box[c]			Downstream[d]			
	Test Start	Test Middle	Test End	Test Start	Test Middle	Test End	Test Start	Test Middle	Test End	Test Start	Test Middle	Test End	
Clay 1	4.83	4.95	4.81	5.02	4.94	4.80	4.62	4.76	4.69	4.79	4.84	4.75	0.103%
Clay 2	4.57	4.65	4.64	4.55	4.61	4.45	4.51	4.47	4.48	4.49	4.46	4.47	0.130%
Clay 3	6.09	6.26	6.18	6.14	6.15	6.12	5.77	5.79	5.86	6.03	5.89	---	0.244%
Clay 4	7.47	7.37	7.36	7.24	7.17	7.24	7.07	7.06	7.14	6.81	6.92	6.89	0.458%
Clay 5	6.56	6.63	6.65	6.47	6.65	6.65	6.39	6.50	6.75	6.79	6.73	6.72	0.090%*

[a]0.5 m upstream of upstream soil edge; [b]6.5 cm upstream of upstream soil edge; [c]6.5 cm downstream of downstream soil edge; [d]0.5 m downstream of downstream soil edge; *excludes downstream data

Table D.19. Flume clay applied shear stress from law of the wall (LOW) and velocity defect law (VDL).

	LOW						Velocity Defect Law					
	Profile 1		Profile 2		Profile 3		Profile 1		Profile 2		Profile 3	
Run Number	τ (Pa)	R^2	τ (Pa)	R^2	τ (Pa)	R^2	τ (Pa)	R^2	τ (Pa)	R^2	τ (Pa)	R^2
Clay Loam 1	0.356	0.965	0.313	0.957	0.313	0.945	0.322	0.967	0.528	0.951	0.412	0.996
Clay Loam 2	0.580	0.962	0.452	0.991	0.499	0.990	0.307	0.973	0.447	0.989	0.534	0.989
Clay Loam 3	0.710	0.992	0.792	0.997	0.739	0.971	0.760	0.991	0.815	0.965	0.864	0.996
Clay Loam 4	1.209	0.986	1.188	0.976	1.092	0.969	1.346	0.982	1.371	0.989	1.423	0.982
Clay Loam 5	0.961	0.953	0.991	0.972	0.573	0.981	1.230	0.987	0.657	0.981	1.209	0.990

Table D.20. Flume clay Run 1 velocity data.

		Profile 1			Profile 2			Profile 3		
Point Gage Depth (cm)	Height above bed (cm)	Average Velocity (cm/s)	Min Velocity (cm/s)	Max Velocity (cm/s)	Average Velocity (cm/s)	Min Velocity (cm/s)	Max Velocity (cm/s)	Average Velocity (cm/s)	Min Velocity (cm/s)	Max Velocity (cm/s)
43.678	0.80	29.5	23.2	37.4	30.6	23.8	39.0	30.7	22.8	38.5
43.922	1.04	30.6	24.4	37.8	32.6	22.9	40.0	32.0	25.2	38.8
44.166	1.29	30.8*	23.5	36.6	33.0	25.4	39.4	32.7	25.0	39.5
44.653	1.78	32.2	24.8	37.8	34.9	25.9	40.7	34.5	27.6	41.7
45.141	2.26	33.9	25.4	40.5	35.7	27.0	43.4	35.9	26.6	41.9
45.629	2.75	34.9	27.9	39.9	36.8	29.0	43.9	36.9	30.0	44.0
46.634	3.76	37.1	28.3	42.3	38.3	32.0	43.4	37.7^{+}	29.5	41.7
47.244	4.37	36.3	31.8	82.3**	37.1	31.9	42.7	37.1^{++}	31.7	42.7

*Something jammed propeller for most of measurements (0:07 - 0:57 sec), average based on measurements before and after jam (250 measurements); **Velocity spike: 2nd to max = 42.5 cm/s; $^{+}$Short on time, only 37 sec of measurements; $^{++}$Short on time, only 26 sec of measurements

Table D.21. Flume clay Run 2 velocity data.

		Profile 1			Profile 2			Profile 3		
Point Gage Depth (cm)	Height above bed (cm)	Average Velocity (cm/s)	Min Velocity (cm/s)	Max Velocity (cm/s)	Average Velocity (cm/s)	Min Velocity (cm/s)	Max Velocity (cm/s)	Average Velocity (cm/s)	Min Velocity (cm/s)	Max Velocity (cm/s)
43.708	0.80	30.9	23.8	39.8	33.1	26.2	41.8	33.0	25.6	40.1
43.952	1.04	32.0	25.1	39.5	34.4	27.0	42.1	34.3	27.6	41.2
44.196	1.29	32.4	25.7	41.4	35.8	28.5	42.5	35.8	27.3	42.8
44.684	1.78	33.9	26.7	40.0	36.9	28.7	44.0	37.1	29.5	43.2
45.171	2.26	35.5	27.8	42.9	38.7	30.9	45.9	39.1	29.9	47.2
45.659	2.75	37.3	29.7	43.1	40.2	30.7	46.2	39.4	32.6	46.2
46.147	3.24	38.4	32.6	43.7	41.1	30.6	46.7	---	---	---
46.787	3.88	40.2	33.9	57.7	41.4	33.6	46.4	41.2*	33.8	47.7

*Out of time, only 37 sec of measurements

Table D.22. Flume clay Run 3 velocity data.

		Profile 1			Profile 2			Profile 3		
Point Gage Depth (cm)	Height above bed (cm)	Average Velocity (cm/s)	Min Velocity (cm/s)	Max Velocity (cm/s)	Average Velocity (cm/s)	Min Velocity (cm/s)	Max Velocity (cm/s)	Average Velocity (cm/s)	Min Velocity (cm/s)	Max Velocity (cm/s)
43.739	0.80	40.0	30.6	51.6	40.4	29.9	51.4	39.3	29.7	48.9
43.983	1.04	41.8	32.2	51.1	41.1	30.0	52.7	41.5	31.1	51.6
44.226	1.29	42.7	32.6	52.6	42.4	31.4	55.6	42.5	31.8	52.5
44.714	1.78	45.0	33.4	54.6	44.6	36.0	54.6	44.9	35.5	55.2
45.202	2.26	47.4	37.2	57.2	47.6	37.3	57.4	47.1	36.2	55.4
45.690	2.75	48.2	37.6	59.0	48.2	37.5	56.9	48.4	38.8	56.6
46.695	3.76	50.7	38.7	57.8	51.0	41.8	58.5	50.4	40.1	57.9
48.250	5.31	52.0	43.9	60.9	51.4	41.6	59.0	52.4*	42.6	58.4

*Out of time, only 44 sec of measurements

Table D.23. Flume clay Run 4 velocity data.

		Profile 1			Profile 2			Profile 3		
Point Gage Depth (cm)	Height above bed (cm)	Average Velocity (cm/s)	Min Velocity (cm/s)	Max Velocity (cm/s)	Average Velocity (cm/s)	Min Velocity (cm/s)	Max Velocity (cm/s)	Average Velocity (cm/s)	Min Velocity (cm/s)	Max Velocity (cm/s)
43.739	0.80	46.8	35.0	58.1	46.3	34.9	59.0	45.9	34.2	57.5
43.983	1.04	47.6	37.3	59.3	48.2	37.2	58.0	48.0	32.9	60.0
44.226	1.29	50.1	38.0	62.0	49.7	36.7	61.3	49.9	35.7	62.4
44.714	1.78	52.2	39.1	64.8	52.1	40.1	62.6	51.5	38.7	65.1
45.202	2.26	55.5	40.5	66.9	55.0	40.1	65.4	55.2	42.2	67.0
45.690	2.75	56.6	43.1	66.9	57.0	42.1	65.1	56.5	44.6	68.1
46.695	3.76	60.5	45.8	68.7	60.5	48.0	69.6	60.6	44.5	68.4
49.469	6.53	63.5	52.9	72.4	61.6	49.3	68.6	62.4	50.2	68.8

Table D.24. Flume clay Run 5 velocity data.

		Profile 1			Profile 2			Profile 3		
Point Gage Depth (cm)	Height above bed (cm)	Average Velocity (cm/s)	Min Velocity (cm/s)	Max Velocity (cm/s)	Average Velocity (cm/s)	Min Velocity (cm/s)	Max Velocity (cm/s)	Average Velocity (cm/s)	Min Velocity (cm/s)	Max Velocity (cm/s)
43.769	0.80	44.6	32.5	54.6	43.8	31.9	54.4	43.3	32.7	53.3
44.013	1.04	45.3	34.3	57.1	45.7	34.9	57.0	45.8	35.4	56.8
44.257	1.29	47.4	37.7	58.3	47.2	36.6	58.1	46.6	35.8	57.4
44.745	1.78	50.3	38.3	60.1	49.5	38.9	59.6	50.5	36.6	61.2
45.232	2.26	52.4	40.7	61.5	49.9	34.0	60.7	51.8	41.0	62.3
45.720	2.75	54.6	42.7	63.7	51.1	40.2	59.0	53.3	41.0	62.4
46.726	3.76	57.4	43.6	66.6	54.2	41.8	61.7	57.0	44.0	65.0
48.951	5.98	57.4	48.2	65.0	55.4	41.9	63.8	57.7	48.4	64.3

Table D.25. Flume clay loam applied shear stresses and erosion rates for different calculation methods.

Flume Clay Run	Applied Bed τ (Pa)			Erosion Rate from Data (mm/hr)		Erosion Rate Adjusted for 5.5g Less of Soil Loss (mm/hr)	
	LOW[a]	VDL[b]	Average Shear Stress	Erosion rate (testing ρ_b[c], pre-test area[d])	Erosion rate (testing ρ_b, testing area[e])	Erosion Rate (testing ρ_b, pre-test area)	Erosion rate (testing ρ_b, testing area)
1	0.327	0.421	0.485	3.305	3.218	3.080	2.998
2	0.510	0.430	0.575	6.130	5.968	5.895	5.739
3	0.747	0.813	1.427	16.946	16.497	16.715	16.272
4	1.163	1.380	3.211	20.391	19.850	20.150	19.617
5	0.842	1.032	0.578	14.784	14.392	14.546	14.161

[a]Law of the Wall; [b]Velocity defect law; [c]Calculated testing bulk density before test; [d]Pre-test soil surface area before swelling (14.8 cm x 14.8 cm); [e]Testing soil surface area after swelling (15 cm x 15 cm)

Table D.26. Flume clay critical shear stress and soil erodibility values using Theil-Sen regression depending on applied shear stress and erosion rate calculation method.

	Erosion Rate Calculation Method					95% CI for Slope (cm^3/N-s)	
τ_a Calculation Method	Erosion Rate[a]	Soil Surface Area[b]	k_d (cm^3/N-s)	τ_c (Pa)	p-value	Lower Limit	Upper Limit
Basic LOW[c]	Test Erosion rate	Pre-test area	5.872	0.171	0.0500	0.0	12.677
Basic LOW	Test Erosion rate	Testing area	5.716	0.171	0.0500	0.0	12.341
Basic LOW	Adjusted Erosion rate	Pre-test area	5.868	0.181	0.0500	0.0	12.681
Basic LOW	Adjusted Erosion rate	Testing area	5.713	0.181	0.0500	0.0	12.345
VDL[d]	Test Erosion rate	Pre-test area	4.712	0.161	0.0500	0.0	87.195
VDL	Test Erosion rate	Testing area	4.587	0.161	0.0500	0.0	84.886
VDL	Adjusted Erosion rate	Pre-test area	4.709	0.174	0.0500	0.0	86.894
VDL	Adjusted Erosion rate	Testing area	4.584	0.174	0.0500	0.0	84.592
Average shear stress	Test Erosion rate	Pre-test area	2.633	0.0	0.0143	0.536	686.775
Average shear stress	Test Erosion rate	Testing area	2.563	0.0	0.0143	0.522	668.583
Average shear stress	Adjusted Erosion rate	Pre-test area	2.632	0.0	0.0143	0.535	686.572
Average shear stress	Adjusted Erosion rate	Testing area	2.563	0.0	0.0143	0.521	668.386

[a]Erosion rate used in regression analysis: test erosion rate – calculated from the test data and testing bulk density; and adjusted erosion rate – calculated from the test soil loss minus 5.5 g of soil and testing bulk density; [b]Soil surface area used to calculate the erosion rate: pre-test area – soil area before swelling (14.8 cm x 14.8 cm); and testing area – soil area after swelling (15 cm x 15 cm); [c]Law of the Wall; [d]Velocity defect law